

Supporting information:

Multi-micron crisscross structures grown from DNA-origami slats

Authors:

Christopher M. Wintersinger^{1,2,3,4*}, Dionis Minev^{1,3,4,*}, Anastasia Ershova^{1,3,4*}, Hiroshi M. Sasaki^{1,6†}, Gokul Gowri^{1,3,4,6}, Jonathan F. Berengut^{1,3,5}, F. Eduardo Corea-Dilbert^{3††}, Peng Yin^{1,6}, William M. Shih^{1,3,4,#}

Affiliations:

¹Wyss Institute for Biologically Inspired Engineering at Harvard University; ²Harvard John A. Paulson School of Engineering and Applied Sciences; ³Department of Cancer Biology, Dana-Farber Cancer Institute, ⁴Department of Biological Chemistry and Molecular Pharmacology, Harvard Medical School; ⁵EMBL Australia Node for Single Molecule Science, School of Medical Sciences, The University of New South Wales, Sydney; ⁶Department of Systems Biology, Harvard Medical School; #Correspondence: William_Shih@dfci.harvard.edu

*Denotes equal contribution

† HMS current address: 10x Genomics, Inc., Pleasanton, CA, USA.

†† FECD current address: Geisel School of Medicine at Dartmouth, Hanover, NH, USA.

Table of contents

Table of contents	1
Supplementary Text 1: Comparison to methods that generate periodic multi-origami assemblies	3
Supplementary Text 2: Design notes regarding the 12HB slat	4
2.1 Derivation of 12HB slats from 6HB slats	4
2.2 Yield differences and the consequence on downstream usage of the slats	4
Supplementary Text 3: Algorithm for selection of the handle sequences	6
3.1 Initial sequence generation	6
3.2 Optimizing for sequence orthogonality	6
3.3 Discussion about the final sequences and pertinence to megastructures	7
Supplementary Text 4: Relationship between the number of unique slats in a design versus the relative rate of growth	8
4.1 Growth slows when large numbers of unique slats are mixed simultaneously	8
4.2 Growth of finite megastructures with large numbers of unique slats can be accelerated by adding the slats in multiple steps	9
Supplementary Text 5: Detailed characterization of binding handles	11
5.1 How the number of binding sites (i.e. v16 or v8) versus temperature influences spontaneous nucleation	11
5.2 How the base-pairing strength of the binding site handles versus temperature influences growth rate and spontaneous nucleation	11
Supplementary Text 6: Kinetics of ribbon assembly	13
6.1 Calculation of the number of slats added to the ribbon	13
6.2 Approximation of growth using pseudo-first order kinetics	13
6.3 How the base-pairing strength of the binding-site handles influences growth rate	14
Supplementary Text 7: Sequence assignment to megastructures from the 2048-handle sequence library, optimization of the Hamming distances of slats within megastructure designs	15
7.1 Increased pairwise complementarity between slats (i.e. minimized Hamming distances) causes drastic slowdown of 1D ribbon growth	15
7.2 Possible mechanism for how complementarity between the slats causes growth slowdown	16
7.3 Discussion of the Hamming distances used in the finite and periodic megastructure designs	17
Supplementary Text 8: Potential future applications	18
	1

Supplementary Figures Fig. S1–Fig. S45	21
Fig. S1–Fig. S8: Slat and seed design and folding, qualitative energetics of crisscross assembly, selection of initial binding-site strength, energies of various binding-handle sets, and need for T-linkers	21
Fig. S9–Fig. S15: Models of finite megastructures, preparation time for each design, and additional TEM results of finite megastructures	29
Fig. S16–Fig. S27: Models of periodic megastructures, growth comparison of different ribbon designs, relationship between growth rate and number of unique slats, and additional TEM results of periodic megastructures	37
Fig. S28–Fig. S31: Model of the DNA nanocube, additional TEM of nanocube patterns, and DNA-PAINT results of 1D ribbons and 2D sheets	48
Fig. S32–Fig. S34: TEM results when no seed added, AGE results of single DNA origami square versus scaffold, representative TEM of megastructures versus concentration of seed	52
Fig. S35–Fig. S40: Standard curve of ribbons, melt temperature of v16 7-nt ribbons, temperature characterization and melt temperature of v8 7-nt, v16/v8 6-nt, and v16/v8 8-nt ribbons, growth versus time for 6-nt and 8-nt v16 ribbons	56
Fig. S41–Fig. S45: Hamming-distance analysis of 1D ribbon growth, mechanistic testing for growth changes to 1D ribbons vs. kinetic trapping of slats resulting from Hamming distance, and optimized Hamming distances of all the megastructure designs tested in this work	64
Table 1–Table 8: Core-strand sequences for 6HB, 12HB, seed, and single origami reference square; Sequences of the 6-, 7-, 8-, 9-, and 10-nt handles; Nanocube strand sequences	70
Supplementary references	87

Supplementary Text 1: Comparison to methods that generate periodic multi-origami assemblies

We believe the method developed by Tikhomirov et al. is the most relevant benchmark for our work, where the key enabling feature is the large number of unique DNA origami that are specifically positioned within the megastructures. In contrast, other reported methods can give rise to megastructures with larger overall mass, however these are periodic structures with a much smaller unit cell.

Xin and colleagues reported a megastructure assembled from DNA origami that is a lattice with a surface area of 19 cm^2 ⁵³. However, this was a periodic assembly, where the size of the unit cell was a single DNA origami.

The Dietz lab has introduced a powerful shape-complementary paradigm for self-assembling periodic DNA megastructures that extinguish their growth at gigadalton size ranges^{16,17,21}. Here the rigid geometry of the origami-sized building blocks enables formation of self-limiting finite assemblies from one or a small number of unique monomers, analogous to self-assembly of viral capsids. However, it is unclear how well this method would scale for assembly of megastructures composed of thousands of unique monomers, such that the entire megastructure would be uniquely addressable, which some applications would demand. Three concerns are listed below:

(i) The apparent second-order rate constant for assembly has been reported as $1.7 \times 10^4 \text{ M}^{-1} \text{ s}^{-1}$ ³⁹, which is ~ 50 times slower than what we have observed here for crisscross polymerization of origami. Therefore assembly with hundreds of distinct shape-complementary components in the same pot would be exceedingly slow.

(ii) A different set of staple strands may be required to generate each of the unique shape-complementary interfaces between building blocks, therefore it likely would be far more expensive to create thousands of unique building blocks (c.f. only modular 2048 strand library required for crisscross origami). Furthermore it remains to be seen whether thousands of functionally orthogonal interfaces could indeed be generated with the shape-complementary architecture.

(iii) A key enabling feature of crisscross polymerization is absolute control over nucleation. With shape-complementary monomers that make contacts only with nearest neighbors, such as what has been demonstrated thus far, nucleation control will be far less robust²⁶. It may be possible to construct architectures that exploit non-nearest neighbor contacts in the context of shape-complementary interactions and thereby achieve robust nucleation control; extending the paradigm of crisscross polymerization in this way would be an interesting next direction to pursue for the field.

Supplementary Text 2: Design notes regarding the 12HB slat

The following section describes how the 12HB slats were derived from the 6HB design and explains the consequences that this choice had for folding and experimental usage.

2.1 Derivation of 12HB slats from 6HB slats

The crossover pattern and staple set for the 12HB slat was derived from the design for the 6HB (Fig. S3). The reason for this was so that we would not have to purchase additional handle strands for the 12HB slats. Rather, we were able to apply the 2048-strand library from the 6HBs to also make the shorter 12HB slats. For the 12HB, a subset of staple strands in the middlemost segment of the 6HB was left out or modified to act as a hinge, so that the 6HB could fold back upon itself to make a half-length 12HB.

2.2 Yield differences and the consequence on downstream usage of the slats

One shortcoming of the approach in Supplementary Text 2.1 was that the yield of 12HBs was much lower compared to the equivalent 6HB (~10% versus ~80%, see Fig. S4). We realized that the process of folding the 6HB back upon itself was inefficient because there was a propensity for the slats to dimerize or else make other higher molecular-weight byproducts. The gel in Fig. S4B indicates that roughly similar amounts of desired monomer and byproduct dimer formed even in the best folding condition. We hypothesized that the hinge did not allow complete freedom for the 6HBs to flex into the desired half-length 12HBs and that this process was perhaps energetically unfavorable. We expect that we could make formation of the half-length 12HB higher yielding by changing the scaffold routing to eliminate this flexing back in the folding pathway. However, that would require purchasing additional handle library strands to accommodate the different scaffold routing.

We note that high yield in the folding of the slats is critical for making downstream preparation of the megastructures easy and straightforward. The ~80% yield of the 6HBs gave us the ability to pool and concentrate the slats into a smaller volume using only PEG precipitation. By contrast, the low ~10% yield of the 12HBs required us to pool the slats, separate them from the undesired dimers by excision from an agarose gel, and then subsequently concentrate the 12HBs into a smaller volume with PEG precipitation. We generally observed ~80% recovery of a pool of raw 6HB slats versus about an order of magnitude decrease for the 12HB slats. We would suggest further optimization of the 12HB design with a different library of staple strands with the 32 possible handles should a user desire to make larger quantities of 12HB

megastructures than as tested here. We also advise any user who conceives of alternative slat designs to optimize design and folding of the slat to make it easier to prepare at high yield for use in megastructures.

Supplementary Text 3: Algorithm for selection of the handle sequences

We generated 6-nt, 7-nt, and 8-nt handle sequences so that each sequence of a given length had roughly similar binding energies and were as orthogonal from one another as reasonably possible. The following section describes the sequence-selection algorithm that we used to choose sequences for the 32 7-nts in the 2048 handle strand library, as well for the 256 6-nts, 7-nts, or 8-nts in the various 512-handle strand libraries. The former 2048 -strand library was used to create the diversity of finite and periodic megastructures, versus the latter 512-strand libraries which were used to make only v16/v8 staggered ribbons to characterize growth and nucleation of different strength binding sites (as detailed in Supplementary Text 4).

3.1 Initial sequence generation

We created all possible 6-nts, 7-nts, and 8-nts using a Python script. We removed the reverse complements for each sequence and sequences with either extremely high or low GC content, and computed the pairwise mean free energy of the sequence with its exact complement in NUPACK 3.0⁵² (using parameters DNA with 25 mM Mg²⁺ and 2 mM Na⁺). We considered this value as the binding energy of the handle. To make the sequences roughly isoenergetic, we removed sequences where the binding energy was some arbitrary number of standard deviations above or below the mean energy of the total set.

3.2 Optimizing for sequence orthogonality

We computed the matrices of pairwise mean free energies between each handle with the other handles, reverse complements of the other handles, and reverse complement of the handle with the reverse complements of the other handles. As a measure of orthogonality of one handle versus another, we normalized the computed free energies in each matrix to the binding energy of the handle in question. We assumed this ratio for a given pair of sequences would lessen if the handles being compared were more orthogonal. As such, we set an arbitrary maximum for this ratio (i.e. a minimum threshold for orthogonality) that we allowed for binding-handle sequences in the library. We removed subsets of sequences that failed to meet this criteria most frequently with other sequences in the library and repeated this process until every handle satisfied the threshold.

3.3 Discussion about the final sequences and pertinence to megastructures

The computed sequence energies of the handles as selected for this study are shown in Fig. S7. We note that only the 6-, 7-, and 8-nt handles were subjected to the selection criteria as above. The 9- and 10-nt handles used initially to test viability of different handle lengths (Fig. S6) were chosen randomly without the careful selection criteria as described above. By linear fitting of the computed energies, we found that each increment of one base pair decreased the mean free energy per handle by $-1.26 \text{ kcal mol}^{-1}$, where the spontaneous nucleation was negligible with 7-nt handles versus prolific with 8-nt handles.

It is unclear to what extent the handle-design process in the prior sections is necessary for the successful assembly of megastructures. In our implementation, we hypothesized that orthogonality of the individual handles would be important so as to limit misbinding of the slats where base pairing is made between a handle other than its appropriate complementary handle. We further hypothesized that by making the relative binding energies of a given length handle similar to one another would make the boundaries clearer between where spontaneous nucleation becomes prevalent versus the threshold length of binding handle. However, we did not seek to accept or refute either of these hypotheses and rather used them as best practices to choose the handle sequences that we thought would be most successful to create megastructures. We also note that our analysis is subject to the shortcomings of the *in silico* tools which we used to measure binding energies. For instance, most of our decisions about whether to use a sequence or not were derived using the pairwise mean free energy in NUPACK 3.0⁵² (with parameters of DNA with 25 mM Mg^{2+} and 2 mM Na^+). We are unclear as to how well these calculations would align to experimental measurements. It might be the case that an experimentalist would be able to create megastructures with less care in the sequence selection of the binding handles, though this topic must be studied further to make any conclusions.

Supplementary Text 4: Relationship between the number of unique slats in a design versus the relative rate of growth

We sought to determine the relationship for the growth of megastructures versus the concentration of the slats and number of unique slats in the design. Our intuition was that a higher concentration of each slat would increase the growth rate of a megastructure, as shown in the middlemost panel of Fig. 5D where there were 16 unique slats in the design. However, we note that the apparent rate of growth seemed noticeably slower as the total concentration of slats was increased past 1 μM (Fig. S22). We speculated that at these concentrations, liquid crystalline behavior of the slats may be occurring, thereby slowing down the rotational diffusion of slats, which may retard the rate of slat addition. This section will describe how this effect was even more dramatic for when more unique slats were added to the design. Using these observations, we describe general best practices for selecting the slat concentration and multi-pot slat addition steps to optimize growth.

4.1 Growth slows when large numbers of unique slats are mixed simultaneously

We realized that the fastest growth is a balance between the concentration of each free slat versus the total concentration of all the slats in the reaction. In Fig. S21, we studied the growth of v16 staggered ribbons versus designs with increasing numbers of unique slats (i.e. decreasing sequence symmetry as shown in Fig. S20). We note that Hamming distances between the different slats are also an important parameter influencing growth, as described in Supplementary Text 7. All the designs with different numbers of unique slats generally had similar Hamming distances (as shown in Fig. S45G–J) so as to not make this a confounding variable.

As expected, the 2x symmetry design with 32 unique slats grew longer per unit of time when 15 nM per slat was added (i.e. 480 nM total slats) versus when 10 nM per slat was added (i.e. 320 nM total slats). Similarly, this also occurred with the 1x symmetry design with 64 unique slats where the 15 nM per slat (i.e. 960 nM total slats) condition grew faster compared to when 5 nM per slat (i.e. 320 nM total slats) was added. However, this relationship of faster growth with higher per slat concentrations was not maintained with the 0.5x symmetry design with 128 unique slats. After 12 hours of growth, there was no measurable assembly with 15 nM per slat (i.e. 1920 nM total slats) versus some measurable assembly when only 2.5 nM or 5 nM per slat (i.e. 320 or 640 nM total slats) was added. While after 38 hours of growth there was some measurable assembly for the 15 nM per slat (i.e. 1920 nM total slats) condition, the ribbons were of comparable length for the 2.5 nM per slat (i.e. 320 nM total slats) condition or even longer for when 5 nM per slat (i.e. 640 nM total slats) was added.

We concluded that although higher concentrations of each slat generally allow for faster growth, there are limits to which trend applies. There is some threshold between 1 and 2 μM where the total concentration of slats seems to cause an impediment to growth. This was further substantiated in Fig. S22, where the relative rate of growth of ribbons (using small 4x symmetry designs with 16 unique slats) was diminished as the total concentration of slats was increased towards 2 μM .

4.2 Growth of finite megastructures with large numbers of unique slats can be accelerated by adding the slats in multiple steps

We predicted that growth of finite megastructures with large numbers of unique slats (e.g. >100) would be slow if all the slats were added simultaneously, because the total concentration of slats would exceed the 1 μM threshold causing growth impediment (see Fig. S21 and explanation in Supplementary Text 4.1). For instance, addition of all slats for the finite 1022-slat sheet at a low concentration of 2 nM per slat would make the total concentration surpass 2 μM . Hence, we considered an alternative approach where we sequentially added the slats in multiple stages to maintain a relatively high per-slat concentration, but without the total slat concentration ever exceeding 1 μM . We note that the initially added seed (and therefore the growing megastructure) is progressively diluted as more slat stages are added, though this was not problematic in this work. Future approaches could attempt to grow megastructures attached to a solid support, enabling circumvention of megastructure dilution.

We initially tested this approach for the elongated 320-slat plus symbol (see Fig. S14). In one approach, we incubated all the slats simultaneously during the initial preparation of the reaction, versus the other approach where half of the total slats (i.e. 160 slats) were added during the initial preparation and incubated for ~38 hours, at which point the remaining 160 slats were added and incubated again for a comparable amount of time. We note that the concentration per slat in the first approach was ~3 nM (i.e. 1000 nM total slats), versus ~5 nM per slat (~800 nM total slats at any given time) in the second approach. We observed that growth using the second approach with multiple slat additions resulted in completed megastructures at an earlier time versus when all the slats were added at once. One explanation of this faster growth with the second approach could be the ~66% higher concentration of a given slat during each stage. Users are advised to keep in mind the observations as explained in Fig. S21 and Supplementary Text 4.1, which suggest that increasing the total slat concentration towards 2 μM would likely impede the growth.

Given all of the above observations, we concluded that growth of the finite megastructures with the largest numbers of unique components should be conducted with the slats being added in multiple stages (see Fig. 2Biii–vi for the final structures, with the different stages shown in Fig. S9C–D and Fig. S10). The

megastructures with the initial set of slats were incubated with 5 nM seed for three days, at which point an aliquot was taken and diluted 2.5x fold into the next series of slats for three more days, with the latter process being repeated five more times until all the slats were added (seed concentration estimated at 50 pM after final dilution). In our implementation, we maintained a concentration per slat for a given stage of ~4–5 nM and ensured that the total concentration of slats did not exceed 1 μ M.

Supplementary Text 5: Detailed characterization of binding handles

To fully characterize how the base-pairing strength of binding handles informs growth and spontaneous nucleation, we studied v16 and v8 ribbons using one of either 6-, 7-, or 8-nt handles at various temperatures. We used the ribbons as a model system for megastructure growth and nucleation because they were easy to identify, had lengths that could be readily measured in low-magnification TEM images, and could be applied to the TEM-grid substrate with high density so as to count many ribbons per image but where the lengths of single particles could still be resolved. All ribbon reactions for assessment of growth versus temperature had 20 nM per slat, 0.5 nM of seed, and 15 mM Mg²⁺. Spontaneous nucleation was quantified by counting ribbons in a control reaction where no seed was added. The following section elaborates and discusses the results from the main text more deeply.

5.1 How the number of binding sites (i.e. v16 or v8) versus temperature influences spontaneous nucleation

To understand how the number and strength of binding sites on the slats inform nucleation and growth, we also tested v8 6-, 7-, and 8-nt ribbons. With fewer binding sites, the v8 designs formed the longest ribbons at lower temperatures where higher spontaneous nucleation was observed. This is evident with the 7-nt design where growth of v16 could be maintained at 31°C, 34°C, 36°C, and 38°C with no observable spontaneous nucleation, versus the v8 design where this could only be maintained at 30.5°C and 32.5°C (Fig. S38, Fig. S39). Similarly, low amounts of spontaneous nucleation (i.e. one order of magnitude greater than the 0.3 pM detection limit) could be maintained at 43.7°C, 47.3°C, and 50.2°C with the v16 8-nt design, versus only over a narrower range (40°C and 42.5°C) with the v8 8-nt design (Fig. S38, Fig. S39). We were not able to observe these differences using the 6-nt binding sites because no spontaneous nucleation was observed at any of the temperatures tested (Fig. S38, Fig. S39). We conclude that the v16 design where more binding sites are used allows growth using a broader window of temperatures where spontaneous nucleation is not observed, which is consistent with prior findings with ssDNA slats³³.

5.2 How the base-pairing strength of the binding site handles versus temperature influences growth rate and spontaneous nucleation

We grew v16 6-, 7-, and 8-nt ribbons with and without the seed for ~16 hours at various isothermal temperatures to determine if fast growth and controlled nucleation could be attained simultaneously (Fig. S38). Additionally, we determined the temperature where grown ribbons melted apart (Fig. S37). We sought to find the breadth of growth temperatures that were below the melting point where no measurable spontaneous nucleation occurred, because the span of this window represents the utility of a particular

length binding site for controlling nucleation of the slats. We can see that the v16 8-nt design is subject to spontaneous nucleation at all temperatures tested (see rightmost Fig. S38A and top panel of Fig. S39). However, no spontaneous nucleation for the v16 6- and 7-nt designs was observed using a large window of temperatures up to $\sim 11^\circ\text{C}$ below the melting temperatures (see left two panels in Fig. S38A and top section of Fig. S39). With the 7-nt design, only minimal spontaneous nucleation that was about an order of magnitude greater than the 0.3 pM detection limit was observed at the lowest 28°C condition tested (middle panel of Fig. S38A). Taken together, we can see that either the 6- or 7-nt binding sites provide leeway with choosing fast assembly conditions that are far below the melting temperature where nucleation is strictly seed dependent. In practice, this window gives the experimentalist freedom to set up origami-megastructure growth reactions at room temperature without the slats becoming aggregated into undesirable byproducts, to be able to accommodate variations in the ion and slat concentrations, and be able to use a breadth of growth temperatures where fast growth and seeded nucleation predominate without significant formation of unseeded byproducts.

In the growth-temperature trials, we also sought to find the “optimal” growth-temperature range where the fastest growth occurred in the window of nucleation control. Temperatures in this window serve as a guideline for reaction conditions that an experimentalist might select for fast, seed-dependent growth. The results are summarized as dark blue bars in the top portion of Fig. S39. We find that the optimal growth temperature ranges were $22.5\text{--}25^\circ\text{C}$, $31\text{--}34^\circ\text{C}$, and $43.7\text{--}47.3^\circ\text{C}$ for the v16 6-, 7-, and 8-nt ribbons, respectively. Thus, each increment of one base pair in the v16 ribbon binding sites increases the optimal temperature range by $\sim 10^\circ\text{C}$. We note that defining exact bounds for an “optimal” temperature range is arbitrary, which would also depend on parameters such as slat and cation concentration.

Supplementary Text 6: Kinetics of ribbon assembly

We determined the kinetics of slat addition by measuring the length of ribbons at different timepoints (see Fig. S40), then converting the length measurements into an estimated number of slat additions, and approximating the second-order rate constant (k_{on}) of assembly by considering the growth as a pseudo-first order phenomenon. The following section explains how these measurements were determined, our assumptions, and how the base-pairing strength of the binding site influences these rates.

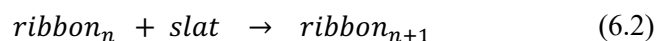
6.1 Calculation of the number of slats added to the ribbon

We assume that each 6HB slat on the v16 staggered ribbons extends the ribbon roughly by ~ 10.1 nm, as explained in Fig. S19C. Hence, the number of slats in a ribbon is given by equation 6.1.

$$\text{number of slats} = \frac{(\text{nm length})}{10.1 \text{ nm slat}^{-1}} \quad (6.1)$$

6.2 Approximation of growth using pseudo-first order kinetics

We consider that growth of an n length ribbon with an additional slat proceeds as a second-order reaction:



The starting concentration of $n = 0$ length ribbons is equal to the concentration of the seed, and the slats were in huge excess with respect to the seed (i.e. 40-fold excess, or ~ 20 nM of each slat and 0.5 nM seed in experiments where ribbon lengths were measured versus time; see Fig. S40). Because of these excesses, the relative concentration of slats does not change appreciably during the early growth times, and we may thus model this reaction as a pseudo-first order phenomenon. It follows that the k_{on} second-order rate constant may be computed as below. In equation 6.3, the length of the ribbons was divided by two to account for how the ribbons grow bidirectionally from the seed.

$$k_{on} = \frac{(\text{nm length})}{2} \frac{1 \text{ slat}}{10.1 \text{ nm}} \frac{1}{[\text{concentration per slat in}]} \quad (6.3)$$

One reasonable criticism of this model would be that the relative concentration of the slats might be depleted after long growth times, to the extent that the pseudo-first order simplification would no longer apply. We note that the ribbon designs tested in Fig. S40 uses 4x sequence symmetry (also see Fig. S20 for explanation of symmetry) and were thus composed of 16 unique periodic slats with 20 nM of each slat. If we imagine that every one of the seeds added triggers growth of a ribbon, then complete depletion of the slats would net ribbons that are each $\sim 6.5 \mu\text{m}$ long. By examination of the data in Fig. S40i, we can see that the mean length of ribbons at the longest time points approach or exceed this $\sim 6.5 \mu\text{m}$ threshold. It follows that slat depletion effects are significant at the longest time points and this might explain the gradual decline of the apparent second-order k_{on} values versus time (as shown in Fig. S40ii). Nonetheless, the pseudo-first order assumptions should explain the length of the much shorter ribbons, such as after one hour of growth.

6.3 How the base-pairing strength of the binding-site handles influences growth rate

The rate of ribbon growth was increasingly faster as the strength of the binding sites were increased from 6, to 7, and to 8 nt. This is shown in Fig. S40 where the length of v16 ribbons was compared at different time intervals using a growth temperature where little to no spontaneous nucleation was observed. The mean lengths for the ribbons after 1 hour of growth were ~ 1 , ~ 1.3 , and $\sim 3.1 \mu\text{m}$ for the v16 6-, 7-, and 8-nt designs, respectively, as shown in Fig. S40Ai, Bi, and Ci. After 16 hours of growth, these increased to ~ 4.2 , ~ 4.9 , and $\sim 8.1 \mu\text{m}$ for the v16 6-, 7-, and 8-nt designs, respectively. This suggests surprisingly fast kinetics for addition of the 6HB slats—converting the mean length of the ribbons (as explained in Supplementary Text 5.1) after 1 hour of growth gives the observed second-order rate constants for growth of $\sim 0.66 \cdot 10^6$, $\sim 0.86 \cdot 10^6$, and $\sim 2.13 \cdot 10^6 \text{ M}^{-1}\text{s}^{-1}$ for the 6-, 7-, and 8-nt ribbons respectfully, as shown in Fig. S40Aii, Bii, and Cii. After 16 hours of growth, the observed second-order rate constants for growth were $\sim 0.18 \cdot 10^6$, $\sim 0.21 \cdot 10^6$, and $\sim 0.35 \cdot 10^6 \text{ M}^{-1}\text{s}^{-1}$ for the 6-, 7-, and 8-nt ribbons. We attribute this decrease in the apparent rate constants over time to accumulation of errors on the slats on a growing ribbon end that might slow further growth, and lack of consideration of depletion of slats in the calculation. As with any folded DNA origami, there is only some probability (e.g. perhaps ~ 80 – 90% per handle) that a 3' handle sequence is available on a 6HB or 12HB slat. A multitude of errors on a ribbon end might temporarily stall or entirely stop the addition of more slats.

Supplementary Text 7: Sequence assignment to megastructures from the 2048-handle sequence library, optimization of the Hamming distances of slats within megastructure designs

The megastructure designs were implemented from the 2048-sequence library by randomly assigning one of the 32 possible handle sequences to each of the intersections in the interface between the perpendicular layers of slats, as explained in Method 2. In the initial explorations with periodic v16 7-nt ribbons as shown in Fig. 3Ai, we discovered that particular random assignments of sequences sometimes resulted in drastic growth differences. We realized that certain designs that grew less prolifically had particular pairs of perpendicular slats where a multitude of complementary handles were matching and aligned to one another. We hypothesized this unintentional alignment of complementary handles caused the formation of kinetic traps with pairs of slats undesirably bound to one another (see Fig. S41). We designated the maximum number of matches between some pair of slats in a megastructure design as having a kinetic trap of k strength. For example, a design with a maximum kinetic trap $k6$ has one or more pairs of slats where the two slats may be aligned with six complementary binding handles engaged together. We quantified this design property of the random sequence assignments for megastructures by measuring Hamming distances between each of the slats in one layer with each of the slats in the other perpendicular layer. This section explains the initial findings with periodic ribbons that suggest the need to maximize Hamming distances (also see Fig. S42), results showing a mechanism for how single kinetic traps in a pair of slats influences ribbon growth (also see Fig. S43), and the Hamming distances of the megastructure designs as implemented in this paper (also see Fig. S44–Fig. S45).

7.1 Increased pairwise complementarity between slats (i.e. minimized Hamming distances) causes drastic slowdown of 1D ribbon growth

We generated random permutations from the strand library of v16 ribbons and selected designs where the minimum Hamming was marginally increased (see Fig. S42A). The designs tested had distributions of slat pairs where there were maximally 6 and 8 complementary binding sites aligning between them (i.e. $k6$ and $k8$ strength kinetic traps, respectively). The length of ribbons as measured by TEM after overnight growth of the $k6$ and $k8$ designs at various temperatures is plotted in Fig. S42B. There was no appreciable growth of the $k8$ ribbons at any of the temperatures tested, versus the $k6$ ribbons which grew prolifically at all the temperatures. Examples of the differences between growth versus no growth for the $k6$ and $k8$ designs are shown in low-magnification TEM images in Fig. S42C–Di. Closer inspection revealed infrequent short, stubby $k8$ ribbons in select higher-magnification images, but their relative number was too few to

quantitatively compare to the $k6$ counterpart (see Fig. S42Dii). To rationalize these extreme growth differences, we considered the Hamming distances in the $k8$ design more closely. We realized that of the total eight top and eight bottom slats in the design, five of the slats from either layer had eight complementary binding sites that could align with one another as a $k8$ strength kinetic trap. We hypothesized that these unintentional “strong” $k8$ interactions between over half of the total slats among themselves prevented the slats from readily being recruited to the ribbons. Regardless of the cause of the varied growth, these results suggested that avoiding low Hamming distances between the slats is important to achieve the best possible growth of a megastructure.

7.2 Possible mechanism for how complementarity between the slats causes growth slowdown

To test our hypothesis that alignment of complementary handles between slat pairs causes the formation of kinetic traps that prevent the slats from freely being added to megastructures, we tested growth of several ribbon designs where we incremented the strength of a kinetic trap between a single pair of slats (see Fig. S43A). The mean length of the ribbons at different temperatures versus the single $k8$, $k10$, and $k12$ traps are shown in Fig. S43B–C, versus a $k6$ control. The ribbons were progressively shorter at all temperatures versus the $k6$ control as the strength of a single kinetic trap k was incremented from $k8$ to $k10$ to $k12$. We also found periodic defects in the $k10$ and $k12$ ribbons with every eighth slat in a particular layer that was frequently missing in close-up images of ribbon segments (see Fig. S43Diii–iv). We note that the designs tested here use 4x sequence symmetry with eight repeating top-slats and eight repeating bottom-slats, such that a particular missing slat in each layer would appear at such intervals (for details regarding symmetry see Fig. S20). The observation of both slower overall growth and missing single slats with the strongest kinetic traps support the mechanism that low Hamming distances cause kinetic trapping of slats that impede their addition to a megastructure. Different segments of other ribbons with the $k10$ and $k12$ traps were observed to have the full set of periodic slats without the missing slat, suggesting that the trapped slat pairs could eventually be added. We suspect ribbon growth where a slat pair is strongly trapped becomes temporarily stalled because it is often missing from the growing ribbon edge. The missing trapped slats are added at a slower rate compared to other free slats and are perhaps skipped and added to the completed segments of ribbon later in time. Henceforth, we concluded that the Hamming distances between slats should be maximized to the greatest extent possible to limit kinetic trapping to best allow free slats to be added to megastructures.

7.3 Discussion of the Hamming distances used in the finite and periodic megastructure designs

For the optimized finite and periodic designs, the multiplicity for each possible number of matching, complementary handles for the slats from one layer with respect to the other layer of slats are shown in Fig. S44–Fig. S45. The largest finite designs in Fig. S44D–F maximally had $k8$ kinetic traps, with the smaller finite designs having weaker traps as the number of slats in the design was lessened. In general, the maximal traps were larger for designs with more unique slats because there are more possible interactions between the various slats. For instance, the 64-slat square had maximally five undesired complementary binding sites between slats (i.e. a $k5$ -strength kinetic trap) versus the 1022-slat sheet which had maximally eight undesired complementary binding sites (i.e. a $k8$ -strength kinetic trap), as shown in Fig. S44A versus Fig. S44F.

We note that the results in Fig. S42 showed that ribbon designs with $k8$ traps either struggled or were incapable of appreciably growing into ribbons, which suggest that the designs in Fig. S44D–F should not be viable for growth. However, we hypothesized that the multi-step addition of slats for the finite designs with the largest numbers of slats (as per Method 10) would have resulted in particular slats being at a different concentrations compared to other diluted slats from prior stages. That is, the growth hindrance resulting from particular kinetic traps could have been lessened because of the differing stoichiometric amounts of particular slats. We also hypothesize that a few isolated “strong” $k8$ kinetic traps in the largest finite designs would be less deleterious to growth compared to a periodic design with a similar-strength trap. With the finite design of unique slats, a single pair of trapped slats would only be skipped once (and perhaps slowly added at some later time), versus periodic designs where skipping of the trapped slat would be encountered repeatedly.

The periodic ribbon designs used to study the nucleation and growth behavior of the origami megastructures were generated from permutations from 256 different 6-, 7-, or 8-nt handles using a 512-strand library, and had maximally $k4$ -strength kinetic traps (see Fig. S45A–B). Other periodic designs that were generated from the 32 different 7-nt handles using the 2048-strand library all had maximally $k6$ -strength kinetic traps (see Fig. S45C–J). We attribute these differences between the maximum-strength kinetic traps to the differences in the number of different handle sequences with each of the different strand libraries.

Supplementary Text 8: Potential applications

We expect the earliest applications will accrue from the ability to construct megastructures with similar functional complexity as a single DNA origami, but simply spanning length scales that are 1–2 orders of magnitude larger.

1. Addressable megastructures could enable positioning of multiple 100 nm+ nanoparticles needed for creation of digital metamaterials that could manipulate visible light⁵⁴, and that could be scaled to high copy number through self-assembly. By contrast, individual DNA origami are too small to organize a large number of nanoparticles in this size range.

2. Artificial cell-surface mimics that span the micrometer length scale could allow investigation of how spatial organization of ligand-receptor pairs on those length scales can dictate cell-cell communication. Some exploration of this issue has been carried out by the laboratory of Jay Groves, using micropatterned surfaces⁵⁵. Crisscross addressable megastructures substantially add to this toolbox by offering much finer pixel pitch for addressing functionalities to a surface, in addition to all the other versatile functional potentials of DNA nanostructures. Furthermore, crisscross addressable megastructures are self-assembled, therefore could be scaled to high copy numbers, and potentially could interact with cells in suspension.

3. Harnesses that are large enough to cup a biological cell could impart polarization on those cells, and thereby enable novel strategies for self-assembly of such cells into artificial tissues, or else to self-assemble micron-scale colloidal particles into larger collections for photonics and other applications. An example of this strategy as applied to imparting addressability to large nanoparticles was reported by Ben Zion et al.⁵⁶ In this case, a construct composed of three DNA origami was used. A crisscross megastructure could be used to impart addressability to a much larger surface area (e.g. surface of a microparticle or biological cell). A large enough crisscross megastructure could directly coordinate the organization of more than a pair of cells.

4. The large size of megastructures enables one to use diffraction-limited optical microscopy to resolve the orientation of those megastructures, instead of requiring more constrained or expensive imaging modalities (e.g. atomic-force microscopy is slow, electron microscopy is limited to samples that are stained or cryopreserved). In this way, research with DNA megastructures can be more accessible than that with individual DNA origami, through reduced barriers to effective imaging.

The more profound advantages may accrue in the longer-term from the ability to construct megastructures with thousands of times the number of functional features as compared to a single DNA origami. This will enable a new dimension of experimental access to two powerful, overlapping metaphors: “wet molecular robots” that are as programmable and sophisticated as macroscale robots, but that can operate on molecules and cells and can be produced in massive copy numbers through self-assembly; “artificial cells” that approach the sophistication of biological cells, but that may operate using very different organizational paradigms, e.g. optionality of membranes; DNA-based artificial cytoskeletons; powered by cycling external fields in addition to or exclusive of chemical fuels, etc. The ability to scaffold arrangements of large numbers of molecular machines on length scales up to 1–10 μm could enable booting up artificial cells to initial conditions (i.e. xyz positions of each agent) that may be difficult to achieve otherwise.

For example, DNA origami have been investigated as breadboards for strand-displacement circuits⁵⁷; localization enables faster computation and increased insulation/modularity. Therefore it is plausible that molecular breadboards supporting thousands to millions of addressable circuit elements may provide a path to more complex and sophisticated wet molecular computation, much as the increase in complexity of integrated circuits has been the key to massive expansion in processing power in the computer industry. Furthermore, large breadboards could support not just a large number of circuit elements that communicate to nearby neighbors, but also nanoscale conveyor belts that could actively shuttle material over micron-scale distances.

Oftentimes cost can be an important consideration for how widely applicable a method can be.

(i) However, there are no other methods known at present, expensive or otherwise, for creating addressable micron-scale megastructures such as what we have demonstrated, i.e. there are no “simpler and easier production methods” currently available. There are methods for assembling periodic megastructures with single-origami unit cells, however these lack the unique addressability that is the key enabling feature of our megastructures.

(ii) Costs in principle could be managed through sharing and collaboration between multiple research groups. The cost of an acoustic liquid handler is comparable to that for a low-end transmission electron microscope, or an atomic-force microscope. Many individual research groups in the nanoscience community have been able to adapt to these instrumental needs by subscribing to institutional core facilities and paying an hourly fee (not inexpensive, but often the only viable option). The cost for the 2048-strand library reported here, which is analogous to printer ink in that it can be used to generate hundreds of distinct

megastructures before being depleted, is around USD\$10k. This material cost would become comparable to other consumable costs in cases where several research groups could collaborate on splitting the costs; ideally state-funded foundries or else commercial entities could offer a form of effective cost sharing in this way. Furthermore, through such collaborative efforts, strand pools could be created in bulk and then aliquoted for distribution to individual laboratories; this would greatly reduce the number of strand transfers that need to be done by a single laboratory. Even for a single laboratory, USD\$10k is not automatically an unthinkable cost, considering that the cost for supporting salary and fringe for a single postdoctoral fellow can be up to an order of magnitude larger figure per year.

(iii) As described above, micron-scale DNA megastructures can be designed with features that can be resolved by diffraction-limited optical microscopy. Thus our method could lower the cost for doing research with DNA nanostructures, through bypassing the need for an electron microscope or atomic-force microscope.

Supplementary Figures Fig. S1–Fig. S45

Fig. S1–Fig. S8: Slat and seed design and folding, qualitative energetics of crisscross assembly, selection of initial binding-site strength, energies of various binding-handle sets, and need for T-linkers

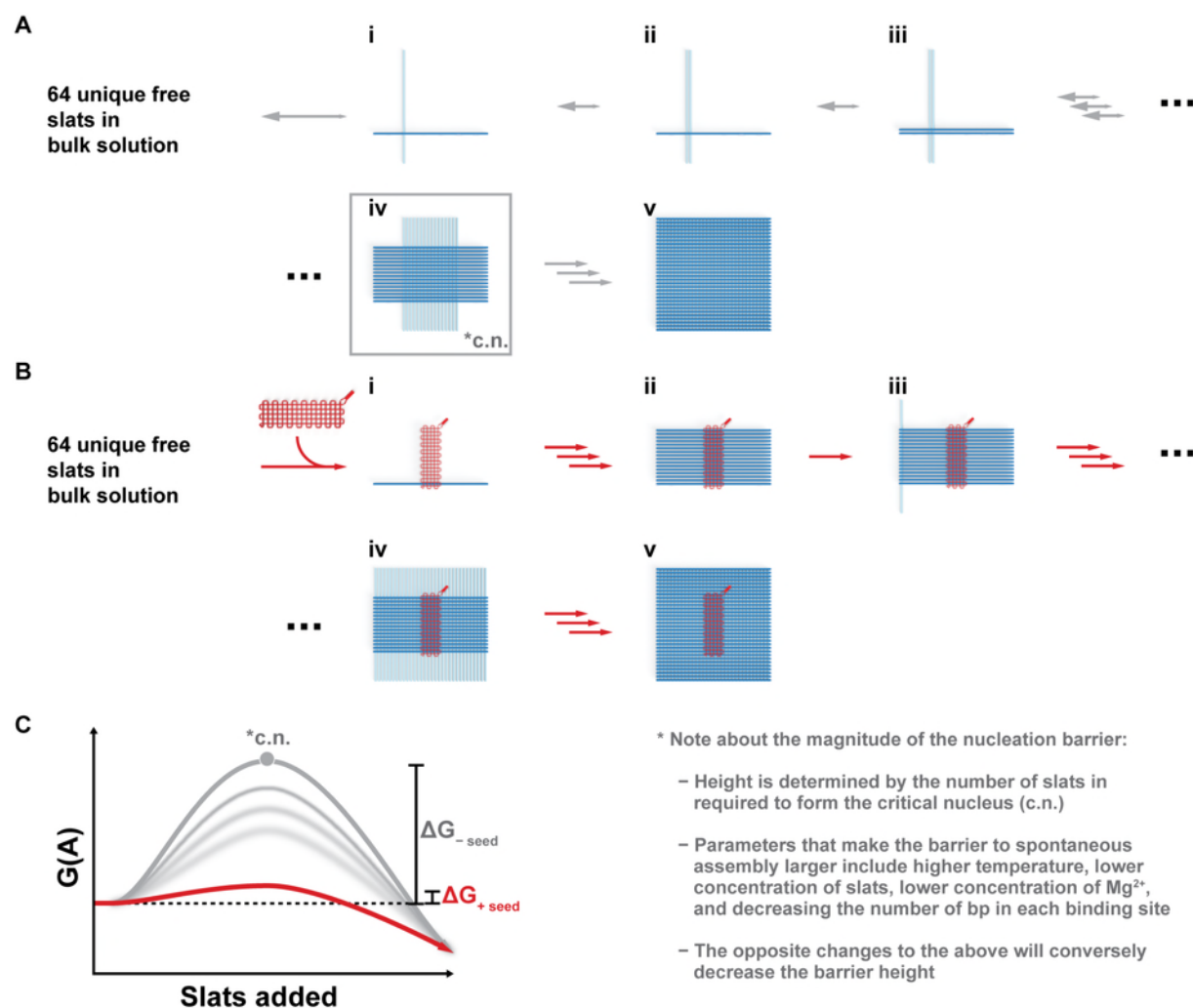


Figure S1 Qualitative energy landscape of the nucleation barrier in crisscross assembly for the 64 6HB slat finite megastructure. This figure elaborates on the energetic pathways introduced in Fig. 1C. **A** shows unseeded assembly of the slats when no seed is added to the reaction. Single pairwise interactions between slats are weak and transient, with the reverse reaction of slat dissociation favored over forward assembly, as shown in *Ai–iii*. Stable addition of slats does not occur until the formation of the metastable critical nucleus (c.n.) in *Aiv*. Once the critical nucleus forms, the remaining slats may readily bind to the critical nucleus to complete the megastructure as in *Av*. **B** shows assembly when the seed is added to the reaction.

Each of 16 cells in the seed have binding sites that strongly engage one 6HB slat, as shown in *Bi-ii*. Steps *Biii-v* with the remaining slats (e.g. 48 slats as shown here) bypasses the critical-nucleation pathway, because the parallel 16 slats in *Bii* stably localize columns of weak binding in close proximity. In the experimental assembly, we incubate the reactions initially for 4 hours at a higher temperature that does not let the reaction proceed past *Bii*. Next, the reaction is incubated at a lower temperature that favors binding of the remaining slats with weak binding sites, as in *Biii-v*. These two possible assembly pathways are qualitatively plotted, as shown in C. The various experimental and design parameters that influence the magnitude of the energy barrier to spontaneous assembly are described in the notes on the right.

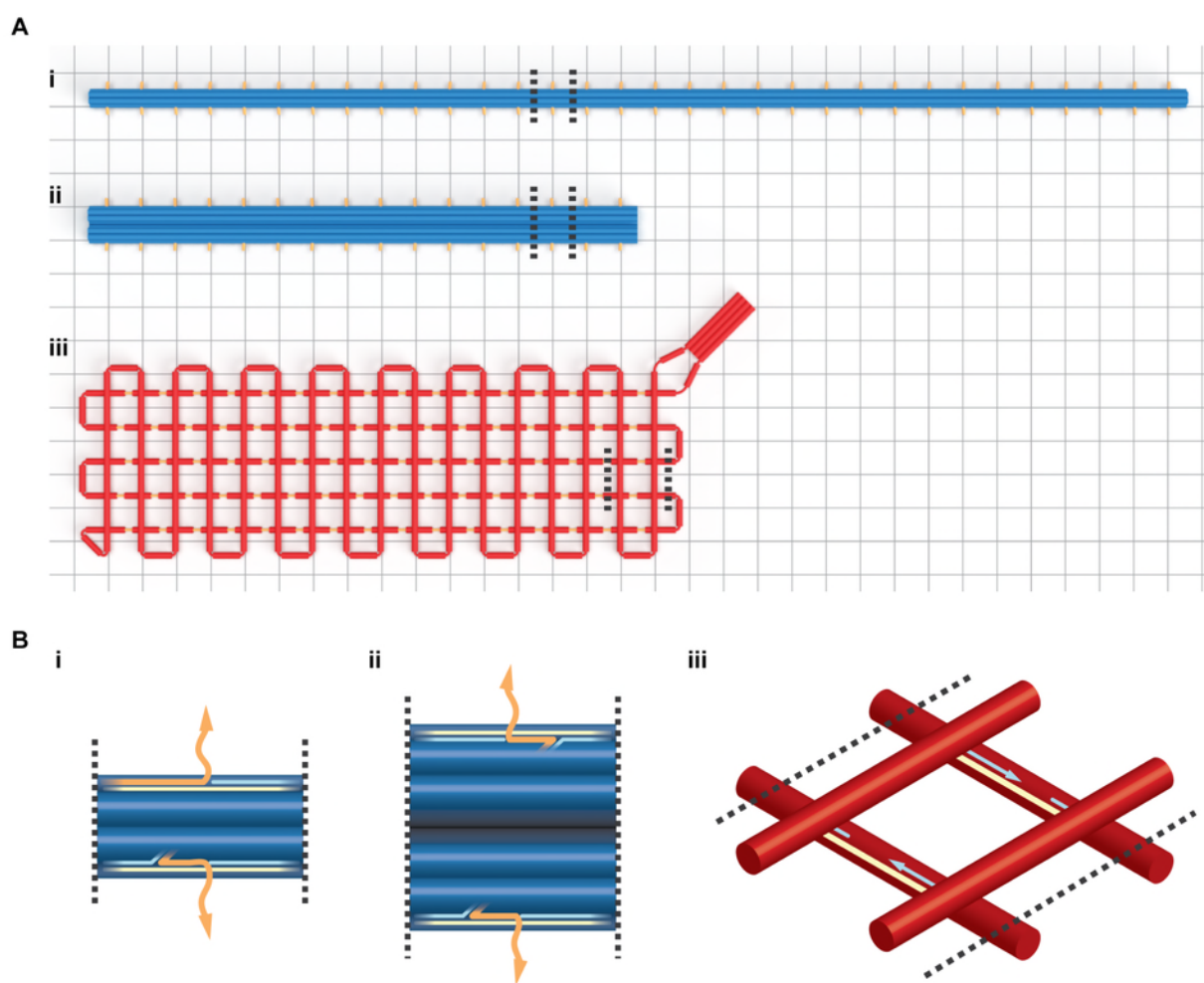


Figure S2 Large renderings of designs for the 6HB slat, 12HB slat, and gridiron seed. Panel A shows the overall structure of each origami component, with the background grid representing 42 bp. The orange ssDNA sites along the top and bottom of each slat are the nodes which may be arbitrarily addressed with cargos as modifications to a staple will allow. In particular, we used these nodes for weak handles to bind

the slats to other slats, for strong 10-nt handles to bind the slats to the sockets on the seed, for strong 16-nt handles to bind DNA nanocubes (see Fig. S28), or as 3' biotin sites to bind DNA megastructures to substrates for DNA-PAINT imaging. The orange notches in the seed in *Aiii* are exposed 10-nt regions of scaffold which serve as “sockets” to strongly bind slats via complementary “plug” handles. The seed has 16 columns as oriented, where five horizontal helices (i.e. five sockets) in each column may cooperatively engage a single slat with five strong 10-nt handles. The black lines indicate the region shown more closely in panel **B**, where the orange line represents the staple strands for addressable nodes on a slat, light yellow lines represent the scaffold strand, and cyan lines as other core staple stands.

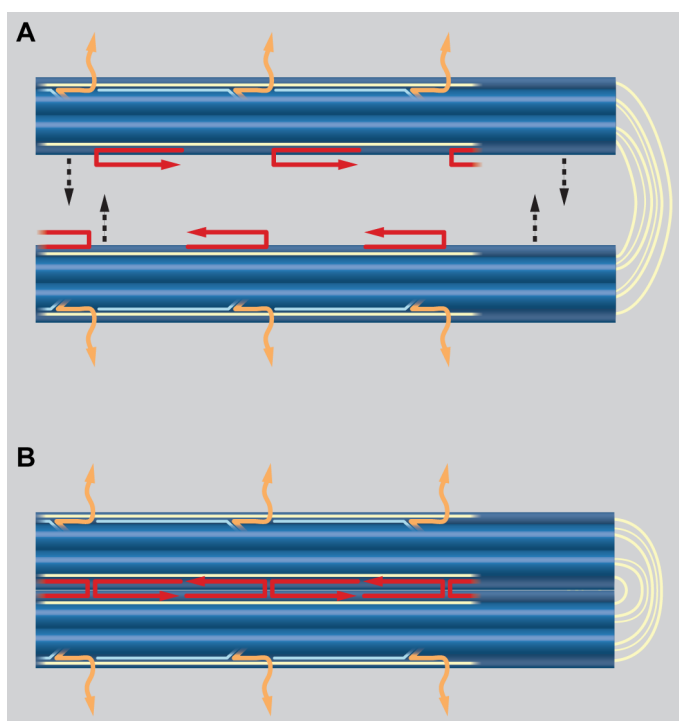


Figure S3 Strategy in which the 6HB slat folds back upon itself to make a half-length 12HB slat. Extreme right in panel **A** shows a region of light yellow scaffold that was left as ssDNA without any staple strands. This region acts as a hinge to allow the 6HB to fold back into a 12HB, using the red staple strands to bridge opposite ends of the top helix together. Panel **B** shows a segment of completed 12HB that was properly folded back. This scaffold routing allows us to use the same base staple sequences (i.e. the orange staple strands) for the 12HB as is used with the 6HB, so that the same 2048 7-nt strand library can be applied to either slat. The consequence of this design on the final slat

yield is explained in Supplementary Text 2 and shown in Fig. S4.

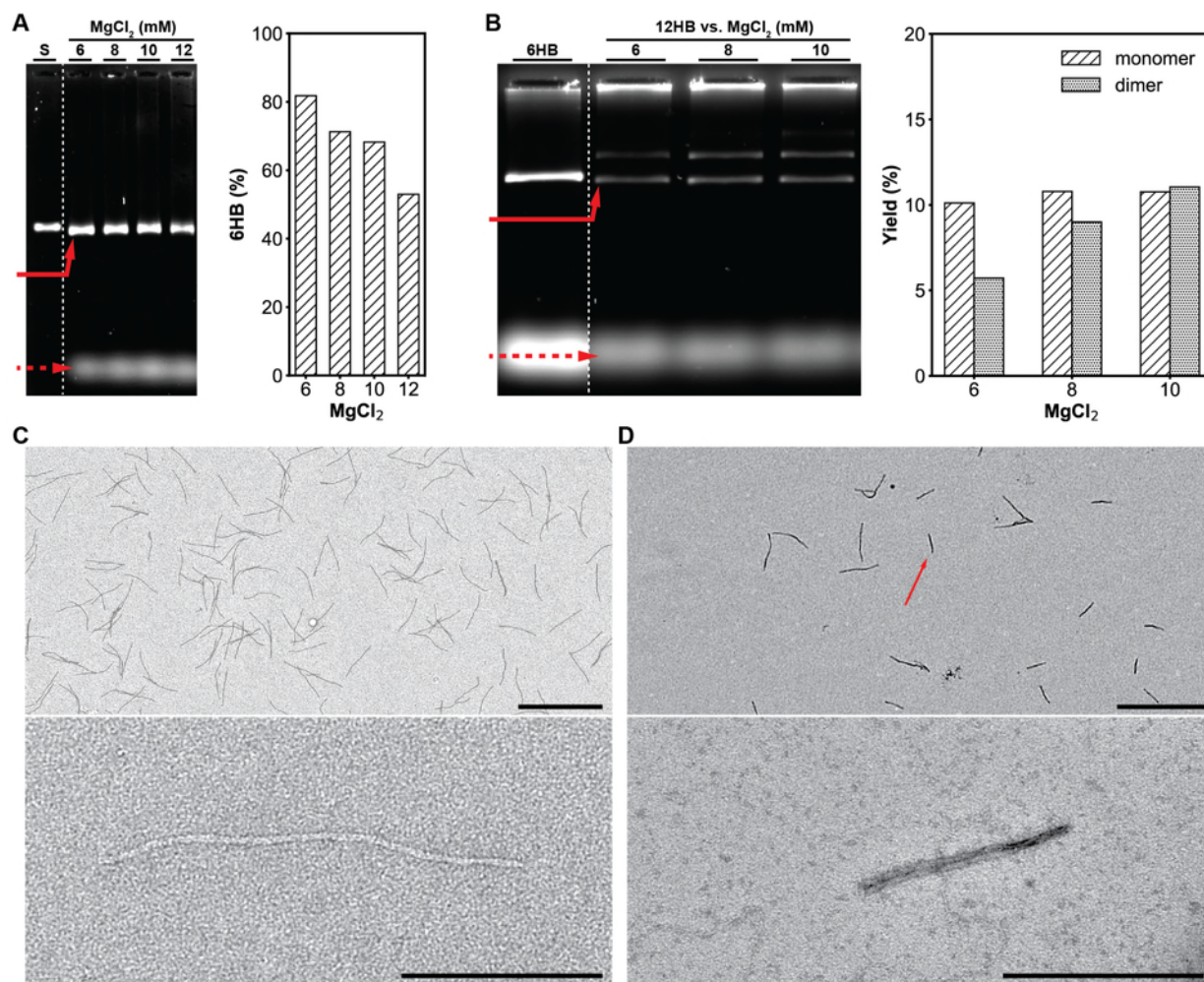


Figure S4 Folding of the DNA-origami 6HB and 12HB slats. Leftmost **A** and **B** show agarose gels to optimize MgCl₂ for folding of the 6HB and 12HB slats respectively, with the solid red arrow pointing to the slats and the dashed arrow pointing to excess staple strands. Control lanes (S) is the scaffold only for the 6HB in **A**, versus a 6HB reference for the 12HB in **B**. The folding yields were determined in the rightmost of **A** and **B** using densitometry of the agarose gel, where the intensity of the desired slat band was compared to the overall intensity of all the elements that migrated slower than the staple band. Roughly 80% yield for 6HB slats was obtained in the 6 mM MgCl₂ condition, versus 10% yield for monomeric 12HB slats in the 8 mM MgCl₂ condition. See Supplementary Text 1 for further explanation of the differences between these slats. TEM images of the raw, folded 6HB and 12HB slats are shown in **C** and **D**, respectively. Only the monomeric 6HB is observed, versus the 12HB where there is a mixture of the desired 12HB monomer (as shown with the red arrow) and an undesired double length 12HB dimer. Scale bars are 1 μ m and 200 nm in the top and lower images of **C** and **D**, respectively.

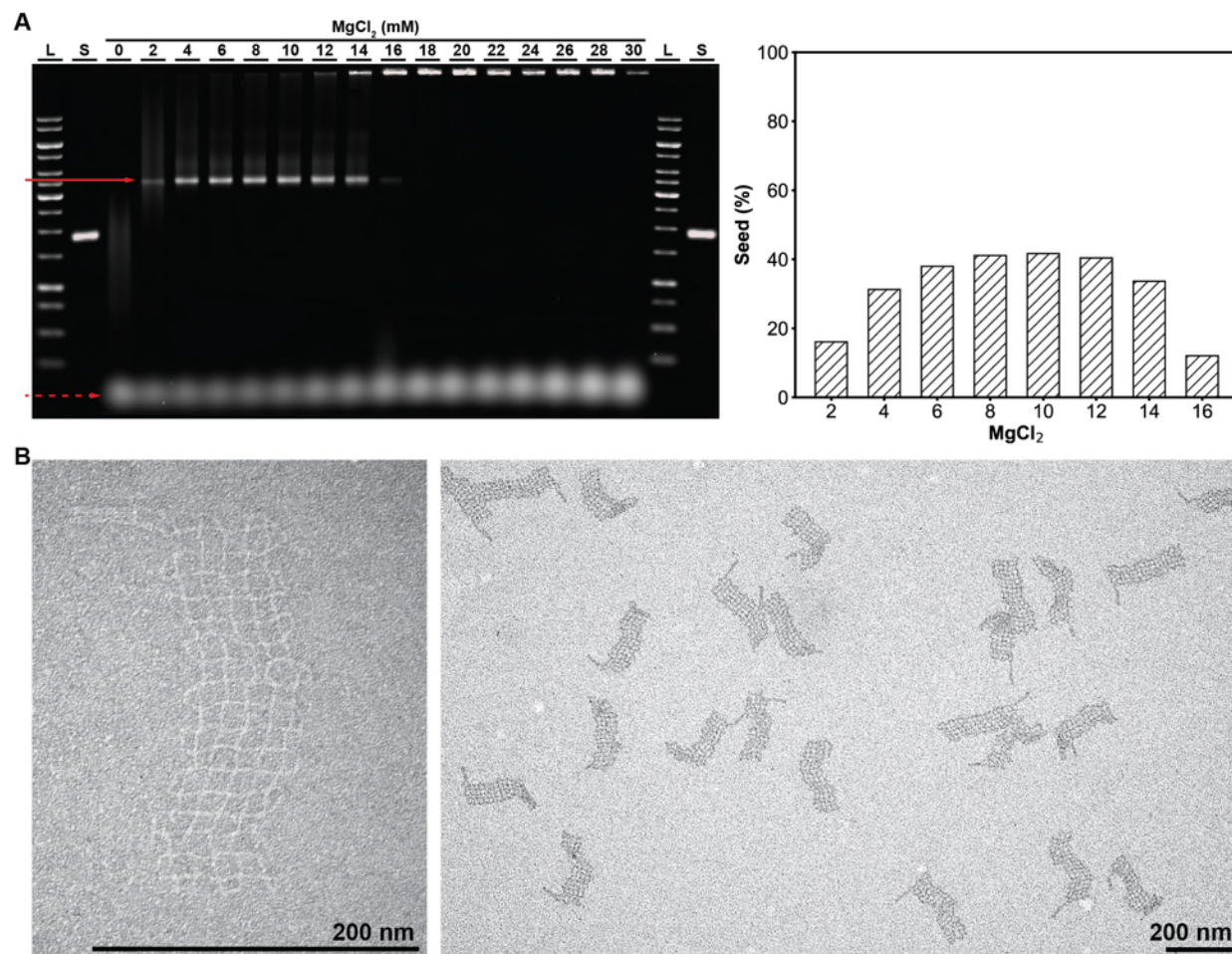


Figure S5 Folding of the gridiron DNA-origami seed. Leftmost **A** shows an agarose gel to optimize MgCl_2 for folding of the seed, with the solid red arrow pointing to the seed band and the dashed arrow pointing to the staple strands. Lanes (L) indicate ladder and (S) indicate scaffold only. The folding yields were determined in rightmost **A** using densitometry of the agarose gel, where the intensity of the seed band was compared to the overall intensity of the elements that migrated slower than the staple band. Roughly 40% of seed monomer was obtained for the 8 mM and 10 mM MgCl_2 conditions, which we deemed to be the folding conditions with the highest yield. **B** shows TEM images of negatively (left) and positively (right) uranyl-formate-stained gridiron seeds. We note that only a single design seed with the same scaffold register was used for all the megastructures in this work, such that the socket sequences needed for each structure were universal. Scale bars are 200 nm.

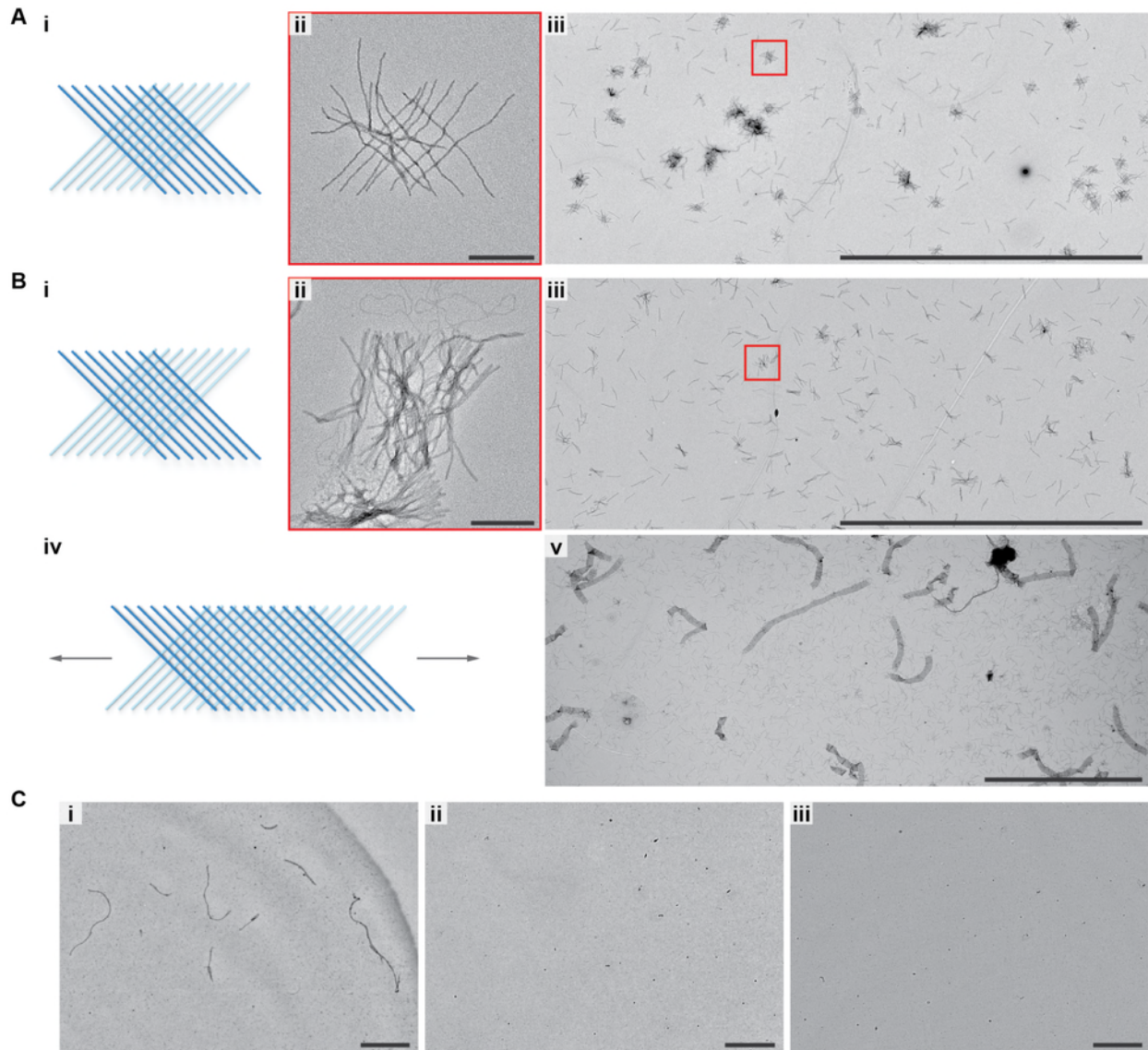


Figure S6 Qualitative assessment of unseeded spontaneous nucleation of 10-, 9-, 8-, 7-, and 6-nt binding sites for crisscross assembly. Binding-site designs where nucleation of assemblies was observed using typical conditions that might be encountered in routine experimental procedures were determined not suitable for seeded nucleation control. **A** shows that 10-nt binding sites had prolific error-prone assembly of the finite 16-slat assembly (*Ai*), as shown by TEM (*Aii-iii*). Similarly, spontaneous assembly of something assumed to be some portion of the 16-slat test structure was also observed with 9-nt binding sites, in **Bi-iii**. Structures similar to the closeup from panel *ii* are highlighted in red in panel *iii*. In **Biv-v**, the propensity of spontaneous nucleation with the 9-nt design was further shown using a v8 ribbon design. As such, we further tested v8 ribbons using 8-, 7-, and 6-nt binding sites, in **Ci-iii** respectively. Prolific ribbon growth occurred using the 8-nt design. However, it was not observed for either the 7- or 6-nt designs such that we concluded either these strength binding sites would be suitable for seeded nucleation control

of the origami slats. Assembly of the 16-slat test structure was for 16 hours at 25°C in 10 mM MgCl₂ using 2 nM of each slat, and assembly of the v8 ribbons was for 16 hours at 32.5°C in 15 mM MgCl₂ using either ~6.6 nM or 20 nM (in *Biv-v* and *C*, respectively) of each slat. Scale bars are 200 nm in *Aii* and *Bii*, and 10 μm in all other images.

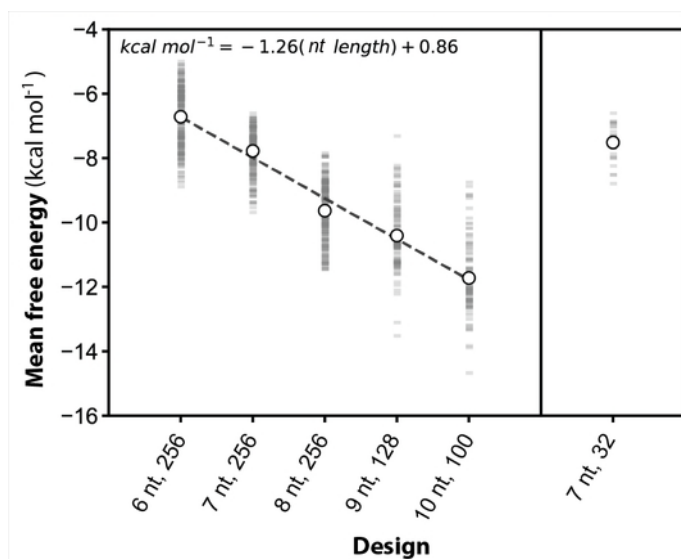


Figure S7 Calculated mean free energy of the sequence handles versus their base-pair length, as determined in NUPACK 3.0⁵². More negative free energy indicates a stronger interaction. Each faint gray bar plotted is the energy of a single handle, with the circular data points indicating the mean energy of the library tested. The 6-, 7-, and 8-nt sequences were selected as described in Supplementary Text 3. The 256-sequence set was used to characterize growth and nucleation of origami megastructures as

described in Supplementary Text 4, and the rightward 7-nt 32-sequence set was used for the 2048-strand library to create a diversity of megastructures. The strongest 9-nt 128-sequence and 10-nt 100-sequence sets were used only for initial testing of sequence-handle length (see Fig. S6). For the leftward sequences, a linear fit suggests that each single-nt increment of the handle increases the binding energy by -1.26 kcal mol⁻¹.

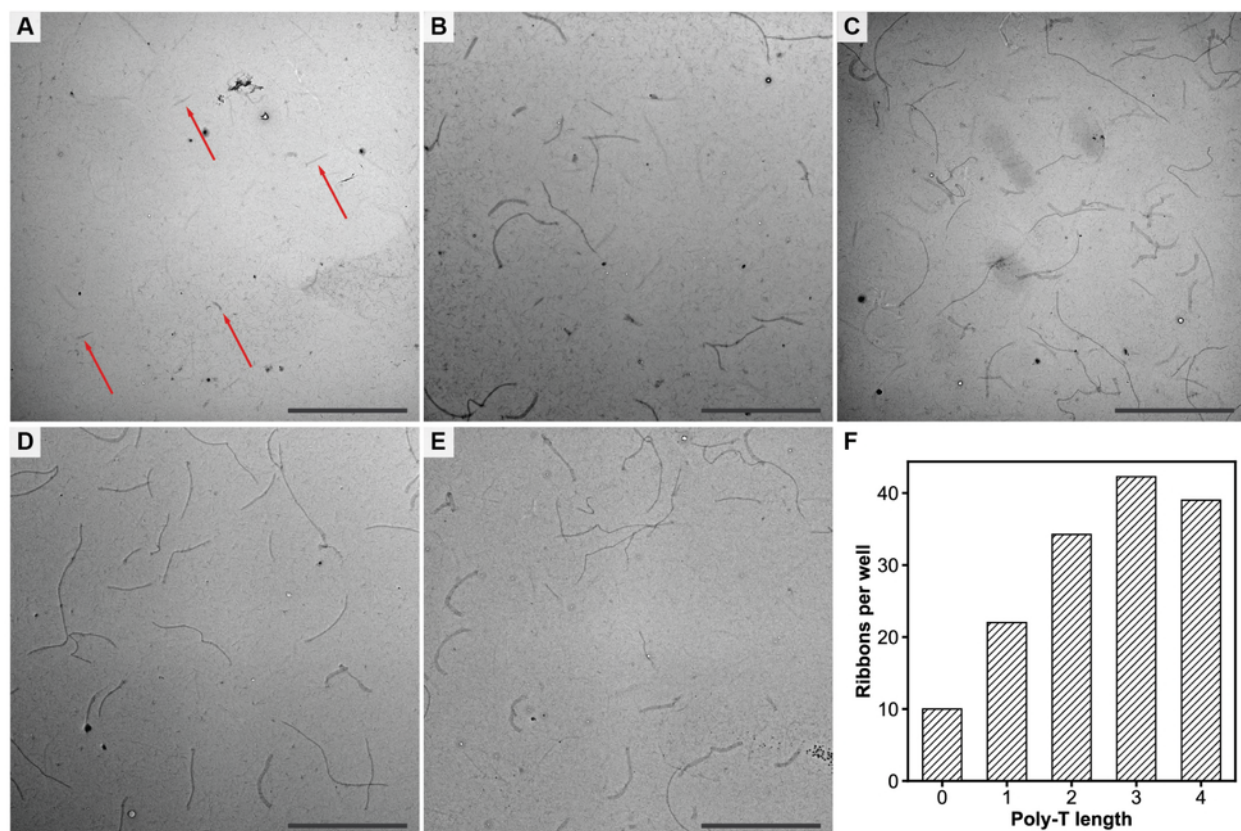


Figure S8 Addition of a poly-T-linker before the binding sites is necessary for allowing assembly of megastructures from DNA-origami slats. The relative number of seeded v8 8-nt ribbons as counted on TEM grids was increased if a 1T, 2T, 3T, or 4T linker was used to separate the handle from the core staple sequence versus if no linker was used. Representative TEM images for the 0–4T linkers are in panels A–E respectively, with the average number of ribbons counted per defined imaging area plotted in F. The red arrows in panel A point to the stubby ribbons that were much shorter compared to the longer ribbons that formed when a linker was used. This observation may be due to relaxation of electrostatic repulsion of the slats that would otherwise impede megastructure assembly. The relative difference in the number of ribbons counted was similar for 2T, 3T, and 4T linkers. We therefore decided to use 2T linkers for the 8-, 7-, and 6-nt handle designs, as shown in Fig. 1Di. We further note that the 9- and 10-nt binding sites as tested in Fig. S6A–B did not use any T-linker, though were still able to nucleate prolifically into unseeded crisscross test structures. We conclude that T-linkers are necessary to allow the assembly of DNA-origami megastructures using weak binding sites that are less than or equal to 8 nt. This observation does not seem to hold true for when stronger handles are used, though we did not study this phenomenon with such designs. Scale bars are 10 μm . $N = 3$ images were counted for the 0T design, and $N = 4$ images were counted for all the other designs.

Fig. S9–Fig. S15: Models of finite megastructures, preparation time for each design, and additional TEM results of finite megastructures

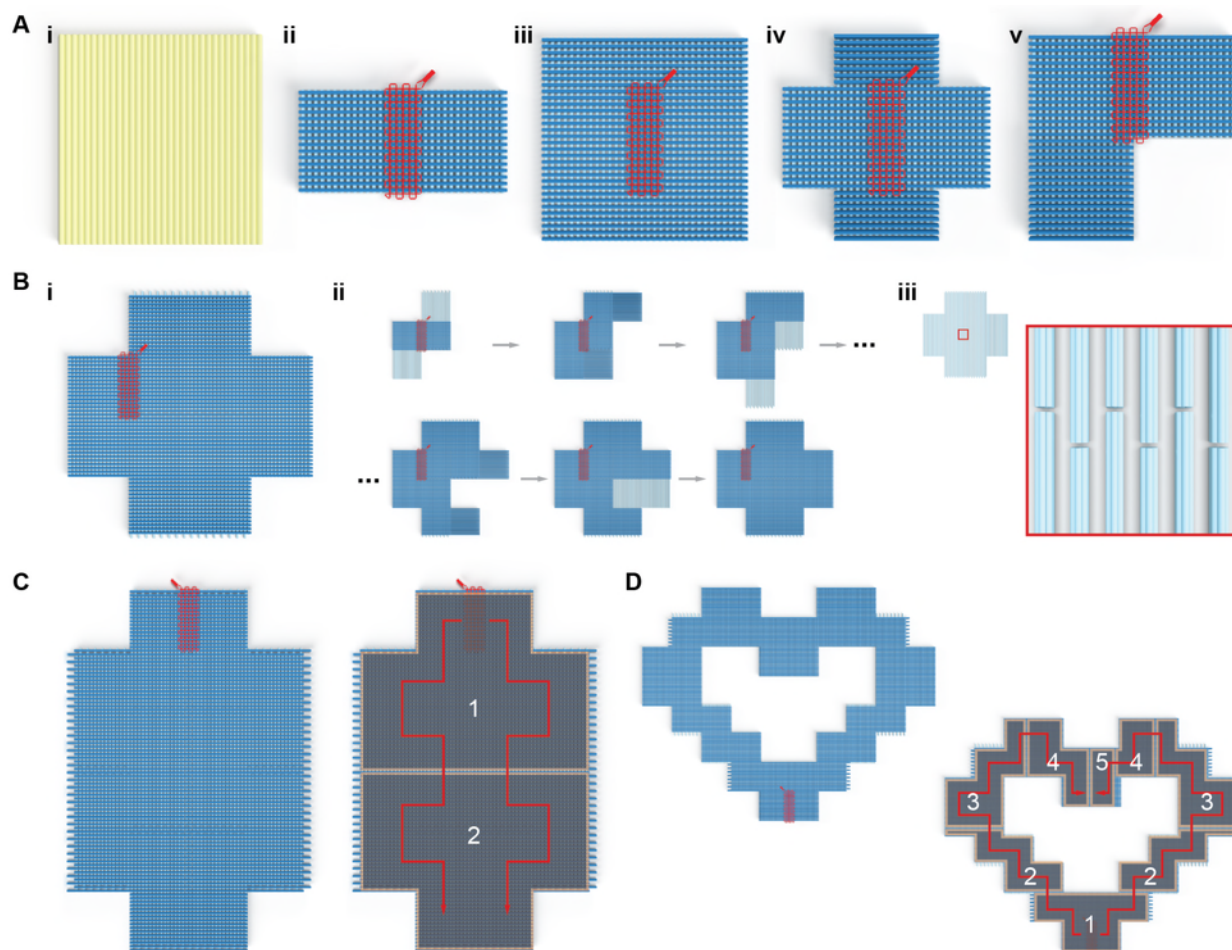


Figure S9 Enlarged design renders of the various finite origamis and megastructures from Fig. 1C. **Ai** is a single-layer flat-sheet DNA origami that is folded from the same scaffold that is used to make the slats, **Aii** is a 48-slat rectangle composed of 16 6HBs and 32 12HBs, **Aiii** is a 64-slat square composed of entirely 6HBs, **Aiv** is a 64-slat plus symbol composed of 32 6HBs and 32 12HBs, and **Av** is a 64-slat L symbol composed of 32 6HBs and 32 12HBs. Panel **Bi** is a larger 191-slat plus symbol composed entirely of 6HBs, with various steps in its raster-fill growth in **Bii**, and **Biii** showing how the bottom-most vertical cyan slats were staggered to seal the middlemost horizontal seam. Such seams exist between the abutting edges of each ribbon-like section of the megastructure. The slats in one or both of the two layers can be staggered, such as done with the finite megastructures in *C–D* and Fig. S10, and the ribbon in Fig. 3iii. **C** leftward is the 320-slat elongated plus symbol. **D** leftward is the 568-slat heart. Rightward panels in **C** and **D** show the raster-fill growth as a red line, with the darkened overlays showing each of the distinct stages where up to

200 slats were added. The megastructures were incubated for about three days of isothermal growth before additional slats for the next stage were added. Images are not drawn to scale.

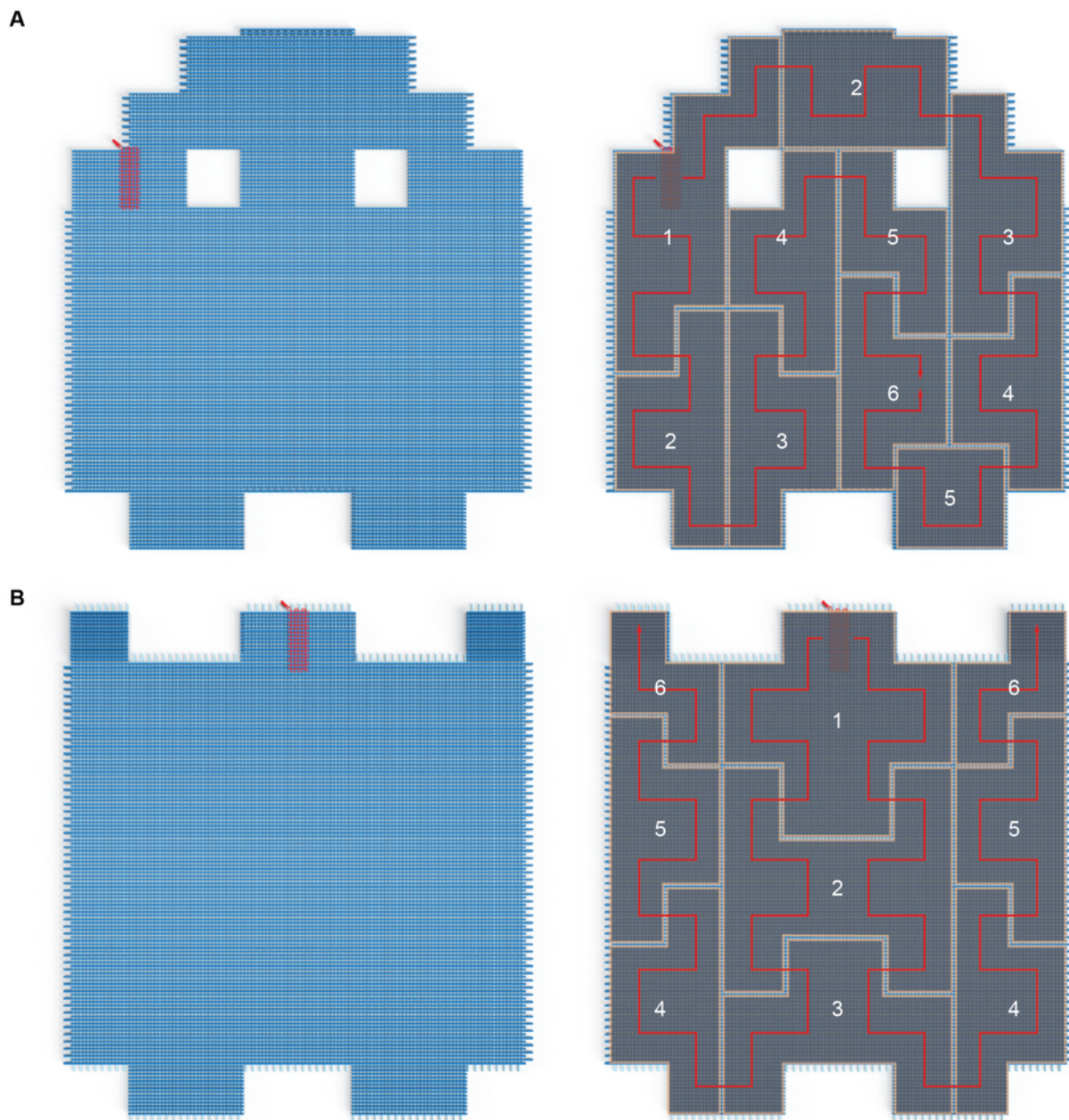


Figure S10 Enlarged renders of the largest designs in Fig. 1C. **A** leftward is the 968-slat ghost and **B** leftward is the 1022-slat sheet. Rightward panels in *A* and *B* show the raster-fill growth as a red line, with the darkened overlays showing each of the distinct stages where up to 200 slats were added. The megastructures were incubated for about three days of isothermal growth before additional slats for the next stage were added. Images are not drawn to scale.

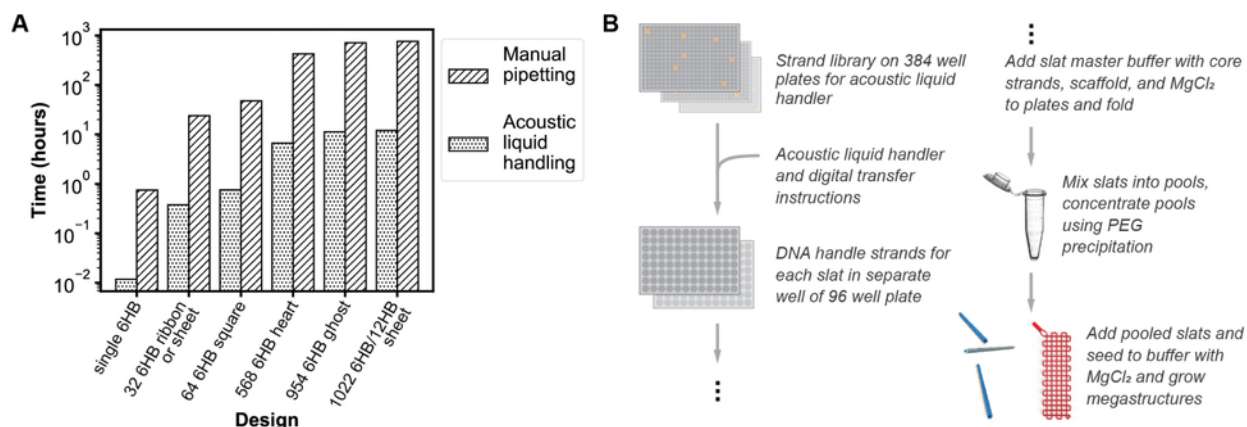


Figure S11 General workflow to assemble DNA megastructures from slats. **A** shows approximate time to mix DNA handle strands for various crisscross megastructures from the 2048-strand library using an automated Labcyte Echo acoustic liquid handler versus a single-channel manual pipette. We determined an average transfer time of 42 seconds per strand using a manual pipette versus 0.66 seconds per strand using the liquid handler, as extrapolated using each method. These timings allow for preparations including manual loading of plates into the liquid handler, manual application of seals to the plates after automated strand transfer, and limited break times for the user. It would be untenable to make the largest megastructures from the strand library using a manual pipette. For instance, the 1022-slat finite sheet requires over 65,000 total strand transfers from the library and would require about one month of manual pipetting versus ~12 hours using the acoustic liquid handler. We note that the need for the acoustic liquid handler could be circumvented by purchasing the strands needed to make the slats for a given design arranged in an order where they could be manually combined using a multichannel pipette. However, this latter approach would not be amenable to having the strands readily rearranged into different crisscross megastructures. **B** shows the workflow for how megastructures are experimentally implemented from the strand library.

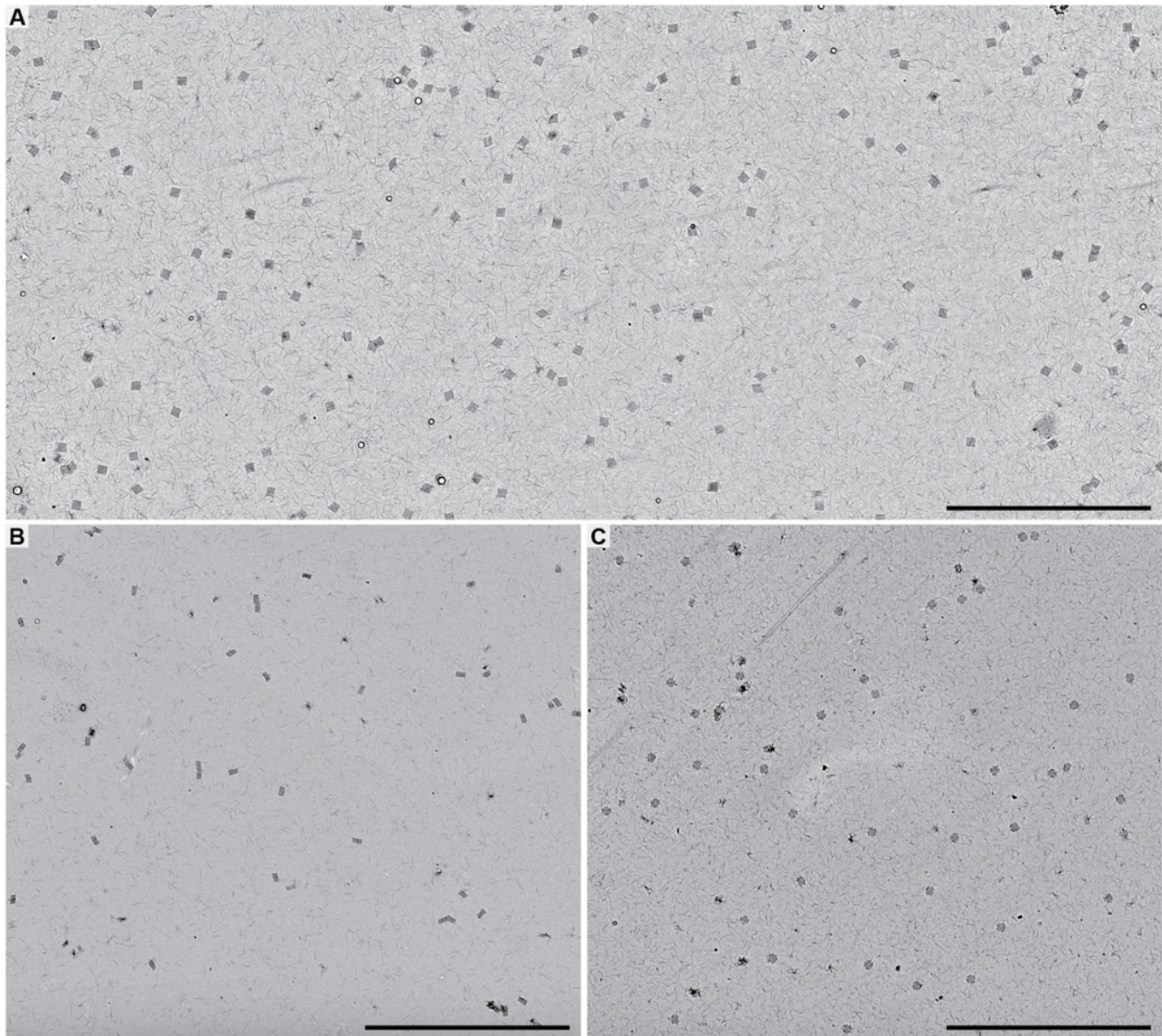


Figure S12 Low-magnification TEM images of small finite shapes showing that they assemble as dispersed, single particles. **A** is the 64-slat square assembled with 6 nM seed (also see design in Fig. S9Aiii), **B** is the 48-slat square assembled with 1.5 nM seed (also see design in Fig. S9Aii), and **C** is the 64-slat plus symbol assembled with 6 nM seed (also see design in Fig. S9Aiv). Scale bars are 10 μm .

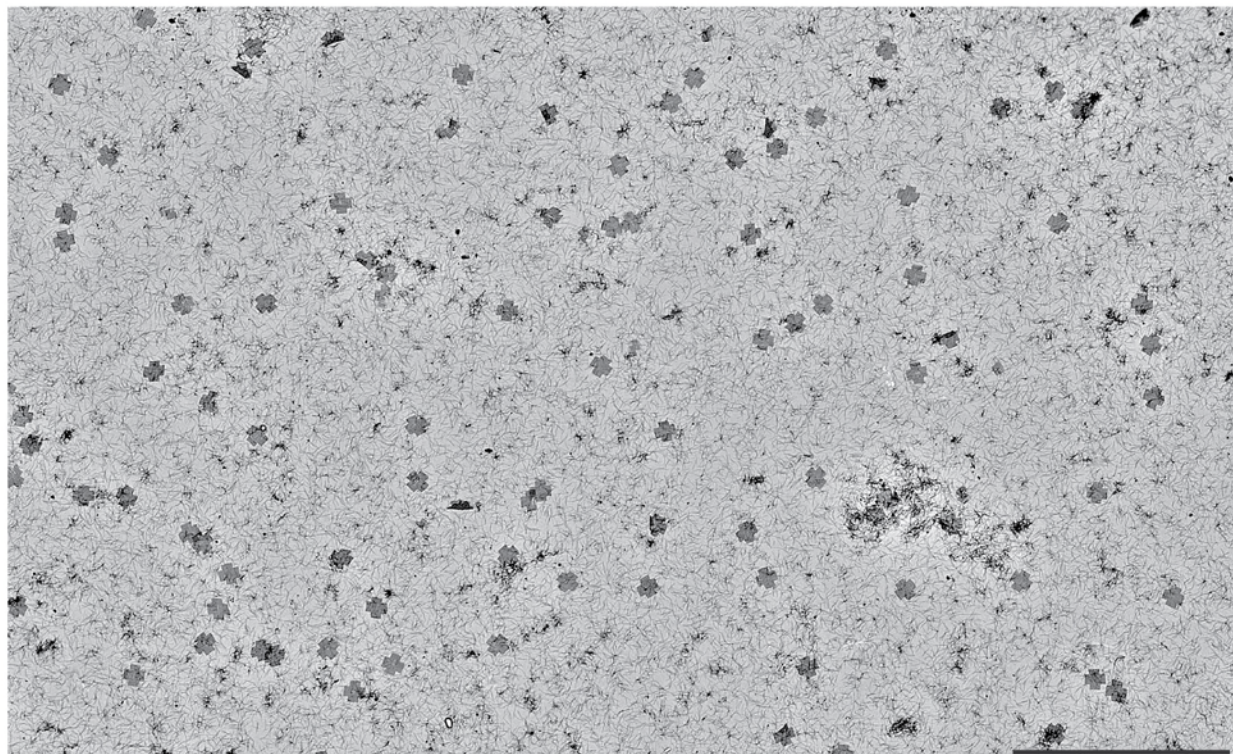


Figure S13 Low-magnification TEM image of the rastering 191-slat plus symbol showing that it assembles as dispersed, single particles, with all slats added simultaneously to the reaction mixture. The raw assembly reaction used 1 nM seed with all the slats added simultaneously and a total isothermal incubation time of ~1.5 weeks. We note that ~3 days was a more typical incubation time for this number of slats, and the longer incubation time may explain why almost all the structures above have gone to completion. An aliquot of the final reaction was concentrated (and also to remove some of the excess slats) by centrifugation about 25-fold, so that it could be imaged with a higher density of particles as above. The scale bar is 10 μm .

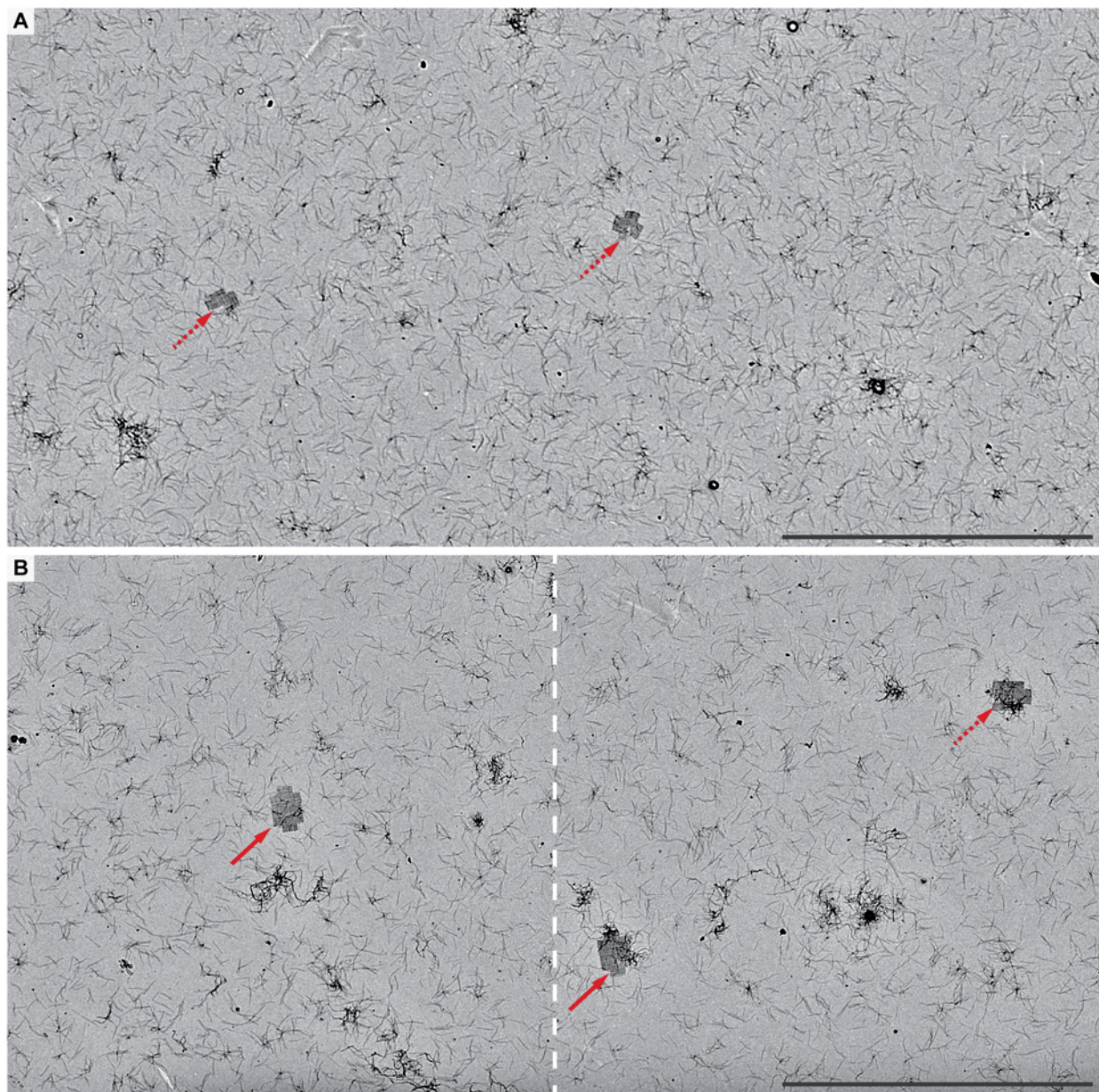


Figure S14 Low-magnification TEM images of the finite elongated 320-slat plus symbol after 90 hours of isothermal growth. Solid-red versus dotted-red arrows show complete and incomplete assemblies respectively. In **A**, all 320 slats were simultaneously added during the initial preparation of the reaction, versus **B** where half of the total slats (i.e. 160 slats) were added during the initial preparation. After 38 hours of growth, the remaining 160 slats were added to the reaction in **B**. The completed shape was not observed after 90 hours using approach **A**, versus **B** where it was frequently observed. We note that the concentration per slat in **A** was ~ 3 nM, versus ~ 5 nM per slat in **B**. This was selected so as to ensure that the total slat concentration did not exceed ~ 1 μ M, because extremely high concentrations of slats tended to impede growth as explained in Supplementary Text 4 and Fig. S21. Scale bars are 10 μ m.

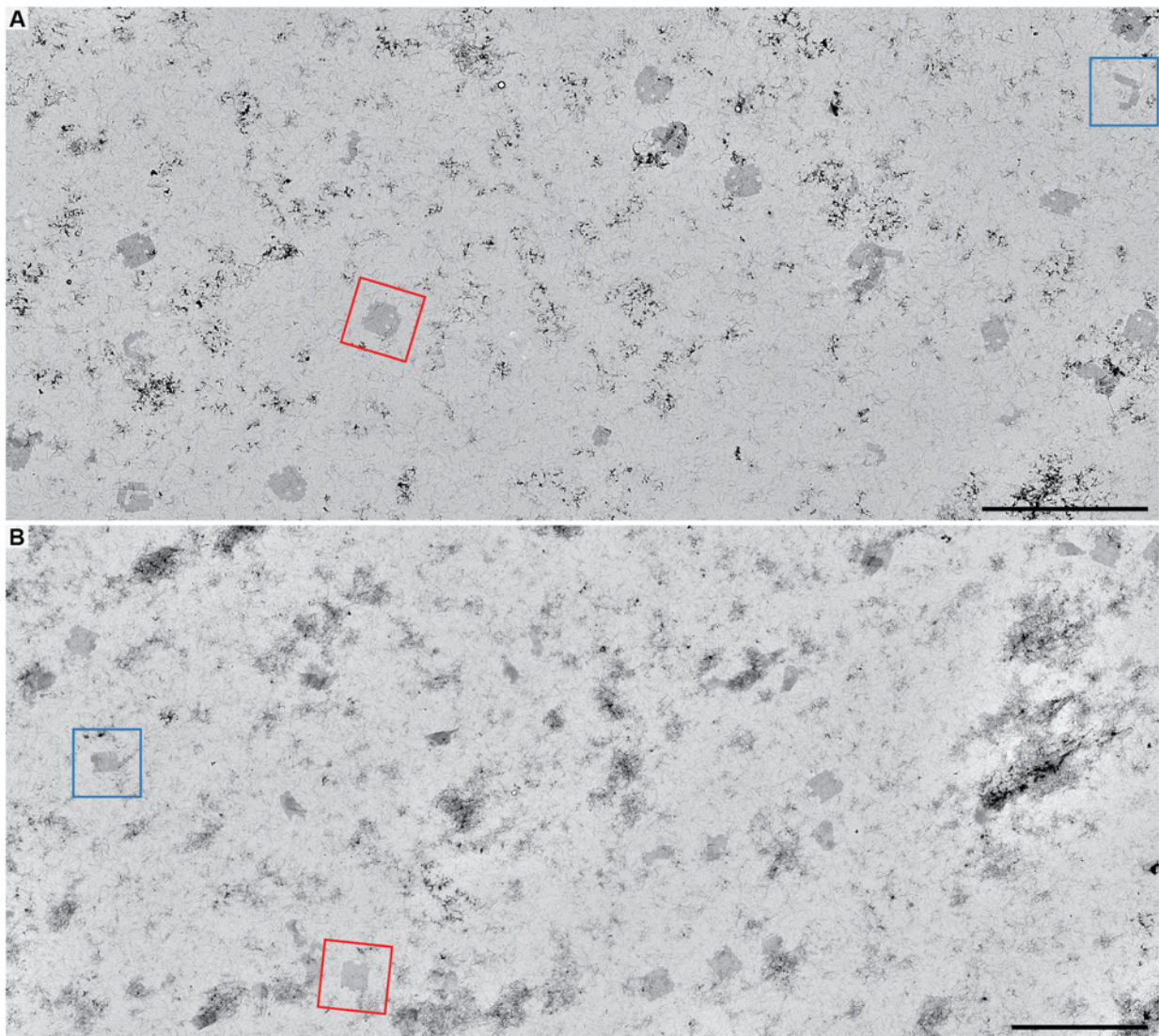


Figure S15 Low-magnification TEM images of the largest finite 954-slat ghost (A) and 1022-slat sheet (B) to assess their relative completion. Completion of the megastructure was deemed all the corners and middle sections of the shape appropriately filled with slats. Examples in red boxes were deemed complete, versus examples in blue boxes were deemed incomplete. Roughly 22.5% of each of the above megastructures were complete by the end of the last stage of assembly. We made the assumption that incomplete structures at the end of a given assembly stage would not be able to continue growth once additional slats were added for the next stage of assembly. This assumes that partially formed structures at the end of a growth period are stalled/trapped because they have accumulated too many defective slats (e.g. those with missing or truncated handles). We considered that by adding more slats for the next growth stage, we would dilute out the remaining free slats needed to recover growth of a given stalled stage, to the extent that recovery would

be exceedingly slow. We postulated that the probability for any given growth stage to go to completion could be treated as the probability of a series of independent events, suggesting that over 75% of the assemblies at each stage were complete and suitable for continuing growth (i.e. $0.225^{1/6}$, as per six distinct stages of assembly). The multi-stage addition of slats is described in Method 10. $N = 225$ seeded particles were counted for the 954-slat ghost, and $N = 267$ particles were counted for the 1022-slat sheet. Scale bars are $10\ \mu\text{m}$.

Fig. S16–Fig. S27: Models of periodic megastructures, growth comparison of different ribbon designs, relationship between growth rate and number of unique slats, and additional TEM results of periodic megastructures

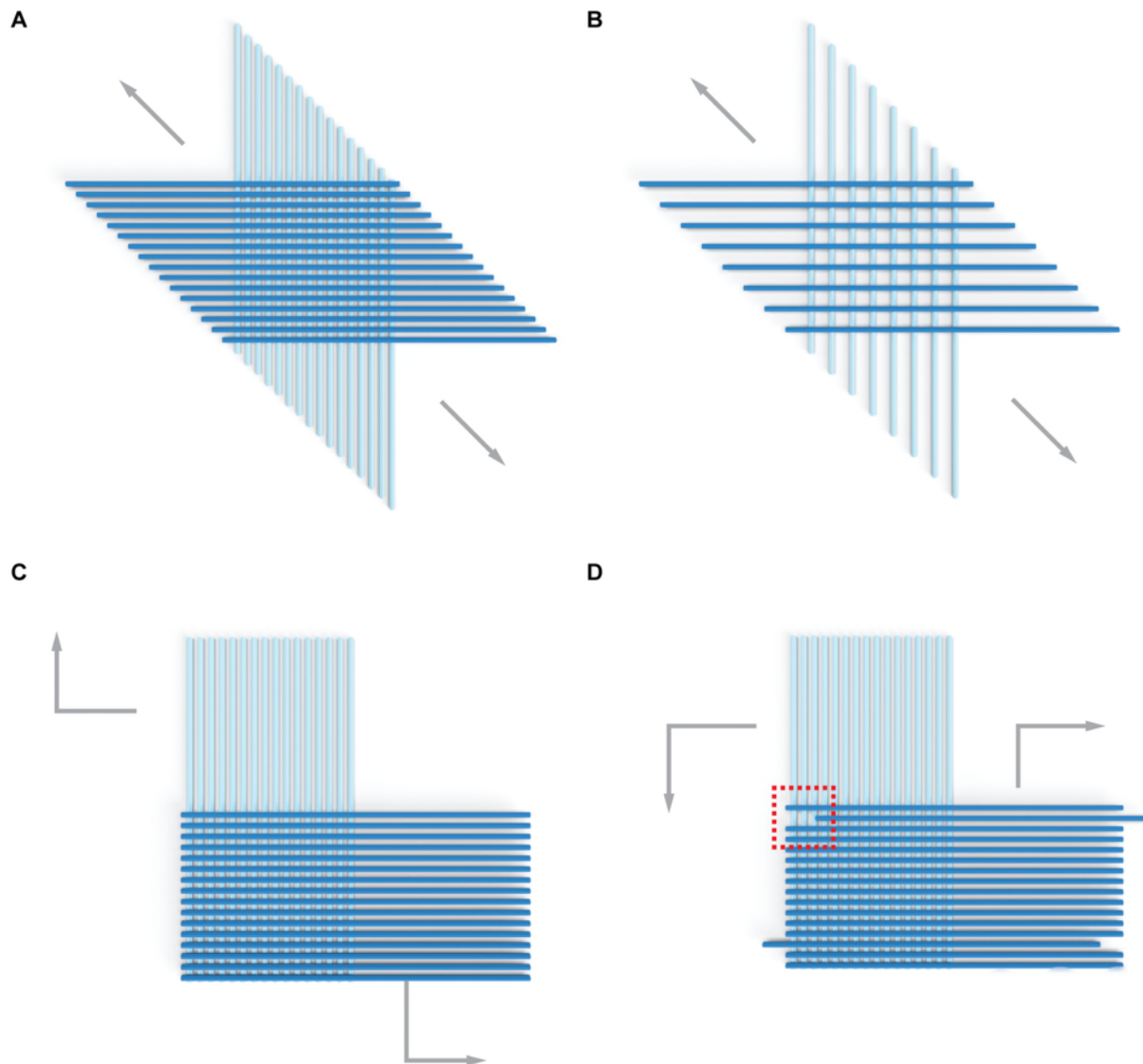


Figure S16 Renders of the ribbon designs shown in Fig. 3. Slats are oriented parallel/perpendicular to the edges of the page to show differences in the staggering of the slats added to the ribbon. In **A** and **B**, each slat added staggers one and two 42-bp spacings respectively, compared to the parallel slat that preceded it. (note: such ribbons within the supplement are defined as the “staggered” designs). The v16 ribbon in **A** is differentiated from v8 ribbon in **B** by the maximum number of binding sites that an incoming slat may make with perpendicular slats on the growing ribbon front (i.e. 16 versus 8 binding sites). In the completed v16 ribbon, a given slat has 32 perpendicular slats bound to all of its 32 possible binding handles, versus v8

which only has 16 slats bound to every other of its 32 possible binding sites. Assuming the binding energy per binding site is the same, the greater number of binding sites allow the v16 designs to be grown under more stringent reaction conditions (e.g. higher temperatures) where the rate of spontaneous nucleation is lower. The differences in nucleation performance are experimentally explained in Supplementary Text 4.1 and Fig. S38, and the energetic models explaining these differences are as discussed previously²⁶. **C** and **D** are v16 ribbons where each slat added does not stagger compared to either immediate parallel slat, creating “zig-zag” ribbons with jagged and flush edges. In **D**, two of the horizontal top blue slats were each staggered by two 42-bp units (as boxed in red) to seal the vertical seams (note: such ribbons within the supplement are defined as the “non-staggered” designs).

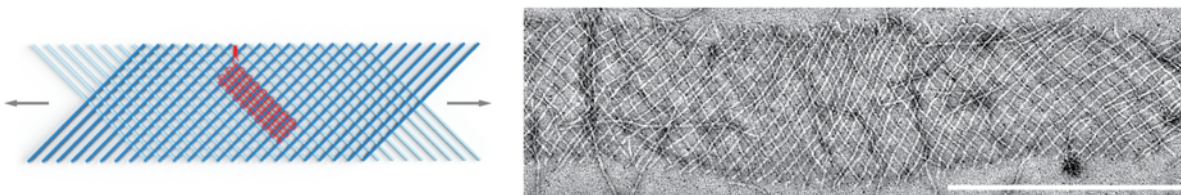


Figure S17 Design and testing of the periodic v8 ribbon. The v8 design uses every other binding site on the 6HB slat, with 16 slats bound to every other of the 32 possible binding sites. There is half the density of slats compared to its v16 counterpart. As such, the v8 ribbons were flexible and had a propensity to stretch and elongate compared to v16 ribbons which remained straighter and flatter (also see Fig. S18B versus Fig. S18A). The close-up rightward negative-stain TEM image shows a flat segment of ribbon, with the inherent flexibility causing the curving, meandering ribbon edge. The scale bar is 500 nm.

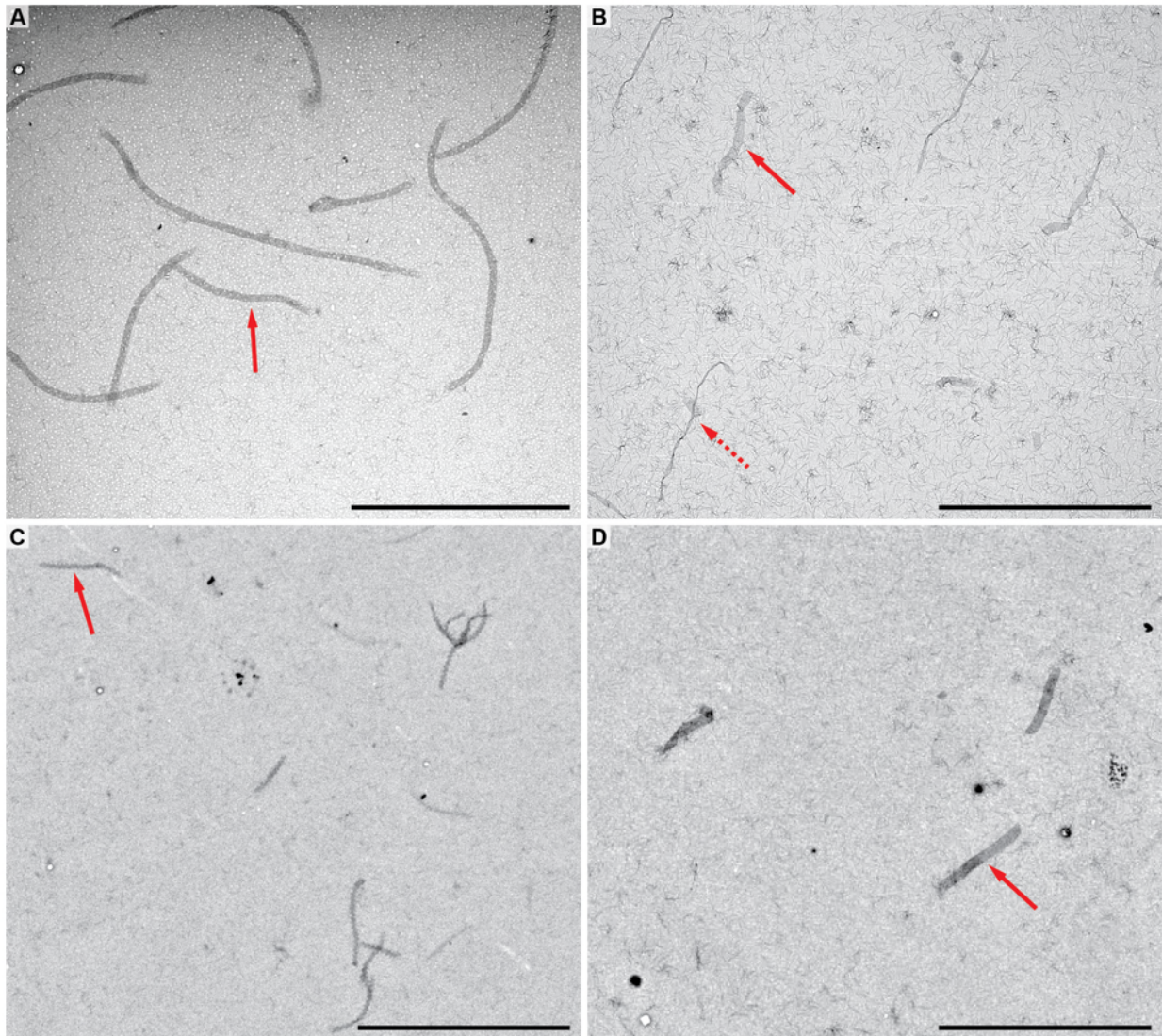


Figure S18 Low-magnification TEM images of periodic 1D ribbons. Images in **A–D** correspond to the designs v16 staggered, v8 staggered, v16 non-staggered jagged, and v16 non-staggered flush ribbons respectively (also see Fig. 3i–iv, Fig. S11). Solid-red arrows point to flat-lying ribbons. The dotted-red arrow in *B* shows how the v8 ribbons had a propensity to adopt stretched and elongated morphologies on the TEM grids. Scale bars are 10 μm .

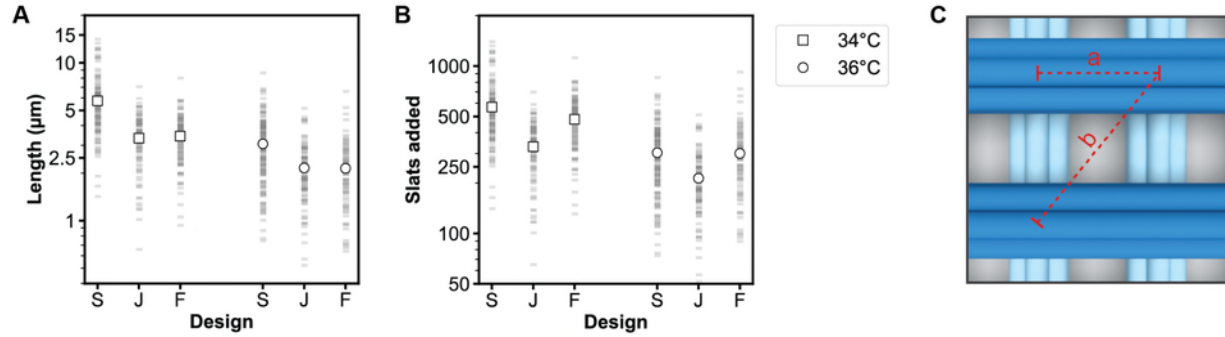


Figure S19 Length comparison of the various designs of v16 ribbons after 16 hours of isothermal growth. **A** shows the lengths as measured in low-magnification TEM images, versus **B** which shows the number of slats per ribbon as extrapolated using the theoretical nm per slat as calculated in **C**. Each faint gray bar in the plots is the measurement of a single ribbon, with the mean lengths shown with either the square or circular data points. ‘S’, ‘J’, and ‘F’ indicate the v16 staggered, non-staggered jagged, and non-staggered flush ribbons. The ribbons for the various designs for a given temperature grew to roughly similar numbers of slats (e.g. 200–300 slats at 36°C), suggesting that the pattern in which the slats are added does not greatly influence the kinetics of assembly. Small differences in growth might be due to small variations in experimental parameters or differences in sequence symmetry of the designs. The v16 staggered ribbons used 4x sequence symmetry, versus 2x sequence symmetry of the v16 non-staggered jagged and flush ribbons (see Supplementary Text 4 for an explanation of the relationship between symmetry and growth). In **C**, dimension ‘a’ is 42 bp or ~14.2 nm, versus dimension ‘b’ which is ~20.2 nm. We can see by considering the pattern of slat as per the design renders in Fig. 3: each pair of slats for the v16 staggered ribbons and v16 non-staggered jagged ribbons add one unit of ‘b’; conversely, each pair of slats for the v16 non-staggered flush ribbons add one unit of ‘a’. $N_{S_{34^{\circ}C}} = 133$, $N_{J_{34^{\circ}C}} = 104$, $N_{F_{34^{\circ}C}} = 109$, $N_{S_{36^{\circ}C}} = 170$, $N_{J_{36^{\circ}C}} = 102$, and $N_{F_{36^{\circ}C}} = 95$ ribbons were measured.

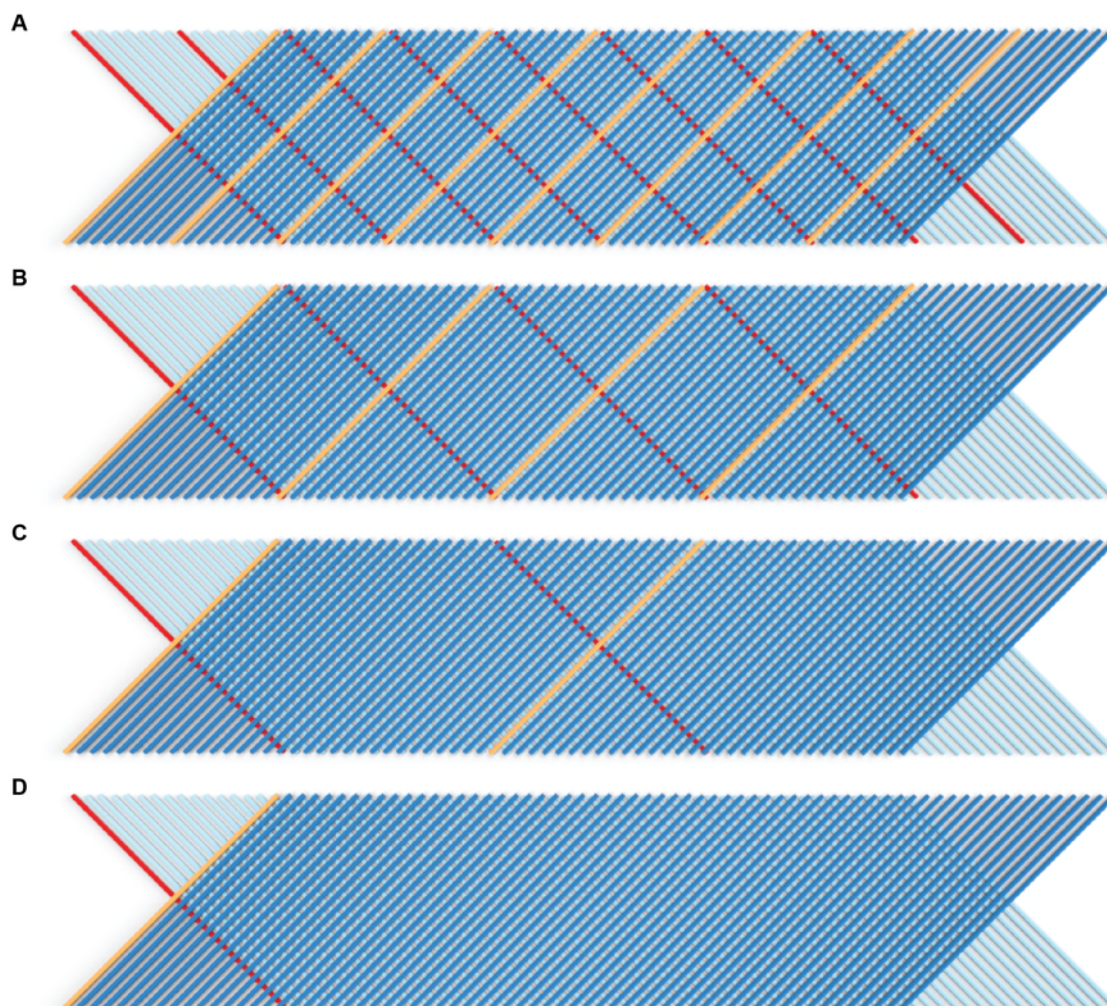


Figure S20 Design renderings showing variable sequence symmetries of the v16 staggered ribbons. That is, the number of slats that repeat in the periodic unit is arbitrary and can be programmed with as many unique slats as desired. Alternatively, sequence symmetry of a given slat is the copy number of another particular slat from the perpendicular direction to which it is bound. This is observed in the above where a given slat from the top-layer is colored orange, and a given slat in the bottom-layer that is colored red. **A** is 4x symmetry with 16 unique slats (i.e. 8+8 slats in each respective perpendicular layer), **B** is 2x symmetry with 32 unique slats (i.e. 16+16), **C** is 1x symmetry with 64 unique slats (i.e. 32+32), and **D** is 0.5x symmetry with 128 unique slats (i.e. 64+64). The v16 staggered ribbons in Fig. 3i use the 4x symmetry, the v8 staggered ribbons in Fig. 3ii use the 2x symmetry, the non-staggered jagged and flush ribbons in Fig. 3iii–iv use the 2x symmetry, the v16 staggered sheets in Fig. 4 and Fig. 5 use the 2x sequence symmetry. All origami crisscross growth characterization with respect to reaction conditions was studied using v16 staggered ribbons with 4x symmetry, or v8 staggered ribbons with 2x symmetry. In Fig. S21, growth versus symmetry design as shown above are compared.

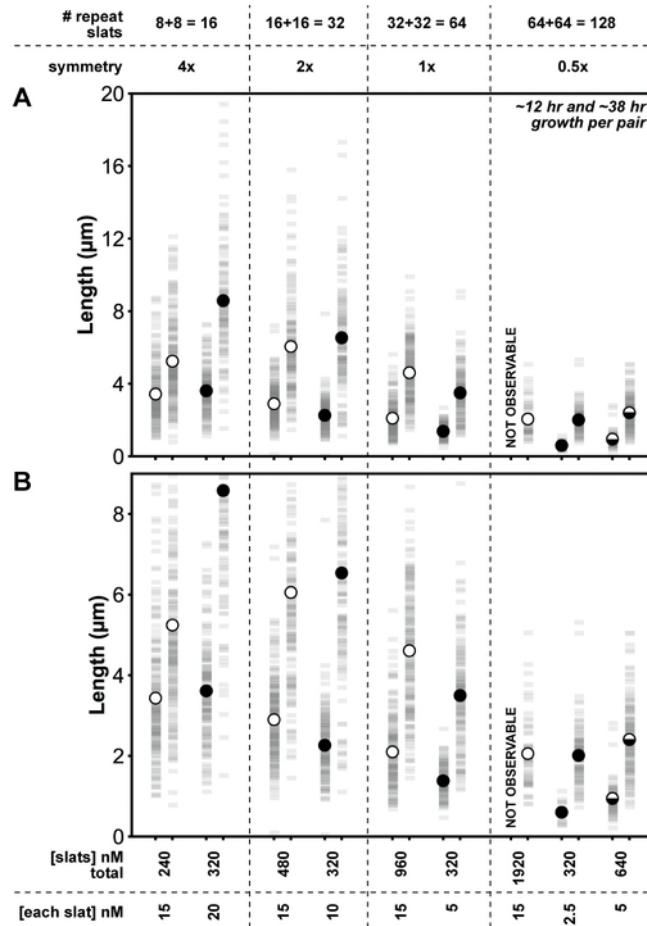


Figure S21 Length of v16 staggered ribbons versus the number of unique slats in the unit repeat of the ribbon (i.e. symmetry as explained in Fig. S20), as obtained by measuring ribbons in TEM images after 12 and 38 hours of isothermal 34°C growth. Panels **A** and **B** are the same data, with the y-axis in **B** over a smaller range to better show the length differences. Each faded rectangle is the measurement of a single ribbon, with circular data points showing the mean length. In general, designs with a larger number of unique slats (i.e. lower symmetry) grew more slowly. We observed that the concentration of the slats is an important determinant for the rate of growth of a given symmetry design. The white data points indicate where we maintained the per slat concentration at 15 nM, versus the black data points where we maintained the total concentration of slats at 320

nM. The following number of ribbons were measured for each condition: $N_{8+8 \text{ slats}; 15 \text{ nM [each slat]}, 12 \text{ hr}} = 177$, $N_{8+8 \text{ slats}; 15 \text{ nM [each slat]}, 38 \text{ hr}} = 192$, $N_{8+8 \text{ slats}; 20 \text{ nM [each slat]}, 12 \text{ hr}} = 147$, $N_{8+8 \text{ slats}; 20 \text{ nM [each slat]}, 38 \text{ hr}} = 117$, $N_{16+16 \text{ slats}; 15 \text{ nM [each slat]}, 12 \text{ hr}} = 217$, $N_{16+16 \text{ slats}; 15 \text{ nM [each slat]}, 38 \text{ hr}} = 147$, $N_{16+16 \text{ slats}; 10 \text{ nM [each slat]}, 12 \text{ hr}} = 146$, $N_{16+16 \text{ slats}; 10 \text{ nM [each slat]}, 38 \text{ hr}} = 129$, $N_{32+32 \text{ slats}; 15 \text{ nM [each slat]}, 12 \text{ hr}} = 169$, $N_{32+32 \text{ slats}; 15 \text{ nM [each slat]}, 38 \text{ hr}} = 179$, $N_{32+32 \text{ slats}; 5 \text{ nM [each slat]}, 12 \text{ hr}} = 117$, $N_{32+32 \text{ slats}; 5 \text{ nM [each slat]}, 38 \text{ hr}} = 143$, $N_{64+64 \text{ slats}; 15 \text{ nM [each slat]}, 12 \text{ hr}} = 0$, $N_{64+64 \text{ slats}; 15 \text{ nM [each slat]}, 38 \text{ hr}} = 58$, $N_{64+64 \text{ slats}; 2.5 \text{ nM [each slat]}, 12 \text{ hr}} = 15$, $N_{64+64 \text{ slats}; 2.5 \text{ nM [each slat]}, 38 \text{ hr}} = 115$, $N_{64+64 \text{ slats}; 5 \text{ nM [each slat]}, 12 \text{ hr}} = 78$, $N_{64+64 \text{ slats}; 5 \text{ nM [each slat]}, 38 \text{ hr}} = 132$.

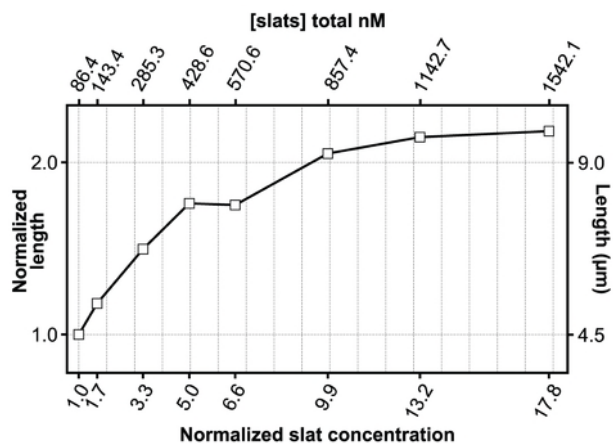


Figure S22 Normalized mean lengths of the ribbons are shown versus the concentration of the slats for the 4x sequence symmetry design (i.e. 16 total unique slats) using a constant concentration of seed. There is roughly a linear change in the mean length versus the slat concentration when the total slat concentration is below 500 nM, versus a lesser increase in length for when higher concentrations of slats were used. This experiment is replotted on a linear axis with the data from Fig. 5D. The dotted

grid lines are spaced to represent an increase in either the length or total slat concentration of one unit compared to the condition to which the data was normalized.

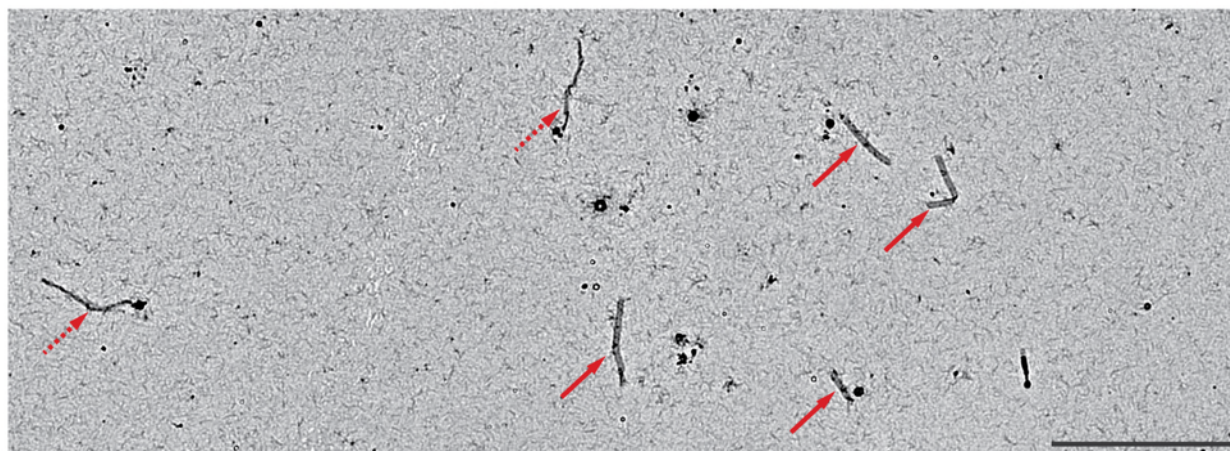


Figure S23 Tri-layer arrangement of slats on a v8 staggered ribbon for 2D growth, as shown in an overview image of the ribbon sample from Fig. 3B. The initial v8 ribbon with two layers of slats was grown isothermally overnight, at which point the additional third layer of slats was added and incubated for two further days. The ribbons with solid red arrows were those where a third layer was successfully added, versus the ribbons with dashed arrows where the third layer did not bind. We note that binding of the third layer appeared to be an all-or-nothing event for a given ribbon. It is unclear why the third layer slats did not bind to certain ribbons and will require further study and optimization to improve its efficiency. The scale bar is 10 µm.

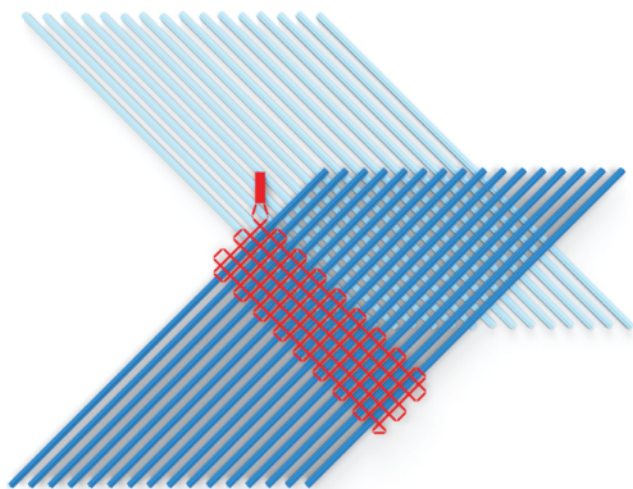


Figure S24 Render of the repeating slat unit for periodic growth of 2D sheets. The pattern of growth is similar to the v16 staggered ribbons (see Fig. S16A), except that here the top- and bottom-layers of slats are shifted with respect to one another. The particular render and designs as tested in this paper used 2x sequence symmetry and were composed of 32 unique slats total.

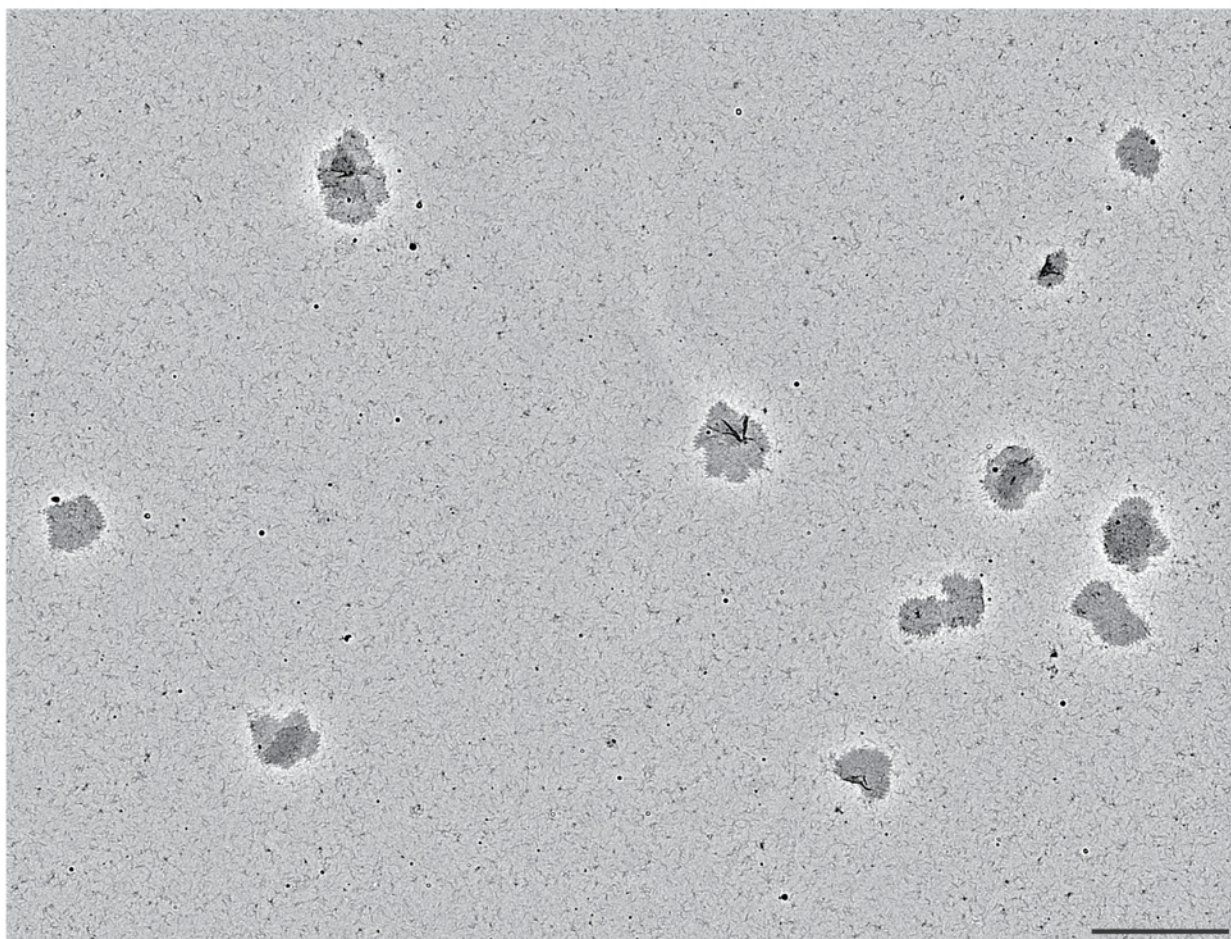


Figure S25 Low-magnification TEM images of the periodic sheets after three days of isothermal growth.

The sheets were grown with 0.2 nM seed and generally appeared as well distributed single particles. The scale bar is 10 μm .

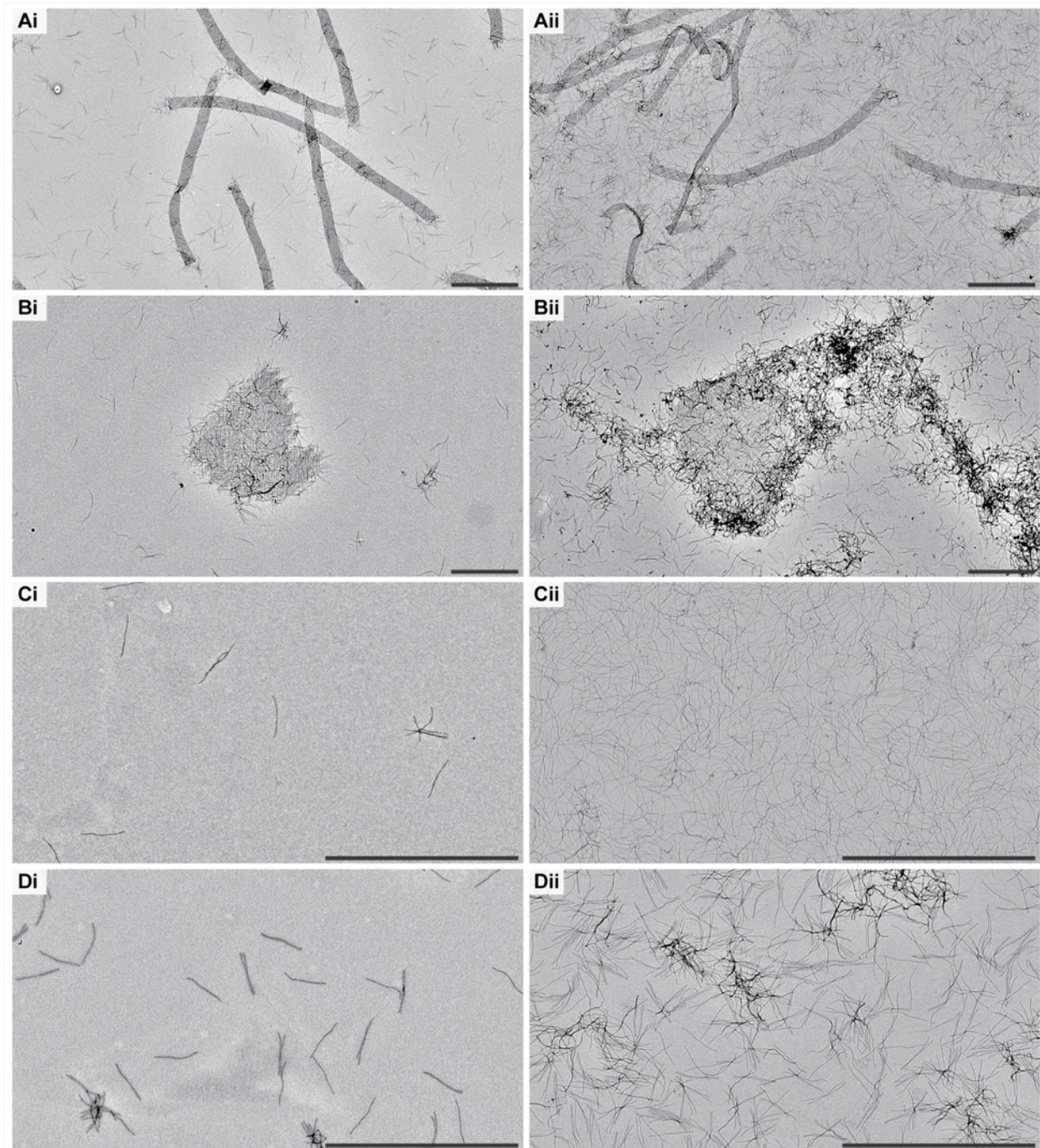


Figure S26 Large periodic megastructures can be purified from excess free slats to a limited extent by low speed centrifugation. Rows **A–D** are ribbons, sheets, one layer of unassembled ribbon slats with no seed as

one control, and both layers of unassembled ribbon slats with no seed as another control, respectively. In column **i**, the samples were purified as described in Method 12, versus column **ii** which is the raw sample with no centrifugation. There are qualitatively fewer background free slats in the resuspended pellets in comparison to the raw samples. We note that the background free slats could be further lessened by repeating the centrifugation process two or more times. However, we were unable to extract all the background slats by centrifugation alone. There was a higher background of free slats in sample *Di* where the control slats had both handles and complementary handles from the other perpendicular layer, versus *Ci* where the control slats only had handles from one layer. We assume that transient interactions between free slats with complementary handles makes them prone to pelleting during centrifugation and that is the reason we could not completely remove the slat background in the megastructures samples in *A* and *B* by centrifugation alone. Further purification could potentially be achieved by attachment of the crisscross structures to microbeads or other surfaces (e.g. via biotin/streptavidin on the seed) and sequential washing away of unbound slats, under more stringent conditions (e.g. higher salt). Indeed, in our low-mag DNA-PAINT images (Figs. S29 and S30), in which flow over attached megastructures provides a degree of washing, qualitatively the background appears more evenly dispersed, with less bias towards overlap with the megastructures themselves. In the TEM images, it is likely that many of the overlapping slats are also trapped underneath the megastructures (in addition to laying on top), hindering their removal during the grid staining procedure. Efforts are underway in our laboratory to investigate these avenues for further purification. Scale bars are 2 μm .

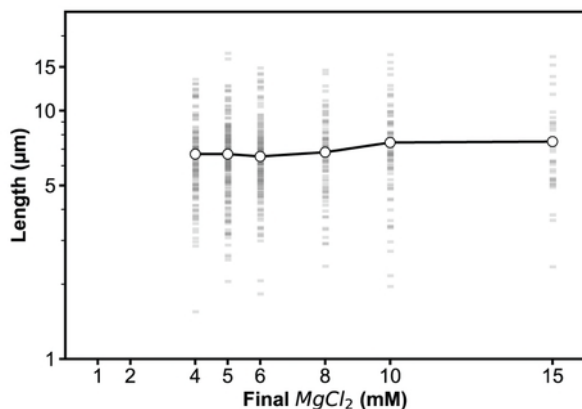


Figure S27 Megastructures (i.e. periodic v16 ribbons) using the 7-nt binding sites were stable in lower-magnesium conditions from which they were initially grown. The ribbons were initially grown in 15 mM MgCl₂, then diluted 15-fold into the concentration of MgCl₂ as listed on the x-axis, incubated for ~48 hours at room temperature. There was negligible difference in the length of the

ribbons that were incubated in 15 mM MgCl₂ versus those that were incubated in 4 mM MgCl₂. No ribbons could be observed in either 1 mM or 2 mM MgCl₂ conditions, where they were presumed to have fallen apart. Possibilities for increasing stability in lower ion concentrations include coating megastructures with PEGylated oligolysine⁵⁸ and/or crosslinking the megastructures post-assembly⁵⁹. Each faint gray bar is the length measurement of a single ribbon, with the mean length indicated by the circular, white data point. N ribbons were measured for the conditions tested: N_{4 mM} = 121, N_{5 mM} = 188, N_{6 mM} = 171, N_{8 mM} = 78, N_{10 mM} = 79, N_{15 mM} = 38.

Fig. S28–Fig. S31: Model of the DNA nanocube, additional TEM of nanocube patterns, and DNA-PAINT results of 1D ribbons and 2D sheets

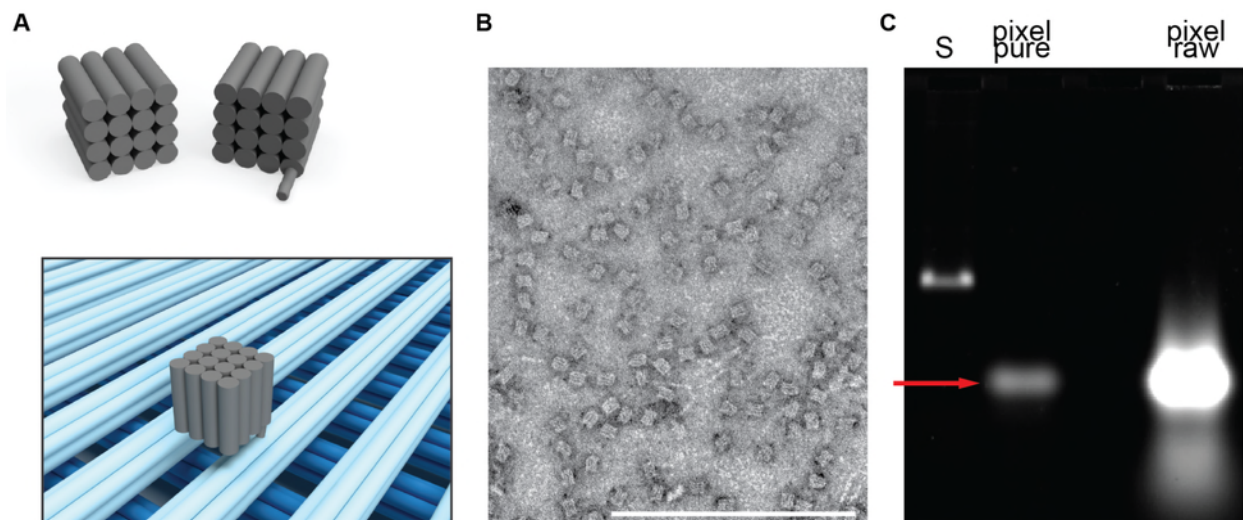


Figure S28 Strategy and folding of the DNA nanocube contrast agent to visualize arbitrary patterns on 6HB megastructure canvases. Uppermost **A** shows a rendering of the $10 \times 10 \times 10 \text{ nm}^3$ DNA nanocube, where we added a 16-nt handle with a 4T linker to the 3' end of one of the strands in the nanocube as published previously³⁷. The lowermost rendering shows the nanocube bound to the top layer of slats in a megastructure. The 3' end of one strand in the top helix of a cyan 6HB was extended with the 16-nt complementary handle at one of the 32 possible addressable sites. The negative-stain TEM image in **B** shows the nanocube after purification by excising them from an agarose gel. **C** shows an agarose gel of the nanocubes after and before purification, with the desired band shown with the solid red arrow. Densitometry of the raw folded nanocube suggests that $\sim 64\%$ of the total material was assembled into the desired structure. The scale bar in the TEM image is 200 nm.

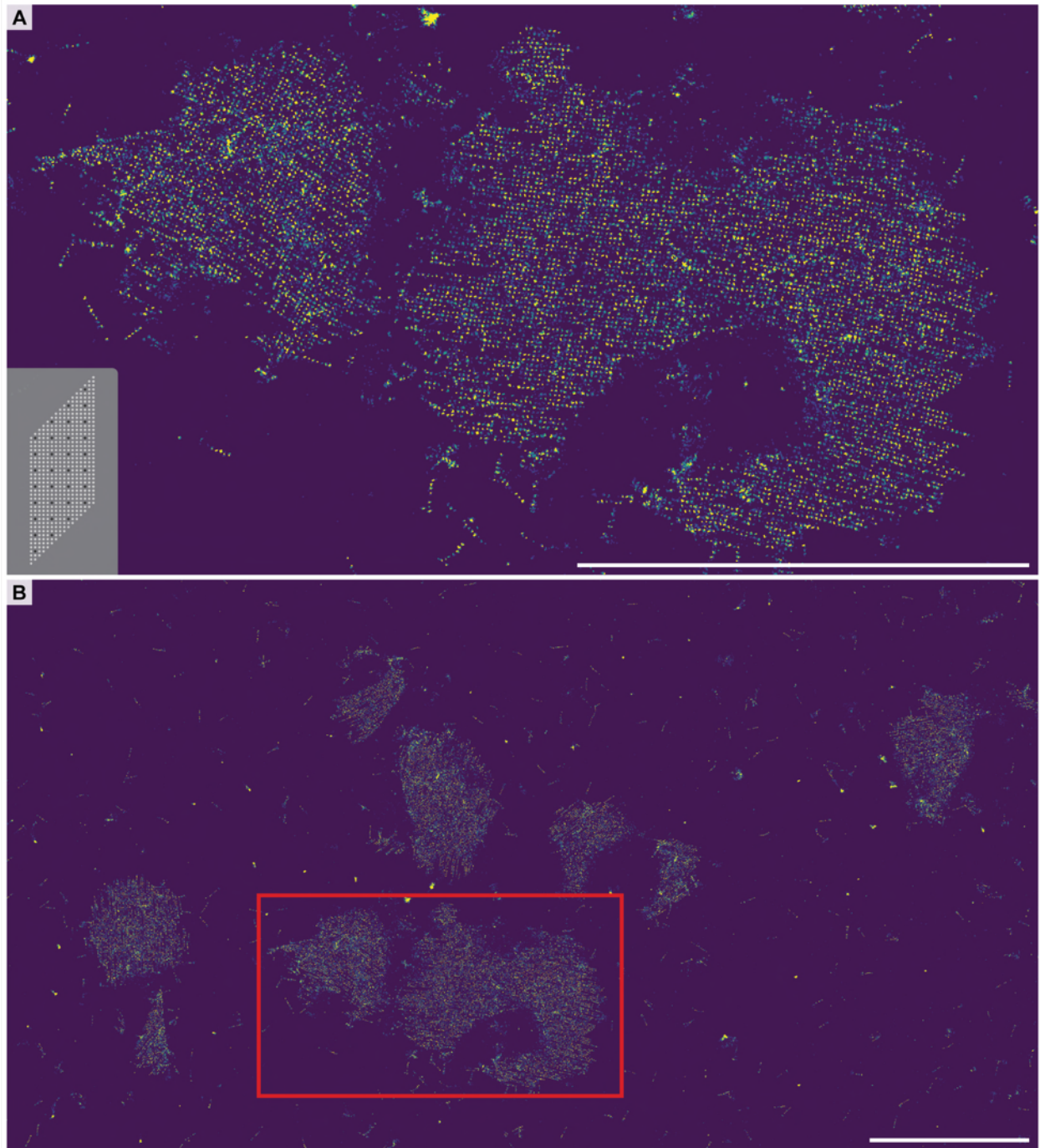


Figure S29 DNA-PAINT overview images of 2D sheets (also note, this is the same sample as shown in Fig. 4C) where the top layer of slats is tagged with complementary handles to the PAINT imager strands. The close-up region shown in **A** was selected from the boxed region in **B**. How the top slats are patterned is shown with the dark dots in the lower left of *A*, where every fourth node (~ 56.3 nm or 168 bp spacings) was decorated. We achieved single handle resolution, with each dot in the above images corresponding to

a single node on the canvas. The base of the sheets were intermittently decorated with biotinylated strands for docking to the imaging substrate. Scale bars are 5 μm .

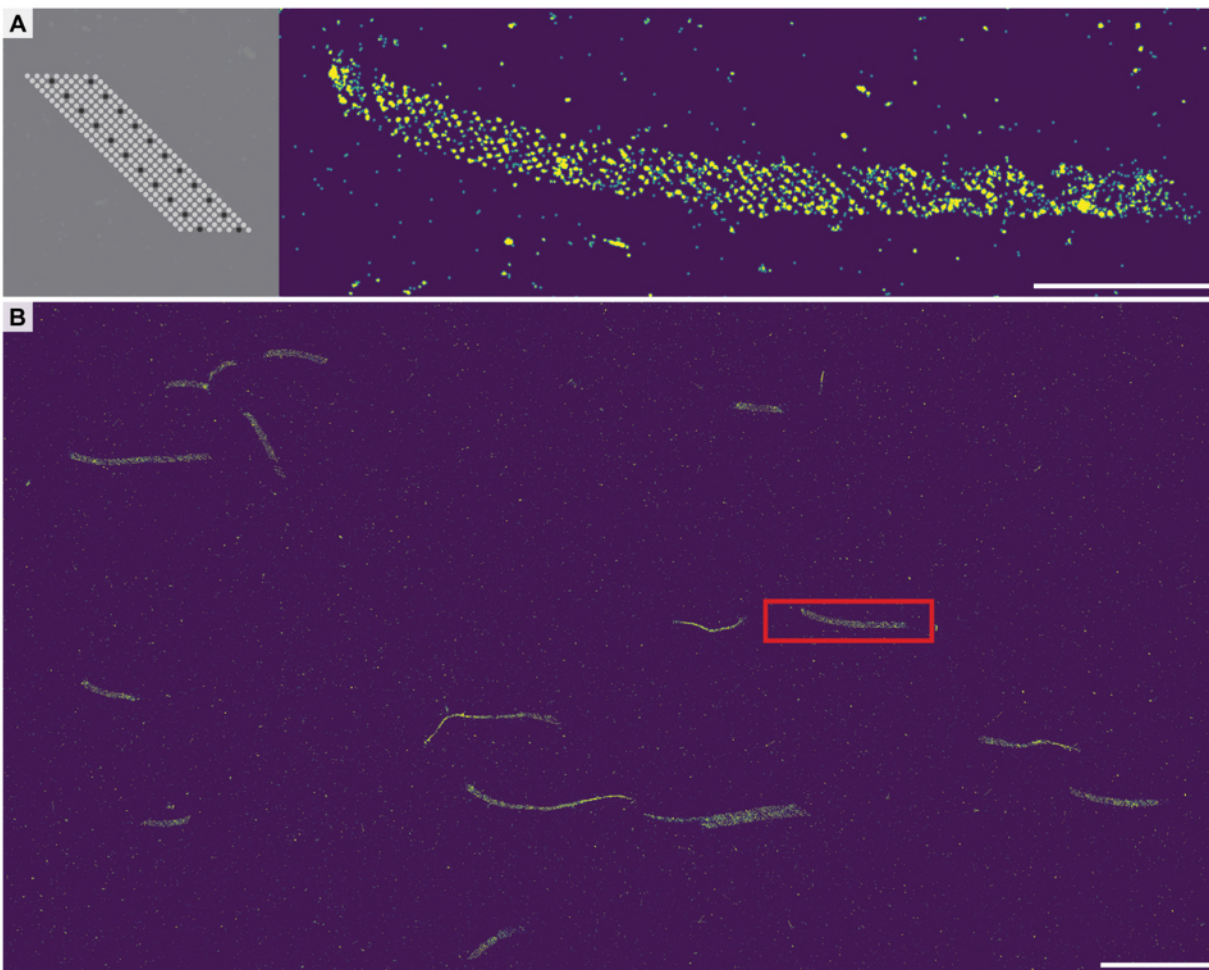


Figure S30 DNA-PAINT overview images of periodic v16 staggered ribbons where the top layer of slats is tagged with complementary handles to the PAINT imager strands. The close-up region shown in **A** was selected from the boxed region in **B**. How the top slats are patterned is shown with the dark dots in the left of **A**, where minimally every third node (~ 42.2 nm or 126 bp spacings) was decorated. We achieved single handle resolution on some examples of slats in **A**, though the resolution of the single handles was not as clear as in Fig. S29. We also note that the ribbons had a propensity to not bind completely flat to the imaging substrate and frequently appeared stretched and elongated. The base of the sheets were intermittently decorated with biotinylated strands for docking to the imaging substrate. Scale bars are 1 μm in **A** and 5 μm in **B**.

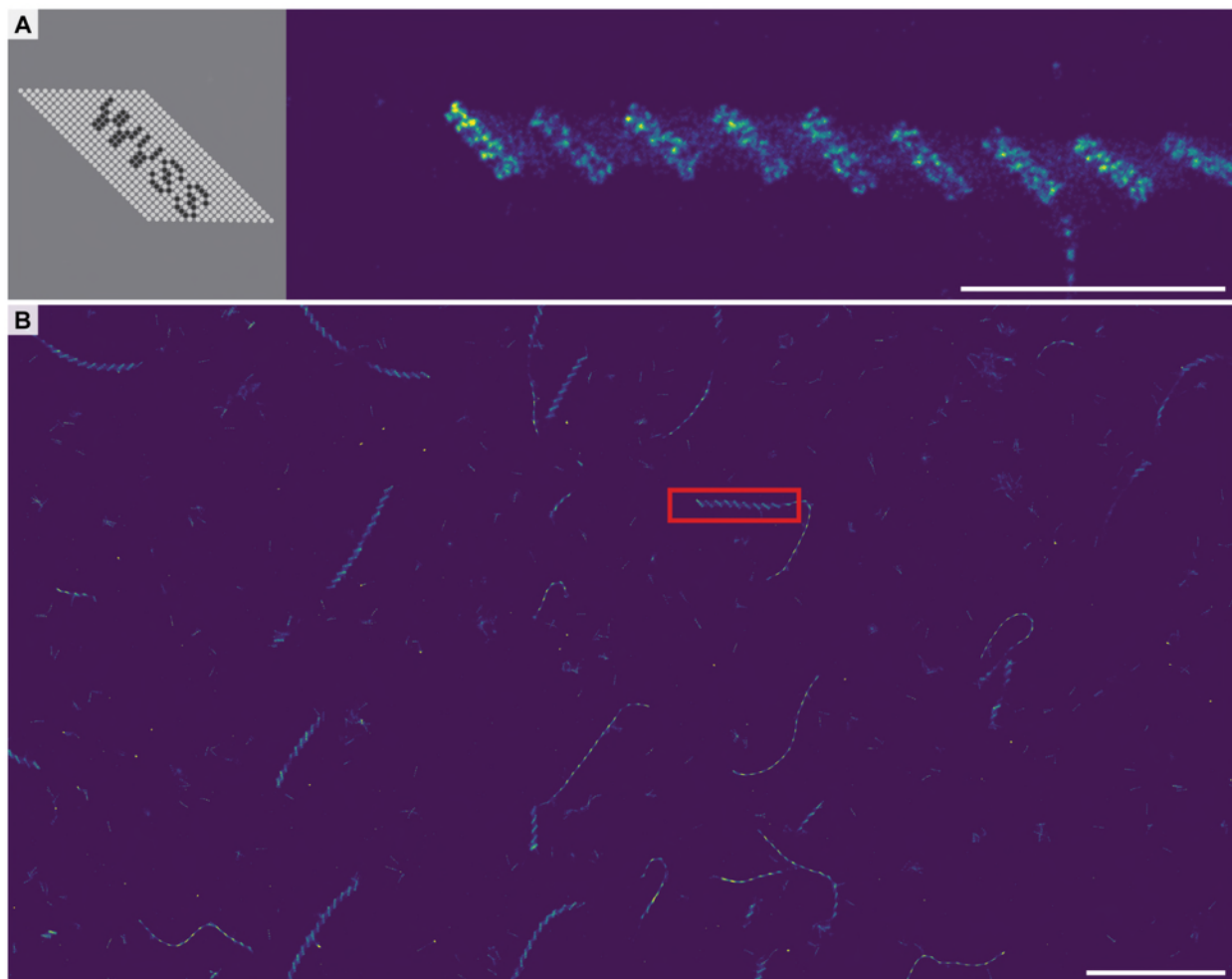


Figure S31 DNA-PAINT overview images of 1D v16 staggered ribbons where the top layer of slats is tagged with complementary handles to the PAINT imager strands, where the pattern resembles the lettering “WYSS.” The close-up region shown in **A** was selected from the boxed region in **B**. How the top slats are patterned is shown with the dark dots in the left of *A*, where minimally every node (~ 14.1 nm or 42 bp spacings) was decorated. The resolution of single handles could not be distinguished, though there is resemblance to the designed pattern. We also note that the ribbons had a propensity to not bind completely flat to the imaging substrate and frequently appeared stretched and elongated. The base of the sheets was intermittently decorated with biotinylated strands for docking to the imaging substrate. Scale bars are 1 μm in *A* and 5 μm in *B*.

Fig. S32–Fig. S34: TEM results when no seed added, AGE results of single DNA origami square versus scaffold, representative TEM of megastructures versus concentration of seed

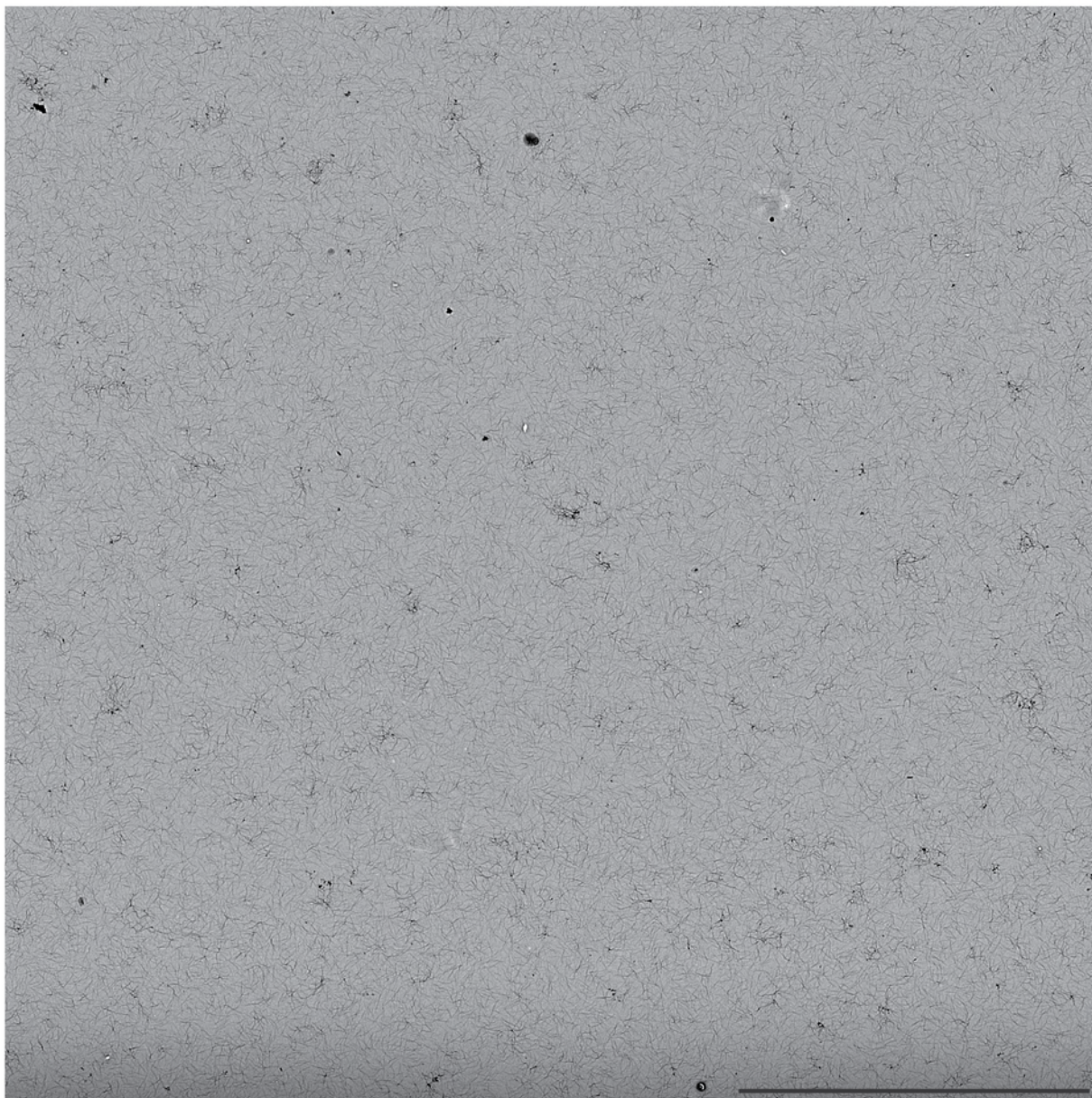


Figure S32 Low-magnification TEM image of a typical megastructure assembly reaction when no seed is added. No assembly was observed in the control for the finite 1022-slat sheet, as above. This was similarly observed in all control reactions for other finite and periodic megastructures from Fig. 2 –Fig. 4, with typical reaction conditions where fast, seeded growth is favored. For brevity, we show only the image of a single design here. The particular reaction as above is perhaps an extreme challenge of the nucleation control attainable with origami slats; slats were added in multiple three-day stages for the largest structures

as explained in Fig. S15. As such, the slats in the above 1022-slat sheet control were incubated at 34°C for over 18 days. In this particular experiment, we also had the thermocycler where we were growing the reaction fail. The reaction sat at room temperature for about one day before we noticed the breakdown, and despite this extended incubation at both these temperatures, no spontaneous growth could be observed. We argue that this leeway with experimental conditions where useful nucleation control can still be attained is a large factor of what makes crisscross assembly of origami a powerful advance to make it easier to create DNA megastructures. The scale bar is 10 μm .

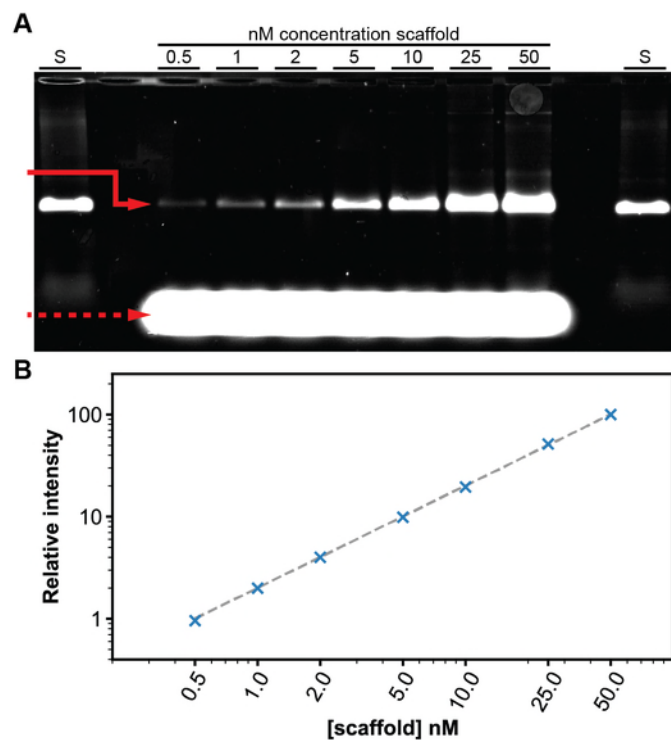


Figure S33 Agarose gel showing the amount of single DNA-origami reference square folded varies precisely with the amount of DNA scaffold added, to serve as a benchmark for nucleation control that we wished to match with assembly of origami-slat megastructures. **A** shows the agarose gel with the solid red arrow indicating the gel band for the square, the dashed red arrow indicating the excess staple strands, and lanes ‘S’ containing just the scaffold. In **B**, the gel density of the solid red gel band with respect to the 50 nM condition is plotted. The dotted line is a linear fitting of the data, indicating an almost perfect stoichiometric relationship between the amount of reference square folded versus

scaffold added. The concentration of scaffold was varied from 0.5–50 nM with the staple strands maintained at 400 nM per strand. This reference square folded as shown above and was also quantified by direct counting TEM images (see Fig. 5Ci).

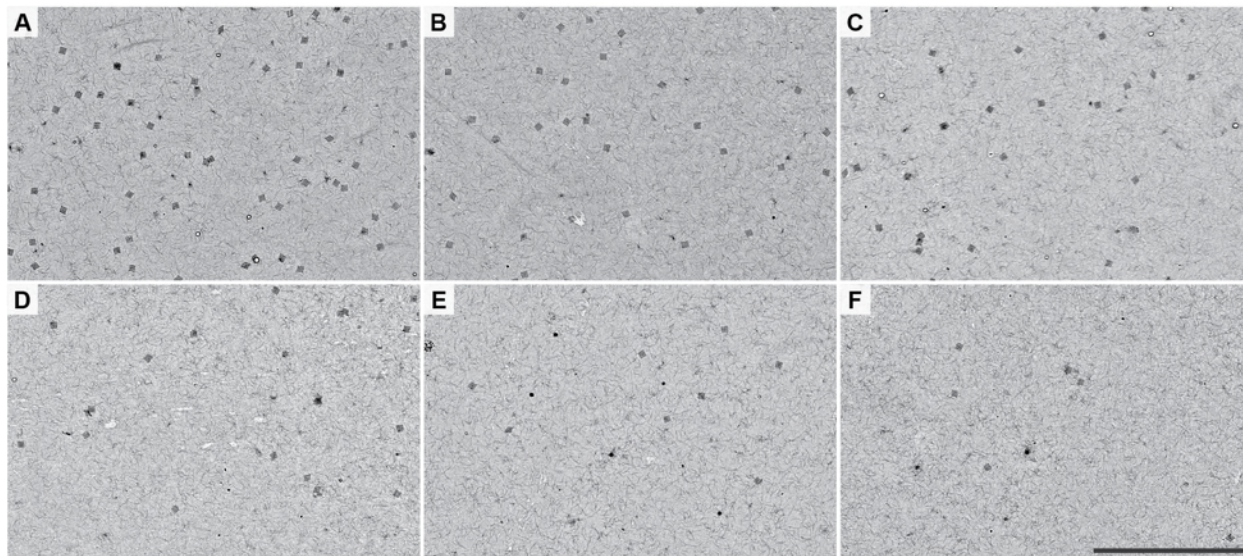


Figure S34 Representative low-magnification TEM images of the 64-slat square versus different concentrations of seed. The concentrations of seed in **A–F** were 6, 4, 2, 1, 0.5, and 0.25 nM, respectively. There is a roughly linear relationship between the mean number of squares counted versus the amount of seed added, as plotted in the leftward panel of Fig. 5Cii. This approach of direct counting from ten TEM images to show control of assembly was also used for the reference origami square and other finite and periodic megastructures, as shown in Fig. 5C. The scale bar (which applies to all images *A–F*) is 10 μm .

Fig. S35–Fig. S40: Standard curve of ribbons, melt temperature of v16 7-nt ribbons, temperature characterization and melt temperature of v8 7-nt, v16/v8 6-nt, and v16/v8 8-nt ribbons, growth versus time for 6-nt and 8-nt v16 ribbons

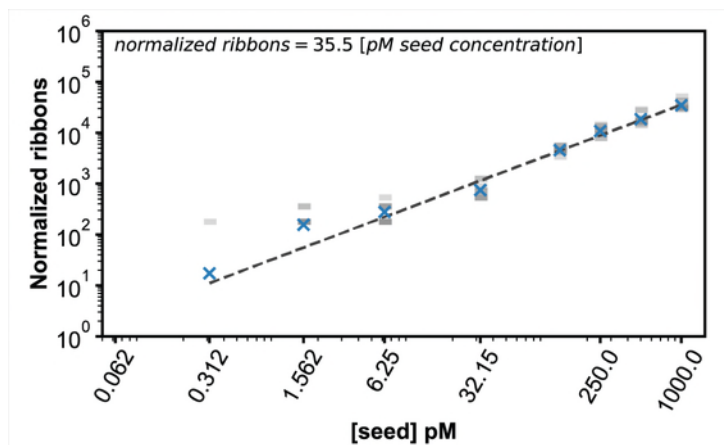


Figure S35 Standard curve of the ribbons as derived from the experiment shown in the leftward panel of Fig. 5Ci. Ribbons were assembled in reactions where the seed was added in different amounts to a constant concentration of slats. The number of ribbons was counted in ten low-magnification (i.e. 400x) TEM images and the number of ribbons was normalized with respect to the factor that the sample

was diluted (i.e. multiply by 250) and to a $100\ \mu\text{m} \times 100\ \mu\text{m}$ area (i.e. divide by ~ 1.44 , which is the number of $100\ \mu\text{m} \times 100\ \mu\text{m}$ regions covered in a 400x image area with our microscope setup). This standard curve shows a $\sim 0.3\ \text{pM}$ limit-of-detection, where a single ribbon was observed in the ten images. We also note that we saw no ribbons in either the sample with no seed or the sample where $\sim 0.062\ \text{pM}$ seed was added. The blue 'x' markers indicate the mean number of ribbons counted per seed concentration. The dotted line and upper left formula is the linear fitting of the data, where the y-intercept was forced through zero to account for how no ribbons were observed when no seed was added. This equation was rearranged to compute the pM amount of spontaneously formed ribbons in Fig. 5D and Fig. S38, with the meaning of the white versus red data points versus the standard curve explained in Fig. S36.





Marker style	x (pM spontaneous nucleation)	Relative unseeded background (vs. 0.5 nM seed)
	$x < 0.3$	$< 0.06\%$
	$0.3 \leq x < 5$	$< 0.99\%$
	$5 \leq x < 50$	$< 9.09\%$
	$50 \leq x < 500$	$< 50\%$

Figure S36 Table of markers used in Fig. 5D and Fig. S38 to denote spontaneous nucleation of ribbons as counted in the control reactions with no seed. There were fewer pM spontaneously nucleated ribbons counted in the average of ten TEM images of unseeded control reactions, as compared to the standard curve of ribbons in the leftmost panel in Fig. 5Ciii. Each seeded reaction was initiated with 500 pM seed, with the assumed relative proportion ribbons that would have been unseeded background for each temperature condition as listed for each marker. We posit that the relative background of

spontaneously nucleated ribbons is especially low for up to and including the red triangle data point, and would be of limited concern for routine nanofabrication of DNA megastructures, though the requirement of nucleation stringency might vary depending on the end application of the crisscross assembly. For instance, one could envision using crisscross growth to amplify some biomarker signal that might require lower background nucleation yet, which might be satisfied using reaction conditions with the white square marker.

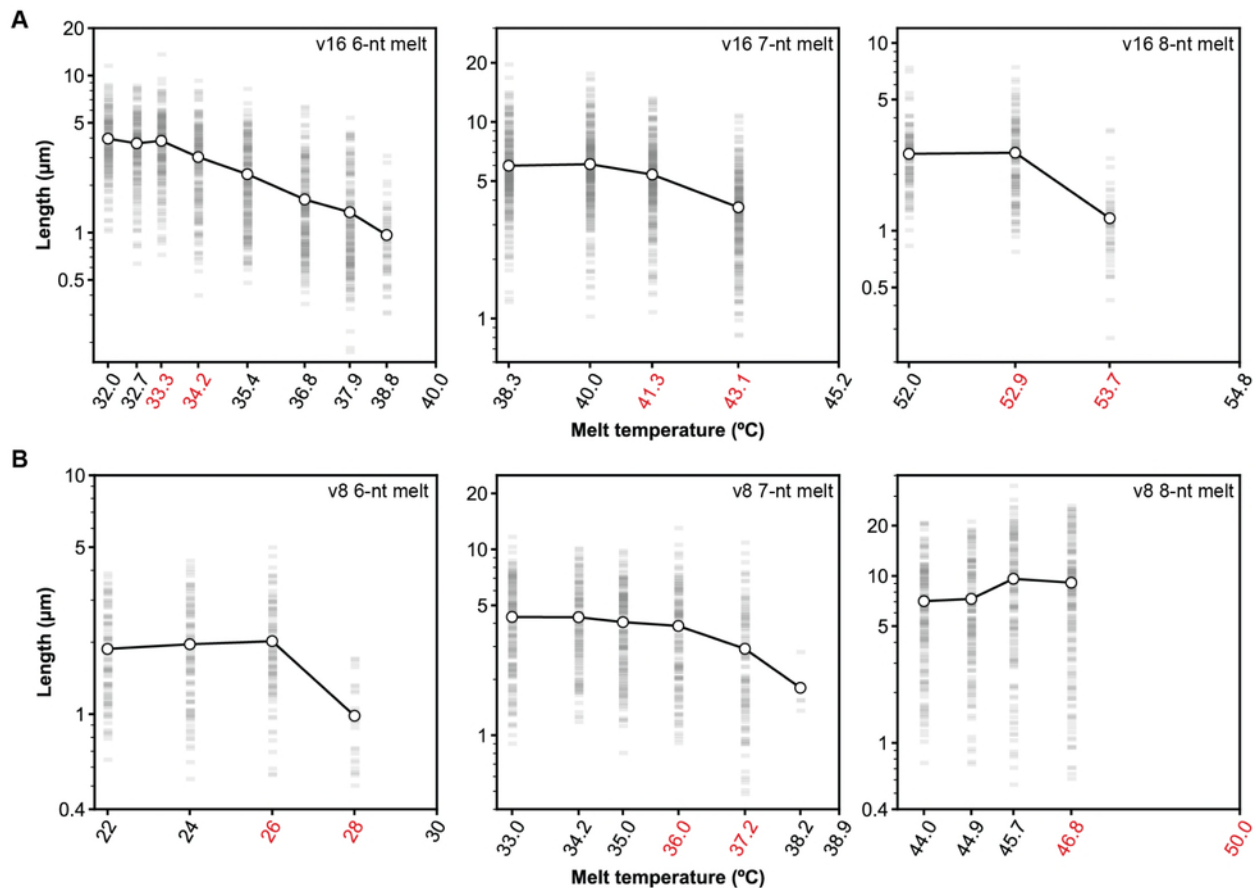


Figure S37 Approximate melting temperatures of the v16 (**A**) and v8 (**B**) staggered ribbons using 6-, 7-, and 8-nt binding sites are within the red temperature bounds in the above plots. Ribbons were grown isothermally for ~12–16 hours at a temperature favoring seeded growth of long ribbons, at which point the temperature was increased across a gradient of possible melt temperatures for 3–4 hours. Samples were collected on TEM grids and the lengths of ribbons were recorded at the putative melt temperatures. The highest temperature tick on the plots is where no ribbons remained, and is hence above the melting temperature. Some range of temperatures below this upper bound was where the ribbons started to fall apart slowly. The shrinkage of the ribbons was typically most noticeable as observed at the second highest temperature tested, to the extent where sometimes only a small number of ribbons could be observed in the sample. The lower and upper temperature bounds containing this melt transition temperature are highlighted in red as above. N ribbons were measured for the conditions tested:

- v16 6-nt: $N_{32^{\circ}\text{C}} = 172$, $N_{32.7^{\circ}\text{C}} = 189$, $N_{33.3^{\circ}\text{C}} = 205$, $N_{34.2^{\circ}\text{C}} = 184$, $N_{35.4^{\circ}\text{C}} = 216$, $N_{36.8^{\circ}\text{C}} = 204$, $N_{37.9^{\circ}\text{C}} = 180$, $N_{38.8^{\circ}\text{C}} = 56$

- v16 7-nt: $N_{38.3^{\circ}\text{C}} = 297$, $N_{40^{\circ}\text{C}} = 337$, $N_{41.3^{\circ}\text{C}} = 305$, $N_{43.1^{\circ}\text{C}} = 283$
- v16 8-nt: $N_{52^{\circ}\text{C}} = 124$, $N_{52.9^{\circ}\text{C}} = 141$, $N_{53.7^{\circ}\text{C}} = 51$
- v8 6-nt: $N_{22^{\circ}\text{C}} = 97$, $N_{24^{\circ}\text{C}} = 101$, $N_{26^{\circ}\text{C}} = 102$, $N_{28^{\circ}\text{C}} = 28$
- v8 7-nt: $N_{33^{\circ}\text{C}} = 174$, $N_{34.2^{\circ}\text{C}} = 148$, $N_{35^{\circ}\text{C}} = 183$, $N_{36^{\circ}\text{C}} = 146$, $N_{37.2^{\circ}\text{C}} = 114$, $N_{38.2^{\circ}\text{C}} = 4$
- v8 8-nt: $N_{44^{\circ}\text{C}} = 183$, $N_{44.9^{\circ}\text{C}} = 166$, $N_{45.7^{\circ}\text{C}} = 151$, $N_{46.8^{\circ}\text{C}} = 177$

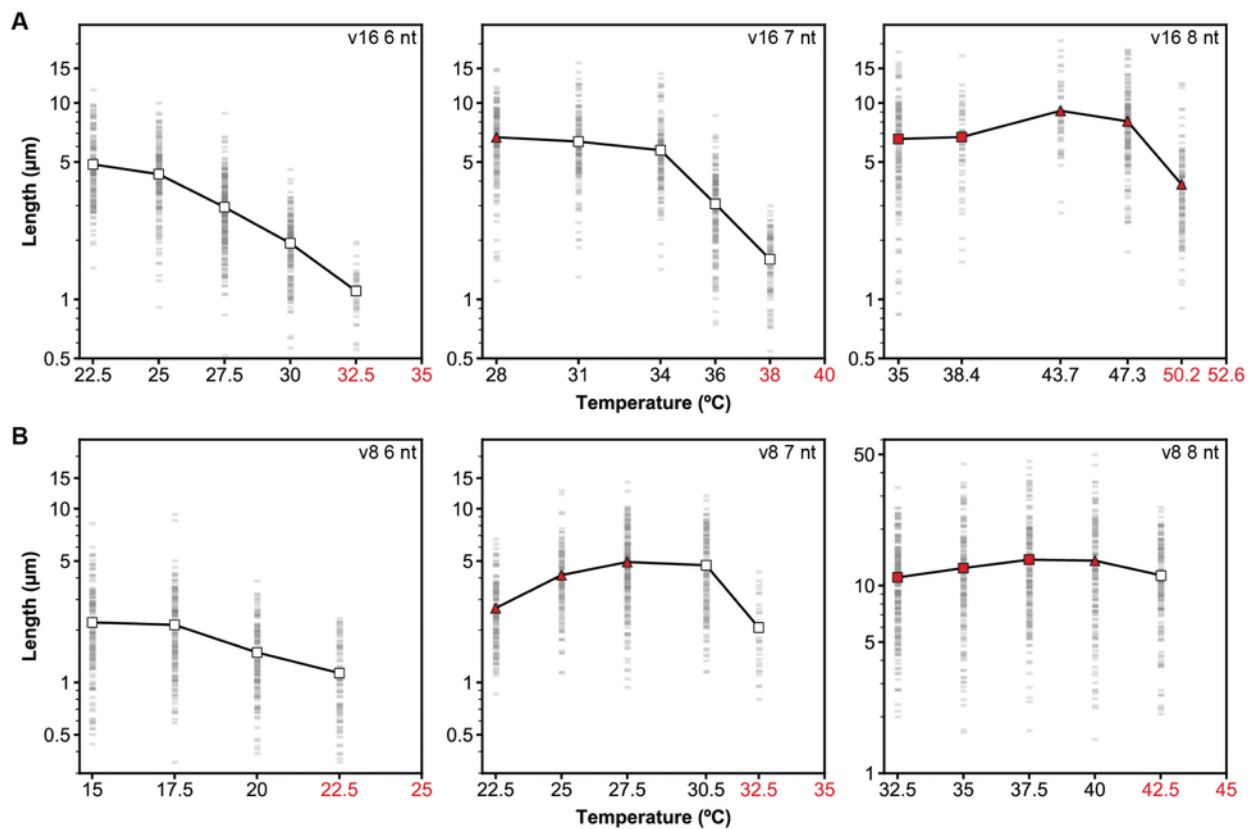


Figure S38 Length of the ribbons versus growth temperature for seeded v16 (**A**) or v8 (**B**) ribbons using either 6-, 7-, or 8-nt binding sites. The v16 7-nt middle plot is the same data as from the leftmost plot in Fig. 5D and is replicated for easy comparison to the other designs. The x-axis ticks shown in red are the growth temperatures flanking the reversible temperature for slat binding to a ribbon end, where the seeded ribbons were first observed to be short and then entirely not observed. The longest seeded ribbons with the fastest growth were generally observed at lower growth temperatures several degrees below reversibility. The shape and color of the mean-length data points represent the number of spontaneously nucleated ribbons as counted in control reactions where no seed was added. White square points are where no

measurable ribbons were observed and were below the 0.3 pM ribbon detection limit, and red points represent some amount of measurable unseeded growth. Details regarding the degradations of these red data points are explained in Fig. S36. Further discussion and consideration of the above results are in Supplementary Text 4 and Fig. S39. Each seeded reaction was mixed together with 20 nM per slat, 0.5 nM of seed, and 15 mM Mg^{2+} and incubated for 4 hours at a temperature above the ribbon melt temperature where binding of slats to the seed was favored. Subsequently, the reaction was incubated isothermally for ~16 hours at the temperature as indicated on the x-axis, at which point was diluted and with images of the ribbons collected by TEM. Each faint gray box is the length measurement of a single ribbon, with the large data point representing the mean length. N ribbons were measured for the conditions tested:

- v16 6-nt: $N_{22.5^{\circ}C} = 156$, $N_{25^{\circ}C} = 154$, $N_{27.5^{\circ}C} = 234$, $N_{30^{\circ}C} = 162$, $N_{32.5^{\circ}C} = 38$
- v16 7-nt: $N_{28^{\circ}C} = 149$, $N_{31^{\circ}C} = 139$, $N_{34^{\circ}C} = 133$, $N_{36^{\circ}C} = 170$, $N_{38^{\circ}C} = 91$
- v16 8-nt: $N_{35^{\circ}C} = 144$, $N_{38.4^{\circ}C} = 51$, $N_{43.7^{\circ}C} = 46$, $N_{47.3^{\circ}C} = 154$, $N_{50.2^{\circ}C} = 120$
- v8 6-nt: $N_{15^{\circ}C} = 145$, $N_{17.5^{\circ}C} = 166$, $N_{20^{\circ}C} = 137$, $N_{22.5^{\circ}C} = 81$
- v8 7-nt: $N_{22.5^{\circ}C} = 141$, $N_{25^{\circ}C} = 128$, $N_{27.5^{\circ}C} = 201$, $N_{30^{\circ}C} = 140$, $N_{32.5^{\circ}C} = 34$
- v8 8-nt: $N_{32.5^{\circ}C} = 206$, $N_{35^{\circ}C} = 150$, $N_{37.5^{\circ}C} = 171$, $N_{40^{\circ}C} = 141$, $N_{42.5^{\circ}C} = 150$

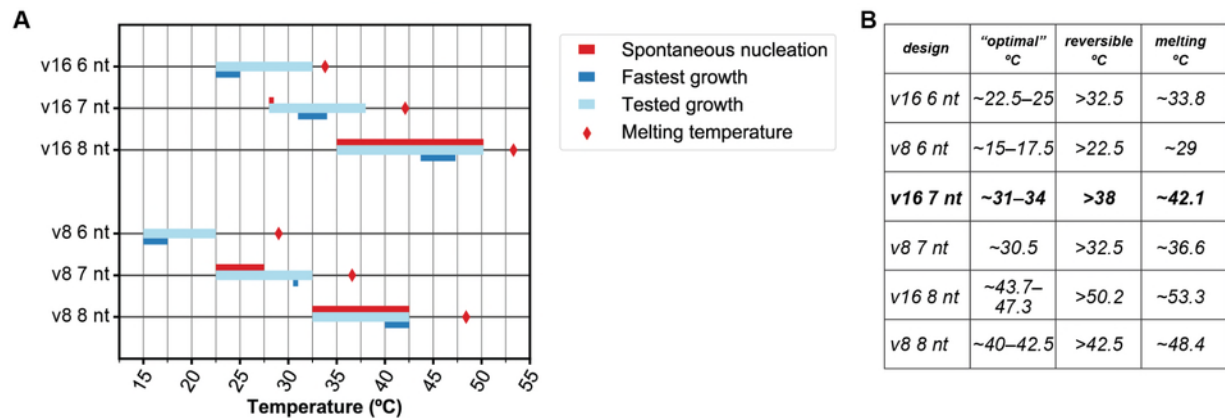


Figure S39 Growth and melt temperatures as determined for various ribbon designs are plotted in **A**, with the plotted data numerically shown in table **B**. The light-blue lines indicate the different temperatures tested in Fig. S38, where growth of ribbons was observed when the seed was added. The highest light-blue points are the temperatures where ribbon growth drastically slowed, and approached the reversible temperature for slats to bind either 16 (for v16) or 8 (for v8) binding handles on a ribbon end. The red diamonds are the average temperatures where previously assembled ribbons were observed to fall apart (i.e. the approximate melt temperature), as determined in Fig. S37. The lowest light-blue points are the lowest growth temperature as tested in Fig. S38, though it would likely be possible to carry out seeded growth at lower temperatures yet. The dark-blue points were designated as the “optimal” growth temperatures favoring fast, seed-driven growth of the ribbons as determined from Fig. S38. We discuss the selection of these temperature optimums in more depth in Supplementary Text 5.1. The red points were where measurable spontaneous nucleation was observed in Fig. S38 that was some amount greater than the 0.3 pM ribbon detection limit.

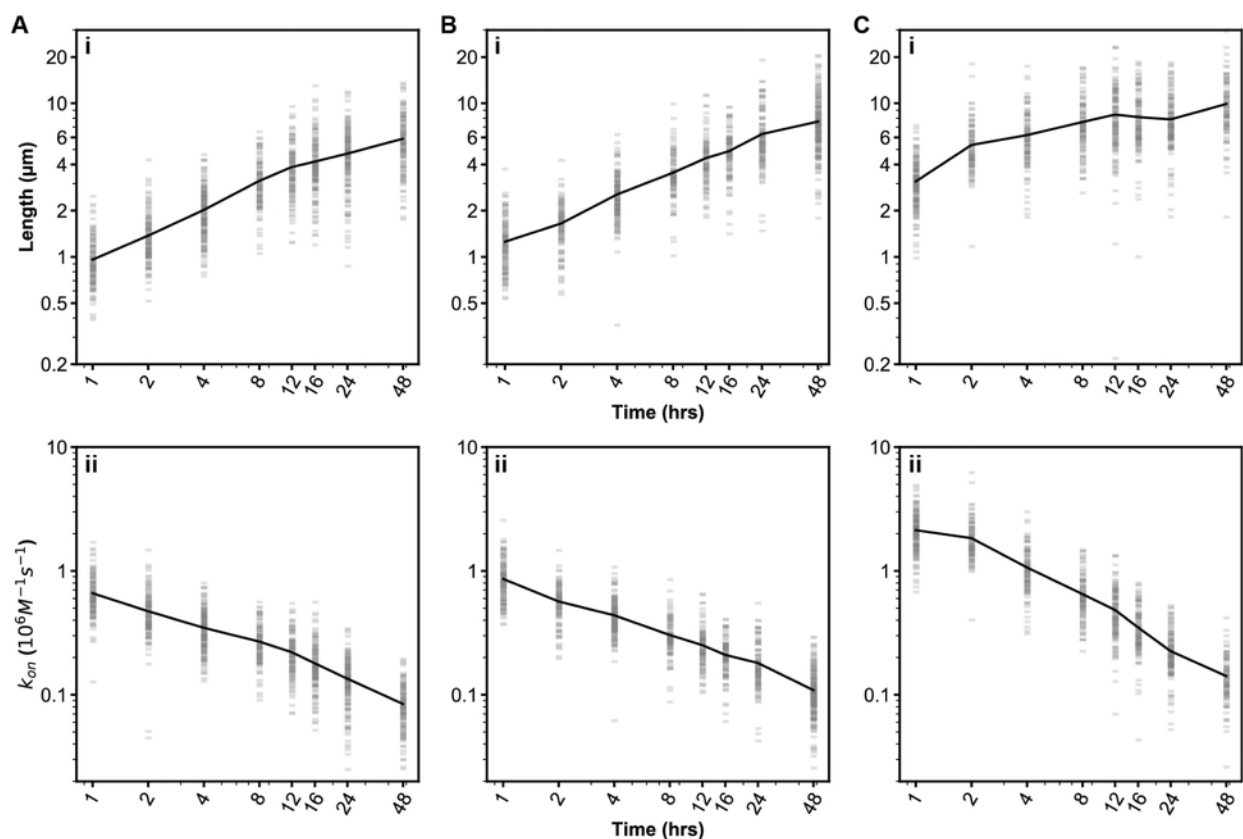


Figure S40 Length of the ribbons (see **i**) and extrapolated kinetics (see **ii**) for v16 6-, 7-, and 8-nt ribbons versus time in **A**, **B**, and **C** respectively. Panel **Bi** is replicated from Fig. 5E for clearer comparison of the three designs. Each faint gray bar represents the length measurement of a single ribbon, with the mean lengths indicated by the line. The mean lengths for the ribbons after 1 hour of growth were ~ 1 , ~ 1.3 , and ~ 3.1 μm , and after 16 hours of growth were ~ 4.2 , ~ 4.9 , and ~ 8.1 μm for the 6-, 7-, and 8-nt designs, respectively. Explanation for how the mean lengths were extrapolated into k_{on} rates are discussed in Supplementary Text 6. The rates of growth were increasingly faster for the 6-, 7-, and 8-nt designs. The observed average forward rate of assembly after one hour of growth was $\sim 0.66 \cdot 10^6$, $\sim 0.86 \cdot 10^6$, and $\sim 2.13 \cdot 10^6$ $\text{M}^{-1}\text{s}^{-1}$ for the 6-, 7-, and 8-nt designs. The average rates were observed to gradually decline over time, such as $\sim 0.18 \cdot 10^6$, $\sim 0.21 \cdot 10^6$, and $\sim 0.35 \cdot 10^6$ $\text{M}^{-1}\text{s}^{-1}$ for the 6-, 7-, and 8-nt designs after 16 hours of growth. We hypothesize that this decline was because of temporary stalling and permanent halting of growth due to accumulation of errors with missing handles on the growing fronts of ribbons, or else due to depletion of the free slats which may have caused inaccuracy of the pseudo-first order kinetic assumptions as explained in Supplementary Text 6.2. All assembly reactions had 20 nM per slat, 0.5 nM of seed, and 15 mM Mg^{2+} and were conducted at growth temperatures where spontaneous nucleation was limited. N ribbons were measured for the conditions tested:

- v16 6-nt: $N_{1 \text{ hr}} = 130$, $N_{2 \text{ hr}} = 141$, $N_{4 \text{ hr}} = 179$, $N_{8 \text{ hr}} = 114$, $N_{12 \text{ hr}} = 119$, $N_{16 \text{ hr}} = 146$, $N_{24 \text{ hr}} = 177$, $N_{48 \text{ hr}} = 128$
- v16 7-nt: $N_{1 \text{ hr}} = 131$, $N_{2 \text{ hr}} = 107$, $N_{4 \text{ hr}} = 158$, $N_{8 \text{ hr}} = 107$, $N_{12 \text{ hr}} = 106$, $N_{16 \text{ hr}} = 106$, $N_{24 \text{ hr}} = 118$, $N_{48 \text{ hr}} = 204$
- v16 8-nt: $N_{1 \text{ hr}} = 188$, $N_{2 \text{ hr}} = 108$, $N_{4 \text{ hr}} = 112$, $N_{8 \text{ hr}} = 108$, $N_{12 \text{ hr}} = 143$, $N_{16 \text{ hr}} = 125$, $N_{24 \text{ hr}} = 148$, $N_{48 \text{ hr}} = 100$

Fig. S41–Fig. S45: Hamming-distance analysis of 1D ribbon growth, mechanistic testing for growth changes to 1D ribbons vs. kinetic trapping of slats resulting from Hamming distance, and optimized Hamming distances of all the megastructure designs tested in this work

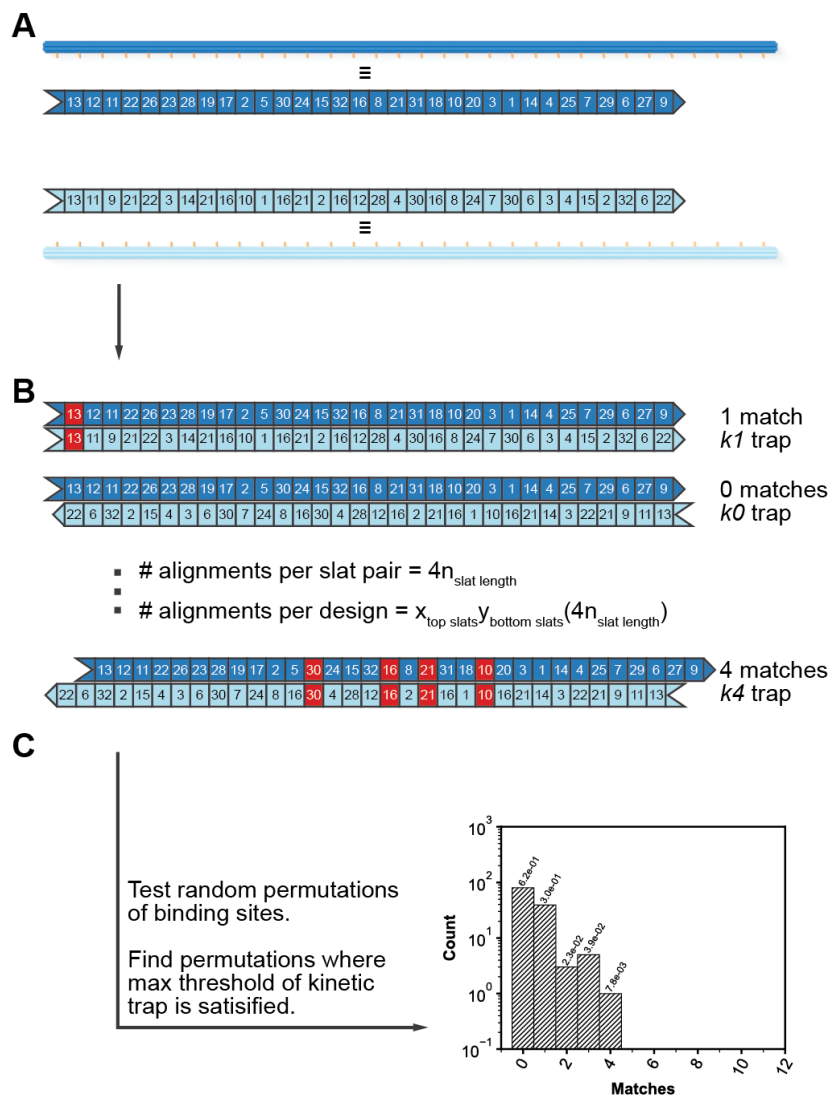


Figure S41 Schematic showing analysis of Hamming distances between a single pair of slats. In **A**, a pair of example slats are extracted from some random permutation of binding sites for a megastructure. Rendered images of 6HB slats are drawn proximally to the numeric representation, where each slat is abstracted as a one-dimensional list which is $n_{\text{slat length}}$ long (i.e. $n = 32$ for the 6HB slat). In **B**, the Hamming distance between the various forward and reverse alignments is measured to determine the number of matching, complementary handles between the pair of slats (where matches in the sample alignments are in red). There are

$4n_{\text{slat length}}$ alignments per slat pair, and $x*y$ slat pairs in a megastructure composed of x top-slats and y bottom-slats. For the example slat pair, the maximum number of matches is four and is designated as a kinetic trap of strength $k4$. In **C**, the strength of the total 128 alignments for the example slat pair are shown in a histogram, with the max-strength kinetic trap shown in the rightmost bin.

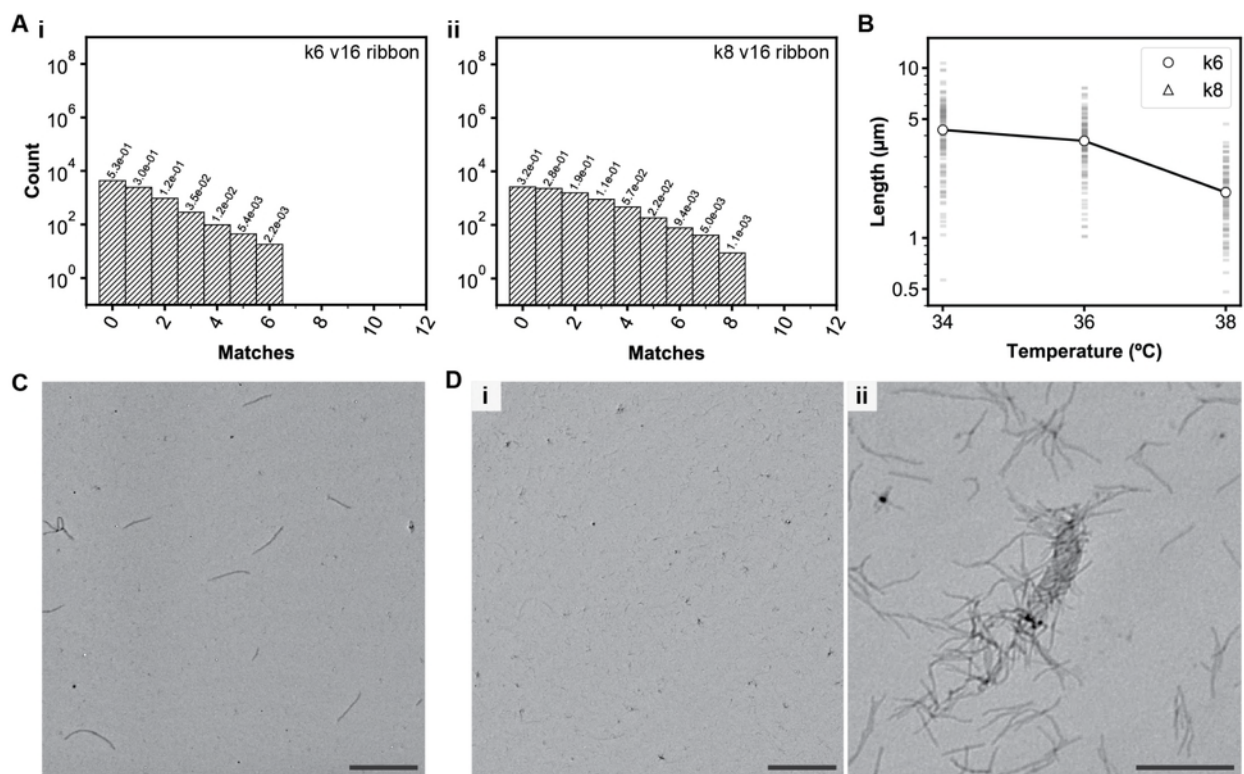


Figure S42 Increasing the k kinetic-trap strength (i.e. the number of matching complementary binding sites between pairs of slats resulting from smaller Hamming distances) nearly stops the growth of v16 7-nt ribbons. The number of kinetic traps between one layer of slats and the other perpendicular layer is shown for two ribbon designs in **Ai–ii**. There are maximally six or eight matching binding sites between the slats (i.e. $k6$ and $k8$ strength kinetic traps) in each of the designs, respectively. The relative fraction of each strength trap of the total interactions measured is shown above each histogram bar. In **B**, the length of ribbons as measured by TEM after overnight growth of the $k6$ and $k8$ designs at various temperatures is plotted. We note that no appreciable growth of the $k8$ ribbons was measured at any of the temperatures tested. Each faint gray box represents the length measurement of a single ribbon, with the circular and triangular white points showing the mean. Low-magnification TEM image of the $k6$ growth is in **C**, versus the unobservable growth of the $k8$ design in **Di** and one of the infrequently observed short $k8$ ribbons in **Dii**. Isothermal growth was conducted for 16 hours using 15 mM Mg^{2+} , with either ribbon design using 4x sequence symmetry with binding sites as selected from the 2048-strand library. Scale bars are 10 μm in **C** and **Di**, and 1 μm in **Dii**. N ribbons were measured for the conditions tested: $N_{k6\ 34^\circ C} = 118$, $N_{k6\ 36^\circ C} = 108$, $N_{k6\ 38^\circ C} = 94$.

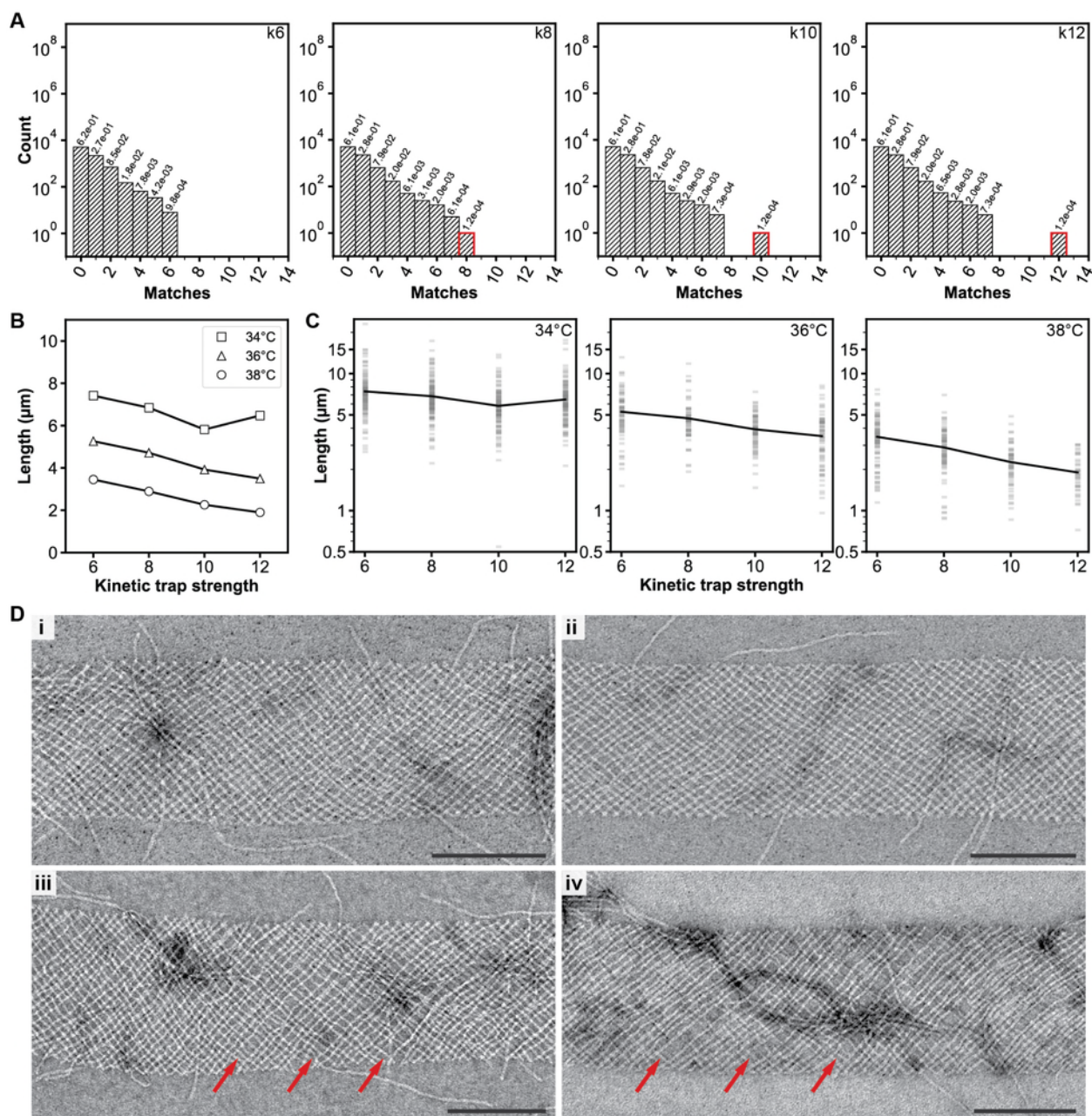


Figure S43 Introducing a single kinetic trap between a single pair of slats of max strength k progressively slows the growth of v16 7-nt ribbons as k is increased. Histograms in **A** show the number of kinetic traps between one layer of slats and the other perpendicular layer in the different ribbon designs tested. The $k6$ sequence permutations is a control with the maximal Hamming distance that we attained for a 4x symmetry ribbon using the 2048-strand library. The $k8$ permutation is distinct from the $k6$ control, with the $k10$ and $k12$ that were generated from small manipulations of the $k8$ design. Each of these latter three designs have only a single kinetic trap of either $k8$, $k10$, or $k12$ strength. The relative fraction that each kinetic trap comprises of the total interactions measured is written above each bar. **B** shows the mean length of the

ribbons at different temperatures versus the different max-strength kinetic traps. In general, the ribbons were shorter at a given temperature when the kinetic trap was stronger with a larger k trap where more matching binding sites entrapped one pair of slats. **C** shows the raw measured-length data of each design for each temperature tested. In **D**, close-up negative-stain TEM images show segments of a ribbon for $k6$, $k8$, $k10$, and $k12$ traps in **i-iv**, respectively. Red arrows point to periodic missing slats in one layer of the ribbon which appeared every eighth slat. Scale bars are 200 nm. The length of N ribbons were for each of the conditions tested above:

- At 34°C: $N_{k6} = 124$, $N_{k8} = 138$, $N_{k10} = 122$, $N_{k12} = 129$.
- At 36°C: $N_{k6} = 77$, $N_{k8} = 61$, $N_{k10} = 78$, $N_{k12} = 72$.
- At 38°C: $N_{k6} = 91$, $N_{k8} = 81$, $N_{k10} = 61$, $N_{k12} = 41$.

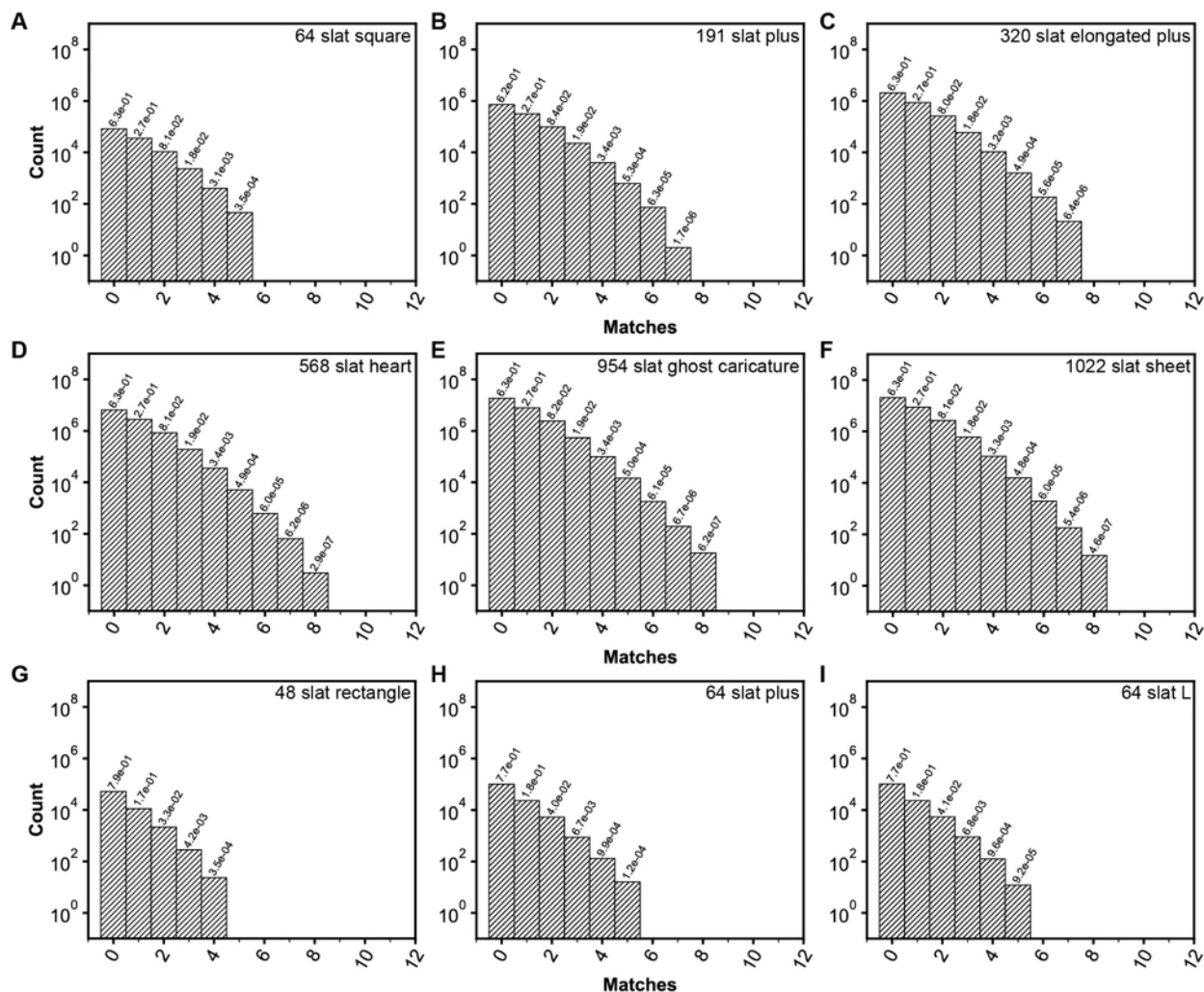


Figure S44 The multiplicity for each possible number of matching, complementary binding sites for each

of the slats from one layer with respect to each of the slats in the other layer are shown as histograms, for the optimized finite megastructure designs as tested in Fig. 3. The relative fraction that each match comprises of the total interactions is written above each bin. We minimized the maximum number of matches for each design as discussed in Method 2 and Supplementary Text 7.4.

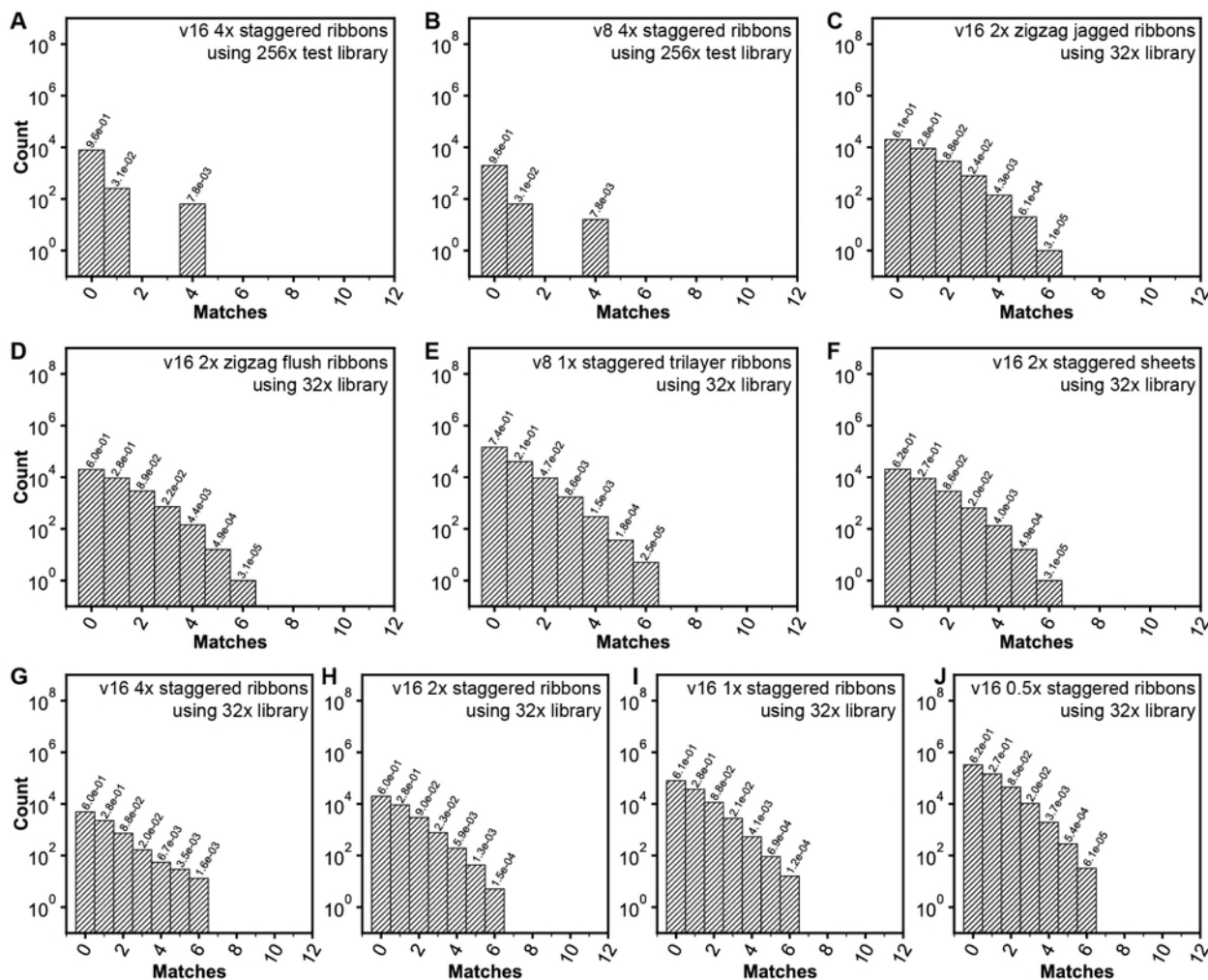


Figure S45 The multiplicity for each possible number of matching, complementary binding sites for each of the slats from one layer with respect to each of the slats in the other layer are shown as histograms, for the optimized periodic megastructures in this paper. The relative fraction that each match comprises of the total interactions is written above each bin. We minimized the maximum number of matches for each design as discussed in Method 2 and Supplementary Text 7.3. The ribbon designs in **A–B** have maximally $k4$ traps, with permutations generated from 256 different 6-, 7-, or 8-nt handles from a 512-strand library. All other periodic designs in **C–J** have maximally $k6$ traps, with permutations generated from 32 different 7-nt handles in the 2048-strand library. Design *A* is for the 4x symmetry v16 staggered ribbon as used in

Fig. 3Ai, Fig. S18A, Fig. S19A–B design ‘S’, Fig. S27, Fig. S35, Fig. 5Ciii ribbons, and v16 ribbon characterization in Fig. 5D–E and Fig. S37–Fig. S40; design *B* is for the 4x symmetry v8 staggered ribbon as used in Fig. S17Aii, Fig. S18B, and v8 ribbon characterization in Fig. S37–Fig. S38; designs *C–D* are for the 2x symmetry v16 non-staggered ribbons as used in Fig. 3Aii–iii, Fig. S18C–D, and Fig. S19A–B designs ‘J’ and ‘F’; design *E* is for all tri-layer designs; design *F* was used for any staggered sheet; designs *G–J* are for the ribbons in Fig. S21.

<pre> AGTTTCGTCACCAGCAGTTGGCAAATCACACCCTCAGAACCG AGGATTAGCGGGGTCTAAAAATCTTTACAGTGCCCGTATAA ATGGAAAGCGCAGTCGTCAAATAGATAAATACCACCACAGAG TTCATAATCAAAATTTACAACAATTCGAATCAGTAGCGACA GTCACCGACTTGAGCGTTATTAATTTAATGGTTTACCAGCG CAGTATGTTAGCAGAACAAAGAAACAGTAGCAGATAGCC GAGCGCTAATATCACCTGATATCAGATATGAAAATAGCAGC ACCAACGTTAACGATGTTGGATTATACGAGCGCTTTAGCG GCACTCATCGAGAACCATATCAAAATAGAAAAATAATATCC TAAAGTACCACAATGCGTAGATTTTCAGCCACCGCTCAACA CCGACCGTGTGATACAGTACCTTTTACACTGATGCAATCCA TAGATTAAAGCGCTATGCTTGAATACCAGTACATAAATCA CCGGCGAACGTGGCAAAATCAAAGAATAGCCGACCTAAAG GCGGGCGTAGGGCTGCATTAATGAATCGGCCCGCAAAATCG GTAACCCACACACACAGTTGAGGATCCCGGGAGTCGGAA GCGTACTATGGTTGTGTGTTTCAGCAAATCGTTATCTTCGCGT CTCGTTAGAATCAGAACCAGAAATGCCAACGGTCAATAAAC AGGGATTTAGACAGTGTACATCGACATAAAAAGTGGTCTG GTTTTTATAATCAGGCCAAGCTTTCAGAGGTGGTTGCCGCCA ATCAGCAAATTAACACTCCAGCCAGCTTTCGGAGCTGTGA AATAACATCACTTGACGCCATCAAAAATAATCCAGTATCGG CTTGC TGGTAATATGTCATTGCTGAGAGTCTGAGCTCATTT AACAGAAAAACGAGAACGCTTTTATTCACGGAGAGATCT AATCGTCTGAAATGTCGAAATGGTCAATAACCTGACCCCTG CACACGACAGTACAGGTCAGGATTAGAGAGTTTGTGTTGA AGAACCCTTCTGACGCTATAAATATTCATTGAAACAGACCG CAATATTTTTGAATCAGTTGAGATTTAGGAATAATAGCGTCC TAGCCCTAAAAACATCATTCACTGAAATAGGCTTTTATTACAG AGCAGAAGATAAAAATAAATTTGTGCAAAATCCAAATCAAC GCCTGCAACAGTGCACGAGGGTAGCAACGGTAAACGGAGATT ATCTAAAGCATCACAAAAGGCTCCAAAAGGACCCAGCAGCGGA AATCAATATCTGGTTACAAACTACAACGCTTTTTCACGTT TTGAGGAAGGTTATTTGCTCAGTACCAGCGGGTAACTG TAATAGATTAGAGCCTCTGAATTTACCCTTCCAAGAAGGATT AGAAGTATTAGACTCAGCGAACCCAGACCCAAAGCCAGA ATCCTTTGCCCGAACCATTTGGGAATTAGAGCCTGCCATCTT ATTATCATTTTGGACGCTAGAAAATACATACATTTATCACC ATTATCATATTTGAGAGATAACCCACAAGACTTATTACG AATATAATCTGATGCTCTTTCCAGACCTAAAGGGTAATT AGGTTAGAACCTACAAGCAAGCCGTTTTTATCTGAAATCTT AGAAATAAAGAAATAAGGTAACATAATCTGTCCCAAGTACC TGAATATACGTAATAAAGGCTTAAATAAGAAAGAGAATA AACGGATTCGCTGGGAAAGAGTCAATAGTAAATTTGAAATA GCGCAGGGCGAATAATACCTGAGCAAAAGAGCGATAGCT </pre>	
--	--

Table 1 Oligonucleotide staple strand sequences for the 6HB slat. The 127 universal core staple strands are unchanging across all the 6HB slats folded, versus the 32 top- and 32 bottom-staple strands which are modified on their 3' end to encode functionality in the slats. The latter top- and bottom-staple strands are arranged in the order in which they are displayed along the length of the slat, where the nodal position is indicated with the leading number. Given top- and bottom-staple strand pairs with the same number overlay one another. In general, we reserved the top-staple strands to append handle or complementary handle sequences to bind the slats to one another. The bottom-staple strands were alternatively appended with strong handle “plug” sequences to bind slats to the gridiron seed, the complementary 16-nt handle sequence to bind the nanocube contrast agent, the complementary handle sequence to bind DNA-PAINT imager strands, with biotin to affix the megastructures to streptavidin coated flow chambers for DNA-PAINT, or with complementary handle sequences to bind other slats in case of the tri-layer ribbon.

12HB universal core staples	12HB top staples
<pre> ACCATCACCAAACTATTAAGAAGCTGGAGAGAGAGTTGCA GCAAGCGGTCCACGGTTTTTCTTTCAACATAAAGCCTGGGG TGCCTAATGAGTGGTGTGAAATGTTATCCCTGGGGCCAGAA TGCAGCGGGCCGTTGCCCGCTCATCAGACGCGGGTGGCG TATGAGCCGGTTCGCTGGAGGTGTCAGCAGCTGCTGGCAG CCTCCGGCCAGAGGGTAAAGTTAAAGCAGGTGAAGGGATA GCTCTCACGGAAGAAACGTACAGCGCCATCCAGCTGGCGAA AGGGGATGTGCTCCATTGAGCTGCGCAAGGGATAGGTCAC GTTGGTGTAGATGGTGGAGCAGTAAACCTATAAGCAATA TTTAAATGTAACATGCTCAATCATATGTAATCACCATCAA TATGATATTCAAATGCTGAGTAAATGTAAGAAATAGCAA </pre>	<pre> 1; CCTGGCCCTCTCCAACGTCAAAGGGCGACTTGACGGGAAAG 2; CATAAAGTGGTGAGACGGCAACAGCTGAGAAAGCGAAAGGA 3; TCTGTGGTGGCTCACAATCCACACAACCGGTACCGTGGCC 4; ATCCGCGGGATCCAGCGCAGTGTCACTCGCCGTACAGGGC 5; TTTTCGTTTCAGCGGGTCAATGCAAGTATAACGTGCTTTC 6; TTTTCGTTTCAGCGGGTCAATGCAAGTATAACGTGCTTTC 7; GCTATTACGGTTTACCAGTCCCGGAATGAACTCTGAGAAGT 8; GACCGTAATCTGTTGGGAAGGGCGATCGAAAAGAGTCTGTCC 9; GGAAGATTGCTGGATTTCCCGTGGGACTTCTTGTGATGAT 10; AGACAGTACCCCGGTTGATATCAGACTCAAATCTCGGC 11; GGCAGGCATAGGTAAGATTCAAAGGCCCGCACCCATTGC </pre>

AATTAAGCAATAAGGCATCAATCTACTAACTAAAGTACGGT
GCTTGGAGTTTCTGGCTTAGAGCTTAATTCATCAAAAAGAT
TAAGAGGAAGCCCCATAAATCAAAAATCAAAAATAGCGAG
AGGCTTTGCAAAACAGGACATAGTAAGAGGCTCATATACC
ACTAAAACACTCACCATTAACGGGTAATAAATACCGATATA
TTCGGTCGCTGAGTCTTAAACAGCTTGATCAACTTCAACA
GTTTCAGCGGAGTAAGTTTGTGCTCTTCGACCCGCCACCC
TCAGAGCCACCACTAGGTGTACCCGTACGCCCTGCCTA
TTTCGGAACCTATGTAATAAGTTTAAACGGATTGACAGGA
GGTTGAGGACGCTCACCTCAGAGCCACCATTGCCCTTAGCG
TCAGACTGTAGGAAACCTCACCAATGAAAAAGGGCGACAT
TCAACCGATTGAGATAAGTTTATTTGTCATACCAAGAGAA
ACCGAGAAACGCCAATAGCTATCTTACCGAATAAATA
AAAACAGGAAAGCTCAAATAGAAACGATCTGCGGGAGG
TTTTGAAGCCTTACAGATATAGAAGGCTTATACGAGCATGT
AGAAACCAATCAAGCCCTGTTTATCAACAATAGAGAATCG
CCATATTTAAACAATCATATGGCTTATACAAAGAACCGGA
GAAAACCTTTTCAACCGCTTAGGTGGGTAGTGAATAACCTTGCT
CACTAAATCGGAAGATAGGGTTGAGTGTGGCAAAATCCTGT
TTGATGGTGTAAACGGGGGGGAGAGGCCGCTGCGCTCAC
TGCCCGCTTCTACCGAGCTCAAAATTCGGGTTTCGCCAGC
ACCGCTGCTGTACGGCATCAGATGCCGGTAAAGGGTAAAG
GTTTCTTGGCTCGAGACCCCTCGGTGCTGCGCCGACTGT
TAGAACGTCAGCAATCCCGTAAAAAAGCGGATCAAACTTAA
ATTTCTGCTCATAGCCGCAAGGAAACGGTAAACCGAGGTT
TTTCCAGTCAGCACCCCTCTGGTGCCATCTGCCATTTG
AGGGACGACGAGGCTCGGCTTCTGTATTCGATTAAT
TTTTGTAAATCGAGCAAAACAGAGAACTAAAGCCGAGAGG
GTAGCTATTTCAAGGATAAAAATTTTAAATCGGTGT
CCAAAACATTATGTTAGCTATATTTCTTCCAAATCTCG
GAACGAGTAGATACCTTAAATGCTCTTCTGTTTAAATCGA
GCTTCAAGCGATCCCGCTCAATGCTTTGTAATAGTAAAA
TGTTTAGACTGGCCACATCAACTAATGCAATAAAACGAAT
AAACAAAGTACACAGAGGCTTTGAGGACTGCCGCTTTGCGG
GATCGTACCCTTAAATGTATCGGTTCTAAGGAATGCG
GAATAAATTTAGCATTCCACAGACGCCAAGCCCAATAGG
AACCCATGTACCAATAGTCCGCTGAGAGTAAAGAGGCTG
AGACTCTCAAGGTAAGCGCTATACATGGATTCAACAACAAA
TAAATCCTTACCGGAACCGCTCCCTCGGTATAGCCCC
CTTATTAGCCTTAGCAAAATCACCACTAGGAGCAAAATATT
CATTAAGGTGAAAAGCTGGCAACATATAAAAAGACTGGCA
TGATTAAGACTCTTGAGTTAAGCCCAATAAATGAACCCCT
GAACAAAGTCAGTTTGGCAGTTACAAAATTTTTCACCCAGC
TACAATTTATCTTCATCGTAGGAATCATATCATTTCCAAGA
ACGGGTATTAACAGACGACGACAATAAAGCAGAGGCAATTT
CGAGCCAGTAAATAAACACCGGAATCATCATCTCTGACC
TAAATTTAATGGTTTATCAAAATCATAGGTTCCCTTAGAATC
GGAGCCCGCTTTTTTTGATTTAGAGAAAACCGCTCATCA
GCAAAATCCCTTATGAGAAAAGGAAATTCGCCCTCACCG
ACCTGTCGTGCCAGGCTGGCAAGTGTAGATACGAGCCGGAAG
CCGTGAGCCTCCTCCGCGCGCTTAAAGGGCGCTGTGCAC
ATCCCTTACACTGGCTTTGACGAGCAGCGCTTTCGCACCTA
GTCCTGTCAGCAGCAGCGGAGCTAAACAAACGCGCTCGCTT
GCAGTTGGCGGTTGGAACGCTACGCCATGTGAGAGATAGAC
AAACGACGGCCAGTTGAGGCCACCGAGTGTGGGGCCTCTC
CCTCAGGAAGATCGCGCTGTAGCAATAAACAACGGCGGAT
TTTAAACCAATAGGACCTGAGTAGAAGAAAAGCCCAAAAACA
ACAAGGCTATCAGCCAGAACATATAGTGAGAAAGGCGCG
AATACTTTGCGGCTCATGGAATACCCTAATAAATCATACA
CCATAGATACATGATTTTACATTTGCTCAACATGTTTAA
GAGCAAACTCCAATAAAAAGGACATCATAGTCAGAAGCAA
AATACTGCGAATCCTGAAAGCTGAAAGTTTACCAGACGAC
GTAGAAGATTCTAGGCTATAGTCTTACCCTATGCGATTT
GTAAACAACTGCTGCCATTAATAAAGGAGCAGATGA
TGTATCATCGCTCGAGAGGTGAGGCGGGCACCACCTAAA
AGACAGCATCGGACACGCTGAGGCCAATGACAACAACCAT
GAAAATCTCAAACTTGTGAACCTCATTTCTGTATGGAT
AGTTTGTGACCCAGCTGGCAATCACCCCTCAGAACCG
AGGATTAGCGGGCTCAAAATATCTTACAGTGCCCGTATAA
ATGAAAAGCGCAGTCGTAATAGATAAATACCACCCAGAG
TTCATAATCAAAATTAACAACAATTCGAATCAGTAGCGACA
GTCACGACTTGAGCGTTTAAATTTAATGGTTTACAGCG
CAGTATGTTAGCAAGAACAAAGAACAGTAGAAGCAGATAGCC
GAGCGCTAATACACTGATATCAGATAGAAAATAGCAGC
ACCAACGCTAACGATTTGGATTATACGAGCGCTTTTAGCG
GCACTATCGAGAACCATATCAAAATAGAAAATAAATATCC
TAAAGTACCAGCAATGCTAGATTTTAGCAGCAAGCTCAACA
CCGACGCTGTGATACGTACTTTTACACTGATGCAAAATCCA
TAGATTAGACGCTATTGCTTGAATACCACTACATAAATCA
CCGGCAACGTGGCAAAATCAAAAGAAATAGCCGACCCATAAG
CGGGCGCTAGGGCCTGCAATTAATGAAATCGGCCCGCAAAATCG
GTAACCAACACACAGTTGAGGATCCCGGGAGTCGGAA
CGCTACTAGGTTGTGTTGAGCAAACTGTTATCTTCCGCT
CTCGTTAGAATCAGAACCGCAAGAAATGCCAACGGTCATAAAC
AGGATTTAGACAGTGTACTCGACATAAAAAGTGGTGTGCT
GTTTTATAATCAGGCCAAGCTTTCAGAGGTGGTTGCCGCA
ATCACGCAAAATTAACACTCCAGCCAGCTTCCGGACGTTGTA
AATAACATCACTTAGCCCATCAAAAATAATTCAGATACCG
CTTGTGTAATATGCTATGCTGAGAGTGTAGCTCATTT
AACAGGAAAACGCAAGCCTTTATTTCAACGGAGAGATCT
AATCGTGAATGTGCAAAATGGTCAATTAACCTGACCCGCT
CACACGACGATACAGGTCAGGATTAGAGACTTACTTTGA
AGAACCTTCTGACGCTCAAAATTAATGAAACCAAGACCG
CAATATTTTGAATCAGTTGAGATTAGGAATAATAGCGTCC
TAGCCCTAAAACATCATTAGTGAATAAGGCTTTTATTACAG
GCTGCAACAGTGCACAGGAGTACCAAGGCTAACGGAGATT
ATCTAAAGCATCAAAAAGGCTCCAAAAGGACCGCAGCAGGA
AATCAATATCTGGTTCAAACTACAACGCTTTTTCACGTT
TTGAGGAAGGTTATTTGCTCAGTACCAGGGGTAACACTG
TAATAGATTAGAGCCTCGAATTTACCGTCCAAAGAGGATT
AGAAGTATTAGACTCACCGGAACCGAGCCCAAAAGCCAGA
ATCCTTTGCCCGAACATTTGGGAATTAGAGCTGCATCTTT

12; AATATGCANTAGTAGCATTAAACATCACATTTGACGCTC
13; AGCGGATGGCTGAATATAATGCTGTAGGACAGATTCACCAGT
14; GATAAAAACCGCTTACCCTGACTTTTGCCCAACAGAGAT
15; TAAGAACTGACACACTATCATAACCCCTCATACGCGGACAGA
16; ACGGTGACACTTTAATCATTGTGAATTAATGCGCGCACTGA

12HB bottom staples

1; TCTGTAATTAACAATTTTCATTTTTTAAATGAAAACAAGTTACAAAAAT
2; ATATATGTGATATAACTATATGTAATGTCGGGAGAAAACAAT
3; ATCGCAAGAAAATTTACCAGTATAAAGTTTAAACGTCAGA
4; GTAGGCTTATAGATAAGTCTGACAAATTTGACAGTAAAAAC
5; CATCCTAATTCGGGATTTAAGAACCTTCTGAATAATGGA
6; AACCTCCCGTTTTTGTAAACGTAAGGATGGAATTCATC
7; CTTTACAGAGAACCCCTTTTAAAGAAAACGGAAGGACCGGA
8; GAACAAGTCAATCAATAGAAAATTCATAAAGTTTGGATGAC
9; CCAAGACACCATCGATAGCAGCACCGTACACTGATTAATA
10; GAATCAAGTCCCTCAGAGCCGCCACAGCAATTTGAGGATTT
11; CCGCCCGAGGGTCACTGCTTGGTAAGGAGCACTAAACAAC
12; ACAGTTAATTCAGGAGTTTGTAGTACCGCACAGTTGAAAGGAA
13; CACCCCTCACAGACTAGTAAATGAAATAATATCAAAACCTC
14; TTTGCTAAACCGATAGTTGCGCGCAGCAGCAATGAAAAC
15; CGCCACCGTCACTAATGCCACTACGAATCAGATTTAACCC
16; ACGAAGAGCCGCACTGACCACTTTGACCGAACCAACCC

<pre> ATTATCATTTTGCGACGTAGAAAATACATACATATTATCACC ATTATCATCATATGAGAGATAACCACAAGACTTATTACG AATATAATCCTGATGCGCTTTCCAGAGCCTAAGGGTAATT AGGGTTAGAACCTACAAGCAAGCCGTTTTTATCTGAACTTT AGAAATAAAGAAAATAAGGTAAGTAATCTGTCCCAAGTACC TGAATATACAGTAAAATAAGCGCTTAAATAAGAAAGAGAATA AACGGATTGCGCTGGAGAAGAGTCAATAGTAAATTTGAAAATA GCCGAGAGGCGAATAATTACCTGAGCAAAGAAAGCGATAGCT AGTCAGGACCTGGAGATGGTTAATTTCAAGACCAGGCTttttttt AGCAGAAGATAAAAATAAATGTGTGCGAAAATCCCAAAATCAACTttttttt ACATTAATTTGGTTTGGCTATTCCTTTTAACTAATATATTT CATACCGGTAATCATGCTCAAGCGCTGTTAGCGCAACAT CTGCGGCTGGTTACCTGCAGCCTAATGCAGAACTAATCGGCT ATAACGAAAGCCATCCACGCTAGCAAGCAAAATAATCAAGAT AGAAACAGCCGCACAGGCGCTATTATCCCAAGCATTAGAC TTAAGTTGGATAAACCCTACCCGAACAATGAAATAAATAAAC TAACCGTGCAGAAACAGGCAAGACACCCAGGAGGAGGAAAG TTTGTAAAAGCCAGCTTTCATAGCAAGCCGCGCTTTCAT TGATAAATGATGAACGGTAACCTCAGAAACCCGACAGGATT GCATAAAGCAGAACCCCTCATACAGGAGTACTTATTCTGAA AACAGTTGAAATTTGGGGCGGTATAGCCCGGAACCTCATT CAAAATATCGTTGATAAAGAGTCTAACGATCTAGAGAATAAGA GCCAGAGGAAACAGTTAGATTCGAGGTGAATGCTTGACGG ATCTACGTTAGATACATAACGATGAGGAAAGTTTCTTTGACC CTCAGAACGAGTAGCGAGGCGCAGACCT CCCCAGCAGTTCCAGTTGGATTAATACATTCTCGCTAT AACGGAAACAACAGCCCTGACGAGAAAACACTGttttttt GAGTTAAAGAAAGACTTTTCCAAAAGGAATAGAAGTTTT AAGGAACAATATCAGCTTGTAAACGAGAATGAGAAAGACTT CAGGGATAGCCTCATAGTTAGCATTTTTGGGAATCCATAT ACATGAAAGGGTTGATATAAGAGCTGAAAAGTAGCCTCAGA GGCCTTGATCTTTGATGATATATTTAAATGCCGTTCTAGC CGGCATTTTCCAGCGCCCACTCGTAAAACCTAGCGTTAATAT GTAAATATTACCATTACCATTCAACATTAATGGCGCATCG GGAATACCCAAAGAAACGAAAAGCGCCATTCGGCAAGGCGGA GGGAGAATATAAGAGCAAGAGAAACAATCGCAAGAGACGC TAGTTGCTAAAACAGCCATCTTTAGTGTAGACACATCCTC GTCTTTCCTTACCAGCCCAAAACAGCTTACGACTGTTGCC GTAATTTAGCAACATGTTACGAGCGGTGCCGTTTCCAGGT TACTTAATTAATTAAGTAAATAGCTTCTTCCAGCTAACCTC TAATTAATTTCTGAGAGACTAGGCGCCAGGCTGCTGTTG CCCAGCGATACTTAGCCGAAATAAATGGGCTTGAAGAAAA ttttttttTTCATTACCGGACCTGCTCCATGTTTATACCAAGCGCG CTTGAAAACATAGATGATGAAACAAAACAAAACAGAGTCCATCAAGTTTTTTGGCCGTAAG ttttttttACGGTCAATCATAAAGGGAAGCAAAAAGAAATAC </pre>	
---	--

Table 2 Oligonucleotide staple strand sequences for the 12HB slat. The 158 universal core staple strands are unchanging across all the 12HB slats folded, versus the 16 top- and 16 bottom-staple strands which are modified on their 3' end to encode functionality in the slats. The latter top- and bottom-staple strands are arranged in the order in which they are displayed along the length of the slat, where the nodal position is indicated with the leading number. Given top- and bottom-staple strand pairs with the same number overlay one another. In general, we reserved the top-staple strands to append handle or complementary handle sequences to bind the slats to one another.

seed universal core staples	seed non-socketed staples
1; TACCGCCACCCCTCAGAACCCGCTCGAGAGGGTTGATATAAG	65c1; GGGAAATTAGAGCCAGCAAAATGTTTATGTAGATGAAGGTATA
2; TCATTAAAGGTGAATATCACTTCTGCAATGTGCGAGAAAATG	66c1; ATTCATATGGTTTACCAGCGCTATCACGAGTACGGTGGAAAC
3; TAGCAAGCAAAATCAGATATAGCAGGGATAGCAAGCCCAATAG	67c1; CCTTGAAAACATAGCGATAGCGAGTTAGAGTCTGAGCAAAA
4; GCTTCTGTAATCGCTGCTATAAACAATATAGATGATTAACCC	68c1; ATTAATTAACATTAACAATTTGCACTCGCGGGGATTTATTTT
5; AGTATTAACACCGCCTGCAACACAGACAGCCCTCATAGTTAG	69c1; TGACGGGAAAGCCGCGCAACCTTACTGTTTCTTACATAAA
6; GCATAAATCGGAACCCATAAATTTGTTTTATGAGAGTGATA	70c2; TAGCAAGGCGGAAACGCTACCGGAACAGCCCTTAGTAAC
7; CAAAGGCGAAAACCAACACAGCTGATTTGCCCTGCGCCAGG	71c2; AGACACCAGGAATAAGTTTATGCAGATCCGGTCTTGTCT
8; AGTCACATATAAAGAAAGAGTTCGACAGCAAGCAAGCGCG	72c2; AGTCAATAGTGAATTTATCAAGTATCTGCATATGATGCTGA
9; TAGGTTGAGTGTGTTGCCCCAGCAGGCGAAAACCTGTGTCG	73c2; CTGAGCAAAAGAGATGATGAGAAACGACATACATTTGCAAGG
10; TTTTTTTTTAATCCCTTATAAATCAGTTCCGAAATCGGCAATTTTTTTTTT	74c2; AAAGCAAAAGGAGCGGCGCTCTGAAATTTCCGCTGCTCTCA
11; TTTTTTTTTTGTGAGAGCGGCGCTCATCA	75c3; CACCGTAATCAGTAGCGACAGGTTCTTGTGTTCCGCATCC
12; GTGTTTTTTGTTTCCCTGTGTGAAA	76c3; AAAATACATACATAAAGTGGCTIATACGGGTTGGAGGTCA
13; CGTATTGGTCAACCGCTGCGCCCTGACGTGGAACCTCAACGT	77c3; CCTTTTAACTCCGGCTTAGTGAGTATTACGAAGGTGTTAT
14; GGGGAGAGATTTCCACAACAATAC	78c3; AGTTACAAAATCGCGCAGGAGAGTGAATCGGTTTTGTAA
15; GAATCGCCGCTCCACCTGTTTTTCCAGTTTGGAAACAAG	79c3; GTCAGCTGCGCGTAACCAACCCAGGAGAACGAGGATATTGC
16; TGCCAGCTGTGTAAGCCTGGGGT	80c4; CAGACTGTAGCGGTTTTTCATAACGAAGACCGCTGTGCTGTT
17; GTCGGGAATCCTGTTGATGTTGAAAGAATAGCCCGAGA	81c4; ATGATTAAAGACTCTTATTACTGCTAAACTGGAAAGCAACGA
18; TTTTTTTTTTGTGCGCTCACGCCAATCATATAATTTGCTTTTTTTTTT	82c4; TAAATGCTGATGCAAAATCAACGAAGTGAAGCAAAATTAATC
19; GTCATAGCTCTTTTACCATTTTTTTTTTTT	83c4; GGGAGAAAACAATAACGGATTTCTGTGAGCTTGAACAGCAAA
20; TTGTTATCCGCTCACAGCGGTTTTG	84c4; CCGCTACAGGCGCGTACTATTTTCCATGAAATGGTAACACC
21; GAGCCGGAAGCATAAAGCATTAAT	85c5; CCTTATTAGCGTTTGCCATCTGCAACAGCAATAAAAATGC
22; GCCTAATGAGTGAGCTGTTTCCA	86c5; CCGAGAAAACGCAATAAATACGTTGCCAGGAGATCTGGAAC

204; GGTAGCTATTTTGGAGAGATCATTAACCGTTGTAGCAATACT
 205; ATGGTCAATAACCTGTTTAGCTTGGCGAACAAGAAACCACC
 206; CTGTAGCTCAACATGTTTAAAAATCCAGAACAAATATTACC
 207; GGCTTTGCAAAAAGAGTTTAGACTTTGCAAAACAATTCGAC
 208; AGATTTAGGAATAGCACATTCAATGGATTATTCAATTGGC
 209; CGAGGCGAGACGGTCAATCAGTTATCAAATATCTTTAGG
 210; CTAACAACACTCATCTTGGCCCTGACCTGAAAGCGTAGAAT
 211; CGAATAATAATTTTTCACGATACACCTTGCTGAACCTCAAA
 212; CGTAACGATCTAAAGTTTGTAAACATGCCATTAAAAATACC

101c8; GAATTGAGTTATTTTAAACCAATAGGAACGCCA
 102c8; AGTATCATATGGACAGTCAAATCACCATCAAT
 103c8; TCAATATAATCGAAGATTGTATAAGCAATAT
 104c8; CCATCAGCAATACAAGGCTATCAGGTCAAT
 105c9; GTCAGACGATTGCATAAAGCTAAATCGGTTGT
 106c9; CAGAGGGTAATGTAAATGTAGGTAAAGATT
 107c9; ACGCTCAACAGTCTACTAATAGTAGTAGCATT
 108c9; GAATTATCATCTGATAAATTAATGCCGGAGAG
 109c9; GTAATAACATCACCATTAGATACATTTCCGCA
 110c10; ATTAAGCCAGCAAATATCGCGTTTAAATTCG
 111c10; CGCATTAGACGCAAGGCAAGAAATTAGCAAA
 112c10; AACCCAAACATTTGCTCCTTTTGTATAGAGGT
 113c10; ACATATCATTTATATTTTTCATTTGGGCGCG
 114c10; GCCTTGCTGTATATGCAACTAAATAGCGTG
 115c11; CCAATAAGCGTAAAAATCAGTCTTTACCCTG
 116c11; AAATAGCAGCCGGAAGCAAACTCCAACAGGTC
 117c11; AATAAGAGAAATCAATCTGCGGAATCGTCATA
 118c11; AAATCCTTTGCGCTTAAATGCTGAATATAATG
 119c11; GCAACAGGAAAATAAAAACCAAAATAGCGAGA
 120c12; CTGGTAATAAGTAATTTCAACTTTAATCATTG
 121c12; AATCCAAATAAAAATGCTTTAAACAGTTCAGA
 122c12; GTCACAGCACATCTACGTTAATAAACGCAAC
 123c12; TTAGAAGTATTGCCAGAGGGGTAATAGTAAA
 124c12; TCAATCGTCTGAACATAATGCAGATACATAACG
 125c13; GCCCGTATAAACGTAACAAGCTGCTCATTCA
 126c13; TAATTTGCCAGAAGAACTGGCTCATTATACCA
 127c13; ACGCGCTGTTCCGGTACAGACCCAGGCGCAT
 128c13; ACTAATAGATTGGTAGAAGATTTCATCAGTTG
 129c13; GTCACACGACCCCTCCATGTTACTTAGCCGGAA
 130c14; ATTATTCTGAAAAAGACAGCATCGGAACGAG
 131c14; ATCCTGAATCTGAGTAATCTTGACAAGAACCG
 132c14; AATAATATCCCGGTAATAACGTAATGCCAC
 133c14; AATTGAGGAAGTAAGGGAACCGAATGACCAA
 134c14; ATAGAACCCTCCAGGATTATACCAAGCGC
 135c15; AAGAGAAGGATGCCACGCATAACCGATATAT
 136c15; TAAATCAAGATTGGAGCTAAAGACTTTTTC
 137c15; AATAATCGGCTGTATCGGTTATCAGCTTGCT
 138c15; TCAATCAATATCGAAGAGGCAAAAGAAATACA
 139c15; GCAATATTTTAAAGAACACTAAAGGAATTG
 140c16; CGGTAAGTCCACCCTCAGAACCCACCCT
 141c16; CGTTTAGCCAGCTTGATACCGATAGTTCCG
 142c16; AAACCAAGTACGAGTTTCGTCACCAGTACAAA
 143c16; AAATCTAAAGCTGAAAAATCTCAAAAAAAGG
 144c16; GATAGCCCTAACGCTTTCCAGACGTTAGTAA

plug sequences for the seed

65c1; GGGAAATTAGA
 66c1; ATTCATATGG
 67c1; CCTTGAAAAC
 68c1; ATTAATTACA
 69c1; TGACGGGGAA
 70c2; TAGCAAGGCC
 71c2; AGACACCAG
 72c2; AGTCAATAGT
 73c2; CTGAGCAAAA
 74c2; AAAGCGAAG
 75c3; CACCGTAATC
 76c3; AAATACATA
 77c3; CCTTTTAAAC
 78c3; AGTTACAAA
 79c3; GTCACGCTGC
 80c4; CAGACTGTAG
 81c4; ATGATTAAGA
 82c4; TAAATGCTGA
 83c4; GGGAGAAACA
 84c4; CCGCTACAGG
 85c5; CCTATTAGC
 86c5; CCGAGGAAC
 87c5; AAAACTTTTT
 88c5; TTTAAGTCA
 89c5; TAACGTGCTT
 90c6; AACCAAGGCC
 91c6; AGAAAAGTAA
 92c6; CTAATTTAA
 93c6; TGCACGTAAA
 94c6; GAGGCCGATT
 95c7; CCTCAGAACC
 96c7; AACAATGAAA
 97c7; GCGTTAAATA
 98c7; CTGAATAATG
 99c7; ATCCTGAGAA
 100c8; CACCAGAAC
 101c8; TAACCCACAA
 102c8; AAGCTGTTT
 103c8; TGGCAATTCA
 104c8; AAGACTCTGT
 105c9; GTTGAGGCG
 106c9; TGAACAAAGT
 107c9; TATAAGCCA
 108c9; AGAAGGAGCG
 109c9; TCTTTGATTA
 110c10; ATAAATCCTC
 111c10; AAACAGGGAA
 112c10; CATATTTAAC
 113c10; AGTTGAGTA
 114c10; CAACTATCG
 115c11; ATTTACCGTT

	116c11; TCAAAAATGA 117c11; TCGAGCCAGT 118c11; AACTCGTATT 119c11; GCCAGCCATT 120c12; CAGGAGTGTA 121c12; TATTTATCCC 122c12; AAGTAATTCT 123c12; ATTTGAGGAT 124c12; ATTTTGACGC 125c13; GAGTAACAGT 126c13; TTCCAGAGCC 127c13; CTAATGCAGA 128c13; AGCACTAACCA 129c13; AGATTCACCA 130c14; TTCGGAACCT 131c14; CTACAATTTT 132c14; GAACAAGAAA 133c14; AGTTGAAAGG 134c14; GCCAACAGAG 135c15; GAGACTCCTC 136c15; TTTGAAGCCT 137c15; GAAACCAATC 138c15; TATCAAAACC 139c15; ACGTGGCACA 140c16; CAGTACCAGG 141c16; GAACCGGAGG 142c16; AACGGGTATT 143c16; AGCAAAATGAA 144c16; TGCGCGAACCT
--	---

Table 3 Oligonucleotide staple strand sequences for the gridiron seed. There are 212 strands in the overall gridiron origami seed, with the leading numbers in front of each strand denoting its identity. Strands 65–144 are necessary for making the 16 seed columns that each bind a single slat using five sockets (see Fig. S2). The non-socketed staples are full length 42-nt strands which will not allow binding of plug handles on slats, versus the socketed staples which have 10-nt removed from their 5' end to form a socket from the exposed seed scaffold. The column location for each of these strand types is denoted with c1–c16, where a matching set of five 10-nt plug sequences must be added to each corresponding slat in the order as written. The universal core staples are not implicated in binding of slats to the seed.

universal reference square staples	universal reference square staples
tttttttAAATCGGCAAAATCCCTTTGATGGTGGTTCCGttttttt tttttttGAAAGGAGCGGGCGCTAGGAAGGAAGAAAGCttttttt tttttttAGTGAAGTAACTACACCTGGGGTGCCTAATGttttttt tttttttAGTAAAAGAGTGTGTCATCAGTGAGGCCACCGttttttt tttttttGTCACTGCGCGCTGTGACAGTCCAGCCAGTttttttt tttttttAAAAGGGACATTCCTGGTCAACAGCCAGTAATttttttt tttttttTCCCAGCAACCCAGTACCGTCGGTGGTCCAttttttt tttttttAAGCATCACCTTGTGGCAAAATGAAAAATCTAttttttt tttttttTTGGCGGTTGTGTAACATTTGCCCGCAGCAGttttttt tttttttGTAACATTAATCATTTTAAATTTAAAAGTTGAttttttt tttttttCGATTAAGTTGGTAAAGGATGTGCTCAAGGttttttt tttttttATCGGGAGAAACAATAAACAAGTACCTTTTACttttttt tttttttACGGCGGATTGACCGTTTCCCGTGGGAACAAttttttt tttttttTTCCCTTAGAATCGTGTGCTAATTAATTAATttttttt tttttttGTAAGTACGATGTCGATGAACGGTAATCttttttt tttttttATACCGACCGTGTGATAATTTAATGGTTGAAttttttt tttttttAGAAGCCTTATTCAGTAATACCTTTTGGGGttttttt tttttttGTCCAGACGACCAAAAAGGTAAGTAATTCttttttt tttttttGATTCGCAATTCGCGATTCCATAAACAAGTttttttt tttttttATAGCAAGCAAAATCAGATCAATACCCGCCAttttttt tttttttAGCGGATTCGATCAAAATTAATGTCAGAAAGTttttttt tttttttTTTGTTTAAGCTCAAAAATTAAGAAAGTttttttt tttttttACGAGGCATAGTAAGAACCCGAAAAGGAATttttttt tttttttAACAAGTTACCGAAGTAAGCAGATAGCCGttttttt tttttttATAAGGCTTGGCCTGAGCTGCTCAATTCAGTGAAtttttt tttttttGGGAGGAAAGTAAATACATTTCAACCGATTGAttttttt tttttttGGCGAAACAAAGTACCCAGCGATTATACCAAttttttt tttttttCTTATAGCGTTTGGCTTTGGTGCATAGCCCTttttttt tttttttTAACCGATATATTGGAAACATCGCCAGCGAttttttt tttttttAGTCTCGAATTTACCCGAAATGGAAAGCGCttttttt tttttttGTCTTCCAGACGTAGATCTAAAGTTTGTCTttttttt tttttttTCGAGAGGTTGATATAGCGGATAAGTCCCGttttttt GGCGAAGAGGGCCTGGCAAGTGGAGAAGT TTAGAGCTGCGTAACCCACCACTTTTGA CTAAATCCCGTACAGGGCGCGCGGAGC	TCATCAACGCATCGTAACCGTGCAGGGCGATC CCGTGGAATGGGATAGGTCAACCCAGCTG CTGACCTAAAATAGGGCTTAAATATATAAAG TTTTCAAAAATCATAATTACTAGAGCAGAGGC CCAATCGTCATATGCGTTATACCCATATTT TTATATAAAAAGCCAACGCATATGATATTCA TTTTGTAAAGCTGATAAAATTAATGGGGTGAGA TAAGCAATTTTGGAGAGATCAGCCTGAGT ATCAAAAATTCCTGAGAGTCTGTTTGTAGA AACACCGGTATTTTAGTTAATGCTTAGA GTTTAGTACAGACAAGAACCGGTGAATTT ACCAGTATCTATATGTAATGCTGCTACCTTT ACCGTCTAAATTCGCATTAATTTTGGGG GGTAGCTAATTTAAATTTGTAATCAAAAAT ATCAGTACAGCCCAAAAACAGGAGCCAGCTT CAAGAGAAAATCATAATGACCCCTAACAC TACCGACAATAACACATGTTTATATTTCA ATTTTCGAGCGGTTTATCAACACCGCACTC AACACAGAAAATAATAATCATCATTC ACAGTAGGCGTGTAGAAATAGTAGCATTA AAGGCCGAAATCATACAGGCAAGCCGAGCT AATGTGTTAAGCAATAAAGCATAACTG ACCTCATAAATCGGTTTACCAATTTGACCA CAGAAGCGCCAGTAATAAGAGAAAGAATA TCCTGAAACCAACATGTAATTTAGAAAAGCCT ATTTACGAGCTTAATGAGAATCGAAATTTCT CATCCAAATAGACAGTCAAAATCACCATCATCA TTAGCAAAAAGGTAAGATTCAAAACCGGAGAG ATAAGCTATATTTTAAATGCAATCAAAAGGT ATGACCTACGCAAGGATAAAAAGAGCAAAA TCGTAGGAATATAGAAAGGCTTATCTTATTTAT ATCGAGAAGCGAGGCGTTTTCAGGTAATTTG AAGAACGGGAGGTTTGAAGCCTTACCAACG ATCAATAATGCTATTTTGCCTCTTTTGATA GAAAAGGTTTTTTCGGGATGGCTTCTCCAACA

(CAAAAG, -5.799)	(CGATCAA, -8.045)	(AACCTGGG, -10.562)
(AAGGAT, -6.269)	(GTTGGAA, -7.975)	(AGAGTCCT, -9.542)
(GACAAC, -6.699)	(CATCGAA, -8.045)	(AAAGTTCG, -9.062)
(CTTACT, -5.599)	(CGTTTTTC, -7.905)	(AACGCAAT, -10.002)
(CGTGAG, -7.709)	(GTCAATC, -7.365)	(AGGGTGTG, -10.612)
(AGGACG, -8.049)	(CCTAGAC, -7.715)	(AGATCGAT, -8.932)
(GCTCAG, -7.619)	(CCTTAAG, -6.975)	(AAGAGTGC, -9.862)
(ACTGAA, -6.439)	(GATGTCCG, -8.535)	(AAGAGCAC, -9.862)
(TTTGCT, -6.939)	(GCGTAAT, -8.255)	(AGCTCCGC, -11.382)
(GGCGTT, -8.709)	(ATTGCCT, -8.585)	(AAAGCTGT, -9.512)
(GGTTTT, -6.299)	(ATATCGC, -7.995)	(AAACTGGG, -9.722)
(CTCCAG, -7.219)	(CTTTCGT, -8.135)	(AAGGGTCG, -10.742)
(GTAGGT, -6.599)	(CGCAAAA, -8.805)	(AAACACCT, -9.272)
(GGTCAG, -7.379)	(GTAACAG, -7.185)	(ACTTACGC, -10.022)
(TTAGCT, -6.349)	(CACAATG, -7.665)	(AAGGAAAG, -8.572)
(CGTGAC, -7.869)	(ATGACTC, -7.595)	(AGGTACGG, -10.462)
(AGATAC, -5.499)	(GTGTAGC, -8.425)	(GATAAAGC, -8.202)
(GCTAAT, -5.999)	(GTCATAG, -6.925)	(GGTATAGT, -7.912)
(CGTAAT, -6.089)	(GTTATGC, -7.585)	(AGCATCCT, -10.092)
(CAAAAC, -5.959)	(GTTCTTG, -7.465)	(AAACCCAT, -9.272)
(ATCGTC, -7.109)	(ATCTCCG, -8.715)	(GCATATAC, -7.972)
(GTTAAG, -5.369)	(GCAACCT, -9.195)	(AGCTCATT, -9.252)
(ACGAGC, -8.449)	(CTGTAAT, -7.415)	(GACGTTAA, -8.802)
(CCTCAG, -7.219)	(TTACTGC, -7.935)	(AGGCTGAG, -10.542)
(CCTCAT, -6.769)	(ACTTCCG, -8.975)	(AACGGTAT, -9.172)
(TTGTGC, -7.599)	(CCTAATC, -6.875)	(AGGCAGAG, -10.542)
(ATACCC, -6.599)	(GAAATCC, -7.315)	(AAGGGAAT, -8.962)
(AAGGAG, -6.719)	(CCACAAA, -8.125)	(ATATGGCC, -9.582)
(GTACTT, -5.759)	(CATTGAG, -7.355)	(AAGTCACT, -9.012)
(GAGACG, -7.559)	(CTCGCAA, -9.385)	(AAACTCCG, -9.902)
(AACTCT, -6.269)	(ATTTCCG, -8.535)	(AGTTCCGG, -10.742)
(CTAGAT, -5.339)	(GTTCCGAT, -8.035)	(AGGTGAAA, -9.132)
(GAATCT, -5.779)	(GGTGAAC, -8.465)	(AACGTCGG, -11.232)
(AACTTG, -6.189)	(CGCTTAA, -8.215)	(AAGTAGC, -9.532)
(GCAAAC, -7.199)	(CCAAAAC, -7.725)	(AAACCGAG, -9.902)
(GTGATT, -6.089)	(CCTATGG, -7.865)	(AGGGGTAC, -10.132)
(AGGTCG, -8.049)	(TTCTTCC, -7.665)	(AACAGGGC, -11.292)
(TTCAGC, -7.289)	(GCTGTAA, -7.935)	(AAGTGACC, -9.622)
(GTTCAA, -6.209)	(GTTTCTG, -7.465)	(AAATGGTC, -8.782)
(CTATCC, -5.949)	(GAAGCAT, -8.095)	(ACATCTCC, -9.362)
(GATCTT, -5.779)	(GTTACAC, -7.345)	(ACGGTACT, -10.012)
(AAGGAC, -6.879)	(CTGTAAG, -7.025)	(AAAGTCCC, -9.572)
(AAGCAC, -7.429)	(GTTGCAA, -8.525)	(AGATGAGT, -8.752)
(GTTTCA, -6.089)	(CCTAAAC, -7.135)	(AGACACAT, -9.062)
(CAACAT, -6.239)	(CTAATCG, -7.205)	(AGGCCAAG, -10.802)
(GCAAAA, -6.709)	(CTTAGAG, -6.715)	(ACGTACAA, -9.362)
(GTAGAC, -6.109)	(GTACCAT, -7.575)	(AAGGGGAG, -10.252)
(GTGCAG, -7.929)	(GCTATTG, -7.425)	(AGAGACAT, -8.752)
(GTACAC, -6.419)	(CCATTAC, -7.185)	(AAAGCCAT, -9.512)
(CATAAC, -5.419)	(CTATCCT, -7.105)	(AACTGCAC, -10.172)
(TTGTCC, -7.379)	(CTCCCAA, -8.655)	(AGCAACAT, -9.562)
(TTGGGG, -7.989)	(CAACCTT, -7.955)	(GCGTATAA, -8.762)
(AGAGCT, -7.349)	(GAGTATC, -6.775)	(AGGGCTAC, -10.372)
(ATCGGG, -8.049)	(CTAACTC, -6.875)	(AGACCTAT, -8.422)
(ATCGAC, -7.109)	(GTGAATC, -7.365)	(AGGATCCT, -9.542)
(AAGGGT, -7.369)	(GCTGAAA, -8.215)	(GACCTAAA, -8.312)
(GTAACT, -5.759)	(GTTGTTG, -7.775)	(AAGCACGT, -10.842)
(GAGTTT, -6.039)	(GCCTAAT, -7.765)	(AACCCGAC, -10.902)
(AAGCAA, -6.939)	(CACCAA, -8.125)	(AGCTTATT, -8.922)
(GTACAA, -5.929)	(TTGAGCG, -9.385)	(AAGCTCCT, -10.042)
(CTTGAC, -6.539)	(TTCGCAA, -9.055)	(ACCTAAGC, -9.532)
(GCTAAC, -6.609)	(CAGTCAA, -7.865)	(AAATCCAC, -8.782)
(CTCGTG, -7.709)	(GTAGGAA, -7.385)	(AGCGAAC, -9.802)
(CAAAC, -6.189)	(CATATGC, -7.475)	(AGCCTTAT, -8.922)
(AGTCAT, -6.319)	(CTACATG, -7.075)	(AAACAGCT, -9.512)
(TTTGGC, -7.549)	(GGTATTC, -7.035)	(AGACTGCT, -10.092)
(GGATAA, -5.619)	(GTGAGTT, -7.855)	(AGGTTGAT, -9.012)
(AACTGT, -6.579)	(CCTTATG, -7.025)	(AAGCGGAG, -10.142)
(CTATAG, -4.669)	(TTGGTCC, -9.145)	(AGCTCGAG, -10.722)
(GAGAAC, -6.389)	(ATTGCTC, -8.095)	(ATATGCCG, -10.312)

(GCCAAG, -7.879)	(GTTGACG, -8.795)	(ACTTACCC, -9.292)
(CTACGG, -7.379)	(CTGAGTT, -7.695)	(ACCATTGT, -9.322)
(TTGCCT, -7.779)	(AAGACAG, -7.695)	(AGAGGAAT, -8.702)
(ATGACC, -6.929)	(TTTACCC, -7.645)	(ACGTTGAT, -9.502)
(CTCAAT, -5.929)	(GTAGAAC, -7.035)	(AGCTGAAC, -9.862)
(ATGTCC, -6.929)	(CATGGAA, -7.865)	(AGATGTGT, -9.062)
(GTCAAT, -6.089)	(GTAGGTT, -7.525)	(ACATAGCC, -9.582)
(ATTTGG, -6.189)	(GTCATTC, -7.365)	(AGCTCTAT, -8.662)
(AGAGAC, -6.619)	(TTAGACC, -7.385)	(AGTGAAGC, -9.862)
(ATTGGC, -7.429)	(CAAAACC, -7.725)	(AGCCTAGG, -10.212)
(CAATGT, -6.239)	(CAGAGAA, -7.555)	(AGGGTGAC, -10.462)
(AATCAG, -5.929)	(ACGATCG, -9.205)	(AGTGACAT, -9.062)
(CAATAG, -5.259)	(CTGATCT, -7.435)	(AGTTGGAT, -9.012)
(AGACAC, -6.929)	(GATTTCC, -7.315)	(AAACGAGG, -9.902)
(ATCAGC, -7.169)	(GCTATAC, -6.995)	(AGATTGCT, -9.252)
(GTGACC, -7.539)	(TTGTGCG, -9.695)	(ACATACGC, -10.072)
(CAATG, -5.849)	(GTCTGAA, -7.715)	(ATTGAGCC, -9.862)
(AGGTGG, -7.869)	(CCTTTTC, -7.415)	(AGCATGGC, -11.252)
(ACCGAG, -8.049)	(CTCACCT, -8.535)	(AGGTACAA, -8.852)
(AAAGCT, -6.769)	(CCAGTAA, -7.535)	(AGCAGAAA, -9.372)
(GCCTAG, -7.289)	(TTGTGTC, -8.025)	(GACTTTAC, -7.962)
(CTTCGT, -7.209)	(CCATTAG, -7.025)	(AGATCGCG, -11.212)
(CGATCG, -7.889)	(GATAACC, -7.035)	(AGCCTAAT, -8.922)
(GGATCG, -7.559)	(CCTAGAA, -7.225)	(AGCTGGAG, -10.542)
(GATCAT, -5.829)	(GCCTATT, -7.765)	(AAATAGCC, -9.022)
(CTTGAA, -6.049)	(CTCAAGG, -8.145)	(AAATAGGC, -8.692)
(CCTAAT, -5.599)	(GCTTTTG, -7.965)	(AACAGGTT, -9.272)
(GATAAG, -5.109)	(CTGTAGG, -7.865)	(ACATAGCC, -9.582)
(GGTAAA, -5.879)	(GTGAGAT, -7.595)	(ACGTGAAT, -9.502)
(GCACAG, -7.929)	(TTCTGCG, -9.385)	(AGGGCTAG, -10.702)
(GTATTG, -5.419)	(CTATTGC, -7.425)	(AGAGCAAC, -9.862)
(ATGTGC, -7.479)	(CTGGAAT, -7.695)	(ACCTACAA, -8.852)
(GTGAGC, -7.779)	(CCCATAA, -7.535)	(AAGGGTGG, -10.562)
(AGGGAG, -7.559)	(CGTCAAA, -8.305)	(AGGATTTT, -8.472)
(CATTAG, -5.259)	(TTGTCTC, -7.715)	(AGCTTCAT, -9.252)
(CTGAAT, -5.929)	(TTCAGTC, -7.715)	(AAGTACGC, -10.022)
(GAATGT, -6.089)	(GTCTCTT, -7.545)	(AAATTGCC, -9.282)
(CGGAAT, -7.209)	(CTTAACC, -7.135)	(AGGCCTAG, -10.212)
(ATTTCC, -6.369)	(CATTTGC, -8.015)	(AACTCCCG, -10.742)
(CGAAGG, -7.659)	(CGTCTAA, -7.715)	(AGGTACGC, -10.862)
(AAACAG, -6.189)	(GTAATCC, -7.035)	(AACCCACG, -11.052)
(ATGCCG, -8.599)	(CTAACTG, -7.025)	(AACACCGC, -11.452)
(CTCAAC, -6.539)	(CTAAAGC, -7.375)	(AGGTGCGAG, -10.482)
(GAAGCG, -8.059)	(CTCATGG, -8.195)	(AGCACAGC, -11.252)
(ACGGAC, -8.209)	(CCTTAAC, -7.135)	(ACGATTTT, -8.962)
(GTAGAA, -5.619)	(CAAGATC, -7.205)	(AAGGATAC, -8.192)
(AGGAGC, -7.959)	(ACTGTCC, -9.025)	(AGGTAGGC, -10.372)
(AAGCAG, -7.269)	(GTCTAAG, -6.875)	(ACCGTAAA, -9.292)
(TTGGAG, -6.889)	(GCTAAAC, -7.535)	(ATTTCCCC, -9.572)
(TTGCGC, -8.899)	(GAATGCG, -9.035)	(ACGTAAAC, -10.022)
(CTTCAC, -6.539)	(CCTGAAT, -7.695)	(AGTTTCGAT, -9.192)
(GGAAAA, -6.159)	(CTGATGC, -8.595)	(AGCAAGGG, -10.802)
(CACAAC, -6.849)	(GTTTCATC, -7.365)	(AGCAATGT, -9.562)
(CTAGAG, -5.789)	(TTGTACC, -7.695)	(ACATTCCT, -9.622)
(CTTGCT, -7.269)	(GTATCTC, -6.775)	(AAAGCTCT, -9.202)
(CTGTTC, -6.539)	(CAAACAG, -7.615)	(AGCATCGC, -11.432)
(GTGAC, -7.719)	(CTCCAAT, -7.695)	(ACCATTTT, -8.782)
(GATCAA, -5.949)	(CCTAGAT, -7.105)	(AGTAGCGC, -11.102)
(GAGATT, -5.779)	(CATAGAG, -6.765)	(ACCTAGAT, -8.422)
(ACACAT, -6.629)	(GTTGTGT, -8.165)	(AGGGCTTC, -10.652)
(CATCTT, -5.929)	(GAACATC, -7.365)	(ACTAACCT, -8.682)
(AGCAAC, -7.429)	(GAAAGTC, -7.315)	(AGCGTTAT, -9.412)
(ACGGAG, -8.049)	(GTAAGTC, -7.035)	(AAAAGCGT, -9.952)
(CCTATC, -5.949)	(GCTAAAG, -7.375)	(AAGAGTGG, -9.462)
(GTGAGG, -7.379)	(CTACATC, -6.925)	(AGGC AAAAT, -9.512)
(ATGGCT, -7.659)	(TTTAGCC, -7.885)	(AAAGCCAC, -10.122)
(CTGAAG, -6.379)	(CTTGTGT, -8.005)	(AAATACCC, -8.452)
(CTACAA, -5.769)	(GTTCTCT, -7.545)	(AGATCAGT, -8.752)
(GAATAG, -5.109)	(GTCTGAT, -7.595)	(AAGGTGTT, -9.272)
(GGAAAT, -6.039)	(CGTTAAG, -7.465)	(AGTCCTAA, -8.542)

(CTACTT, -5.599)	(TTCTGTC, -7.715)	(ATTTGGGC, -10.122)
(CTAAGG, -6.049)	(CCATATC, -6.925)	(AACTCGAC, -9.802)
(GTGACG, -7.869)	(GAAGTTC, -7.315)	(AGTAGAGC, -9.272)
(TTCCAG, -6.889)	(CCTAAGG, -7.815)	(AGGTTGAC, -9.622)
(CTTTAG, -5.209)	(GTCAGAA, -7.715)	(AAAAGGTG, -8.882)
(CTTTGT, -6.189)	(CCATTCT, -7.695)	(AGGGTAGG, -9.972)
(GTACAT, -5.809)	(CCGAAAT, -8.135)	(ACTAGACT, -8.422)
(AACCAA, -6.699)	(GAGATCG, -8.225)	(AGCACTAT, -8.972)
(CAATCT, -5.929)	(CTAATGC, -7.425)	(AGTACGCG, -11.192)
(GTAGAT, -5.499)	(GTTTGTG, -7.775)	(AGGTGGAG, -10.302)
(CTAAGT, -5.599)	(CATAACG, -7.515)	(AAACACGG, -10.212)
(CATGAT, -5.979)	(GCCAAAT, -8.355)	(GAGCTAAT, -8.432)
(GCCATG, -7.929)	(AACAGAG, -7.695)	(AAAAGACG, -9.062)
(CCAAAA, -6.309)	(GTTTGAG, -7.465)	(AGGCTAGC, -10.612)
(TTCACG, -7.379)	(GCAGAAC, -8.705)	(AAACTGGC, -10.122)
(GAATTC, -5.549)	(TTCCAAG, -7.815)	(AGATGCAC, -9.912)
(GAAAAG, -5.649)	(CTGTCCG, -8.195)	(AAGACCCG, -10.742)
(AATGAG, -5.929)	(CCTGAAA, -7.815)	(ACTTAGC, -9.272)
(AGCGAG, -8.289)	(GCTAATG, -7.425)	(AGCACAAA, -9.682)
(GTGAAA, -6.209)	(CAGCTAT, -7.655)	(AGCATGGG, -10.852)
(CATCAA, -6.099)	(AGCCCAA, -9.545)	(AAAAGCAC, -9.282)
(CATAGT, -5.649)	(GTTACTG, -7.185)	(ATAGAGGC, -9.272)
(GAACCG, -7.819)	(AAGTCAG, -7.695)	(AAACAGGG, -9.722)
(CTGAAC, -6.539)	(GTGTATC, -7.085)	(AGGTAGTT, -8.682)
(GTTCGT, -7.369)	(CCAGAAA, -7.815)	(ACATCTGC, -9.912)
(ATGCAC, -7.479)	(CTTGTCT, -7.695)	(AAGCTAAT, -9.172)
(GCAATT, -6.589)	(TTCCTCC, -8.505)	(AAAGTCCG, -9.902)
(CGGTAT, -6.929)	(GTATAAC, -6.755)	(AGACCAAT, -9.012)
(GTCGAG, -7.559)	(GTTAACG, -7.625)	(AAGAGAGG, -9.152)
(GTTTAG, -5.369)	(CGTAGAA, -7.715)	(AATCCGCG, -11.472)
(AATACG, -6.089)	(CACATAG, -7.075)	(ACGTATGT, -9.222)
(CGTTTT, -6.629)	(AAGTGAG, -7.695)	(AGTTAGCT, -8.922)
(GCTGAG, -7.619)	(CCTTACT, -7.365)	(GAATAACC, -7.962)
(GTTGAA, -6.209)	(CGAAAAG, -7.745)	(AAACAGGC, -10.122)
(GACTTT, -6.039)	(GTTCAAC, -7.625)	(AAGCAGAC, -9.862)
(GGTCTC, -6.879)	(GGATATC, -6.775)	(AGAGGAAA, -8.822)
(GTGAAT, -6.089)	(GGAATTC, -7.315)	(ACTGTACC, -9.342)
(ATGCGT, -8.149)	(ACCGTAG, -8.695)	(AGCGTAGC, -11.102)
(TTCTCC, -6.739)	(GTTGATG, -7.515)	(AAAGGACC, -9.572)
(CTTCAT, -5.929)	(CATGCAA, -8.415)	(GATTAAGC, -8.202)
(TTGTCC, -7.049)	(GTTGATC, -7.365)	(AAGCACCT, -10.352)
(CTTGAG, -6.379)	(GTTTCAC, -7.625)	(AAATCGAG, -8.802)
(GAGAGG, -7.069)	(TTGAACC, -7.975)	(AATCGCGG, -11.472)
(GTACCG, -7.539)	(CTACAAG, -7.025)	(ACGGTAGT, -10.012)
(GCTAAA, -6.119)	(CTAGATC, -6.615)	(AACGGAAC, -10.062)
(CATATG, -5.309)	(CCTATTC, -6.875)	(GATTTACC, -7.962)
(TTGCAC, -7.599)	(GTCAGAT, -7.595)	(ACGTACAT, -9.222)
(ATGGGG, -7.869)	(GTTAGTC, -7.035)	(AGGTCGTT, -10.292)
(CAGTTT, -6.189)	(GTATTGC, -7.585)	(AGGACATT, -9.012)
(CATCAT, -5.979)	(ACCTGCT, -9.425)	(AGAGAAGC, -9.552)
(GTAGCG, -7.779)	(GTGTCAT, -7.905)	(ACCTATGT, -8.732)
(CTTTAC, -5.369)	(TTTGTGC, -8.525)	(ATTACGCC, -10.022)
(ACGTCG, -8.539)	(CGGTAAG, -7.975)	(GAGTTAAC, -7.962)
(ATCGCG, -8.779)	(TTAGTCC, -7.385)	(AGCTTTTC, -8.972)
(GATGAT, -5.829)	(GCTCAAA, -8.215)	(AAGTTACC, -9.292)
(CTACCG, -7.379)	(GAAGTCG, -8.485)	(GAGTTATG, -7.852)
(ACTGCT, -7.659)	(CCAAGAA, -7.815)	(ACATCACC, -9.672)
(CTAACT, -5.599)	(TTCGTCC, -8.995)	(ACGCTAAT, -9.412)
(GTGGTG, -7.689)	(CTCATCT, -7.435)	(GATAAACG, -8.292)
(GGAACG, -7.819)	(GTTCCAT, -7.855)	(ACCTAACT, -8.682)
(GATATC, -5.009)	(GTTCCCT, -8.645)	(AGATGGCG, -11.032)
(GTAGTC, -6.109)	(GCTATAG, -6.835)	(AACGGACT, -10.292)
(CATTCG, -6.869)	(CTAAGTG, -7.025)	(AACCGGTT, -11.282)
(AGAAAC, -6.039)	(GCCTAAA, -7.885)	(AAGCCAAC, -10.122)
(AACTAC, -5.759)	(CAAATCG, -7.795)	(AAATGTCC, -8.782)
(ATACGC, -7.329)	(CTGCTAT, -7.655)	(AGGTGATT, -9.012)
(GTTGAT, -6.089)	(CAAGTAG, -7.025)	(AACAGGAC, -9.622)
(CGGAAA, -7.329)	(GTGACTT, -7.855)	(AGTGT CAT, -9.062)
(CATTCT, -5.929)	(GTTTTTCG, -7.905)	(AGTAAGCT, -8.922)
(ATGCGG, -8.599)	(GTGAAAG, -7.465)	(AAAGGTCC, -9.572)

(GTACGG, -7.539)	(GTGATT, -7.365)	(AGGATGAT, -8.752)
(GAACAT, -6.089)	(CTTGCTT, -8.195)	(AACCTGCG, -11.292)
(CTAGCG, -7.619)	(GCTAGAA, -7.625)	(AGGACAAC, -9.622)
(GACAAT, -6.089)	(CGTCACT, -9.025)	(AGCCTGAG, -10.542)
(GGTAAC, -6.369)	(CTAAGTC, -6.875)	(AGGACAAT, -9.012)
(CAACTT, -6.189)	(GTAAACC, -7.295)	(ACCCTAAT, -8.682)
(TTCCCG, -8.169)	(CGTGTA, -8.025)	(AACCTTCT, -8.962)
(GATTAG, -5.109)	(AACGTAG, -7.855)	(AGCTGAAT, -9.252)
(GATTTC, -5.549)	(CGTTTTG, -8.055)	(AAACCCGG, -11.002)
(GCACTG, -7.929)	(CAAGTTC, -7.465)	(AAATGACG, -9.112)
(GACACG, -7.869)	(CCTAGTT, -7.365)	(AGGTGAAT, -9.012)
(GAAAAC, -5.809)	(AGGTTTCG, -8.975)	(AGTCTCAA, -8.872)
(TTGCGT, -8.269)	(CGACTAA, -7.715)	(AGACGCCT, -11.372)

Table 6: The 6-, 7-, and 8-nt handle sequences and their NUPACK 3.0⁵² computed kcal/mol energies. Either the handle or complementary handle sequence from the above was appended to the 3' end of the top- or bottom-staple strand sequence with a TT linker. The majority of megastructures formed in this study used permutations of the 32 7-nt handle sequences, versus the 256 6-, 7-, and 8-nt handle sequences which were used to determine growth and spontaneous nucleation using ribbons.

9-nt, x128	10-nt, x100
(CAGCTACGA, -11.862)	(CTAGTCGACC, -12.404)
(TAATAGCAC, -9.932)	(TATTCATACG, -10.688)
(CAAAGTTTC, -9.318)	(CGCACATAAT, -11.814)
(CACATCAAC, -10.258)	(CCTGATCCTC, -12.244)
(TAACATCCC, -10.812)	(TATGAAACAC, -10.948)
(CGCATAAAA, -10.118)	(CCCTAGACCC, -13.014)
(TTTAAAAAA, -7.328)	(TAACATGGGA, -12.462)
(AATCAAAC, -8.868)	(CTTTTCTGCA, -11.828)
(TTGTCAATC, -9.618)	(TTGACCAATG, -11.534)
(ATCAAAATC, -8.608)	(CAATATCGCA, -11.778)
(TTTCAACT, -9.218)	(TAAATACATT, -9.168)
(CAAGACCCT, -11.228)	(TAATCAACGT, -11.618)
(ATGGCCTTT, -11.278)	(ATTACTCCCG, -12.054)
(ATTGTGCCT, -11.328)	(ATACCATCGG, -12.104)
(TCGAATCTG, -10.802)	(GACTAGCCGT, -13.294)
(TAACCAAAG, -10.072)	(TACGCCTAAA, -12.488)
(TCATCCATG, -10.672)	(CCCGTTTGAT, -12.644)
(CGTTTTCAA, -10.158)	(GGCTAACAAAT, -11.434)
(CATGAAACG, -10.538)	(CTCCGATGTT, -12.384)
(CCAGACTTC, -10.738)	(TCACATTTGC, -12.258)
(CAGCATTCT, -10.678)	(CAATTTGATC, -10.034)
(CGACCGTAT, -11.618)	(CAACCAGTTG, -12.124)
(CAGGTCTGT, -11.278)	(TTGCAATAAC, -10.764)
(TTTCTCCG, -10.688)	(CAGTCTGCCC, -13.894)
(ACACTTCAT, -9.988)	(TTTCGTATTC, -10.394)
(AACATTTCG, -10.428)	(TGGACCACTT, -12.818)
(TACAAAAGC, -10.472)	(CATTGAGCTC, -11.954)
(CCTTAGCTC, -10.648)	(TTGAATTTAA, -8.884)
(CGGGATATC, -10.638)	(TATCCACGTT, -12.458)
(TGAATTTCC, -9.672)	(CTCTCCTGAC, -12.244)
(CTACCAGCT, -11.188)	(ACGTTAACAC, -11.684)
(ACTTTCACC, -10.548)	(AACTCTTGAC, -11.214)
(CGTTTACGT, -12.118)	(GACCCGATCA, -13.348)
(TCTCAGACC, -11.312)	(ACCTACAACC, -12.034)
(TATTCATC, -8.872)	(TCCTTTACCC, -12.168)
(TGCGTAAAC, -11.222)	(CACGTATCAC, -11.924)
(TTTGATTTT, -8.378)	(ACAAATGCAC, -12.074)
(GCGTTCAAT, -11.278)	(CTGGAGGCC, -14.684)
(AATCTTACA, -8.782)	(ATCTTCAAAC, -10.374)
(ATCCACCAG, -11.278)	(CACATCAGCT, -12.494)
(TAACCCTTC, -10.762)	(CACCAATTT, -11.134)
(AAACGATCC, -10.728)	(ACATTCAAAC, -10.684)
(CCTCTCACA, -11.242)	(CAGAACTCGT, -12.384)
(TCATACACC, -10.502)	(ATGCTCAATT, -11.154)
(TTTGCACAT, -10.658)	(TAACCAACTC, -11.738)
(ACAACATCG, -10.928)	(CGTGCAGATA, -13.198)
(CGTTCTCAA, -10.738)	(TCTACAGAGC, -12.198)
(CCATACCAC, -10.768)	(CGGACTATCC, -12.404)
(TGCAAATTT, -9.872)	(GCGTTCAAAT, -12.204)
(TAATTCCTT, -8.472)	(CACGAGAAAC, -12.154)
(ACTGGACCT, -11.618)	(TAAAAGACGG, -12.018)
(GGTACTCAC, -10.618)	(TATTTGTGGA, -11.622)
(CATCCAGGT, -11.278)	(TACATTTCCC, -11.738)
(ACAATATTC, -8.328)	(CTGTCTCCT, -13.224)
(TACATTTCC, -10.302)	(CGACTACCCT, -12.894)
(AGGGTCACC, -12.228)	(AACCAAAATC, -10.634)
(ACCACATTC, -10.598)	(AAAGGCGTTT, -12.644)
(TAACTTGAT, -9.362)	(CGACTATGCA, -12.618)
(GAGGAGGTC, -11.428)	(CAATTCATC, -10.874)
(TGTTTACCG, -10.822)	(TACTTTGTCC, -12.068)
(AACAAACAA, -9.528)	(AATTACGTTT, -10.184)
(AATTACACG, -9.758)	(AAAAACAAAC, -10.054)
(TAGTCCAAC, -10.812)	(ATTCCTTGG, -12.154)
(GAGATCTCG, -10.658)	(CCAGTACCCT, -12.714)

(AAGCAACTC, -10.788)	(CCGTCTTCA, -12.608)
(GTTCTTGCA, -11.062)	(TAATTTCAA, -9.568)
(ACATTACAT, -8.868)	(TCGTACTACC, -12.118)
(TAAAAATTC, -8.242)	(CAAGCCATTT, -11.864)
(CTTTACTACT, -9.268)	(CGGTATCTCC, -12.404)
(TCGAAACTT, -10.562)	(AAAAGTGTCA, -11.138)
(AACACGTT, -10.688)	(ACCTTAGACG, -12.054)
(TATTATTCC, -8.542)	(TCTAAGCAAC, -11.618)
(CTCTGTAGC, -10.698)	(CTTTAACACT, -10.194)
(TAACAAATC, -9.132)	(AGAAAAAAT, -9.134)
(TCAACTTCT, -10.122)	(TTCCAATTCA, -10.998)
(TTAACATGC, -9.838)	(ATCAAAAAT, -9.184)
(CACAAATCT, -9.598)	(GGAGACTTCC, -12.354)
(GACTAGGTG, -10.458)	(CGTTTTTGCA, -12.578)
(CCATCTTCC, -10.738)	(CTGACCGGAC, -13.834)
(TACAAATTA, -9.045)	(AACTTGCAAC, -12.024)
(GTAGGATCG, -10.638)	(TCGCGATTAA, -12.638)
(CCCCGAGGA, -13.532)	(AACAAAATGC, -11.184)
(CCCGGAACC, -13.118)	(GTATCAAAAT, -9.254)
(ACGTACAAC, -10.758)	(CAGTAGCTCC, -12.464)
(CCCTCTTCA, -11.192)	(CCACCATTTG, -12.124)
(TTCATGACA, -10.122)	(TTTGACAAAC, -10.804)
(CAGATCCCA, -11.242)	(TCATTTTTCA, -10.482)
(TATTCTTCC, -9.662)	(CTGGATGACC, -12.554)
(CTACGGACT, -11.128)	(TCCTTTTTCAC, -11.658)
(AACATACTC, -9.168)	(CACTACATCC, -11.434)
(CTAAGAGCC, -10.648)	(CATTGTCCAT, -11.414)
(CGCAATTT, -11.378)	(CTTGCCAGAT, -12.444)
(CTGTTACCC, -10.718)	(TAACGACATC, -11.968)
(GCCTGTACC, -11.958)	(TTAATTCACA, -9.878)
(CCGTAACT, -10.548)	(ATGCAAAACAT, -11.464)
(ATCATTCAT, -8.888)	(GTCCGGTTCT, -13.334)
(CTAAGCCCT, -11.138)	(TACAATTACC, -10.618)
(CTTTTGCGT, -11.378)	(AGTTGAAGCA, -12.218)
(TACTTCCAC, -10.812)	(TCGATTTTCA, -11.502)
(TCGATTCCA, -11.415)	(AATCATTTAA, -8.764)
(TAATGTTGC, -10.522)	
(CCCCAACTT, -11.488)	
(AACTTCACC, -10.548)	
(ATCACTGCA, -11.342)	
(CCATCCTCA, -11.242)	
(AATGCTCC, -10.788)	
(CAGTACCCC, -11.558)	
(ACTTCAAAC, -9.708)	
(CTCACAAC, -10.438)	
(TTCGACATC, -10.638)	
(ATACCTTTT, -8.768)	
(ACGGCTAAT, -11.178)	
(ACTTCGTAA, -9.958)	
(CTACCCCTGG, -11.398)	
(TAACGAATT, -9.802)	
(TAATTCAG, -9.812)	
(AAGATTTTC, -8.558)	
(TTTCCTTTC, -9.518)	
(CTAAGGCTC, -10.648)	
(ACTTTAACC, -9.378)	
(ACTCCTCTG, -10.968)	
(TCTTATGGC, -10.692)	
(TATATTGCA, -9.595)	
(CTGGAGTCA, -11.242)	
(TTTTTAACA, -8.322)	
(CACCCTTT, -10.698)	
(AATCAACAC, -9.758)	
(CCTTCTCAG, -10.578)	

Table 7: The 9- and 10-nt handle sequences and their NUPACK 3.0⁵² computed kcal/mol energies. Either the handle or complementary handle sequence from the above was appended to the 3' end of the top- or

bottom-staple strand sequence with no linker. These handle sequences were used to initially determine the viability of such length handle sequences for controlling nucleation of megastructures, as shown in Fig. S6.

original nanocube strands	modified nanocube strand
<p>GTAAGTTGAAGTAGGAAGCTTTTTCTAGCCATAGCATCGACACTACGACCTGCTTTTCGACAC GGACTGCATTCTGGACAGTAACTGCATTAAGTACGTCGCCAACATAAGTACGTCCTCAGCAG TTGAAAATTATCTCGATAAGCAGAAGGACCTGTATAACTGGCAAGAGACAAAGCCGCTCAGAA AGGATAGCCGGACCGTATTAATGCCCGCCCAACGGTTTCCCGGACCTAGTGTCTATCAAGTCTA TTCATGAAACCAATCTCGGGTCGAGCGGGTCACTGTTGTGACCTACGAGAAGCGTATAGATGT TCCGCGGAATAGCTCACAGGCGAAGTACGTATGAATTGGTTTAAACGTCCTCGGGAATTAAT ACGACAGTGGCAACCACCTCCGATGTCAGCGCCGCATACCATTACTGTGAATTTCCACAC CGAGGATTCGAGGTCCATGGGATTCACCAAGCTCGTATACACCCTGATTCTCCATGGCAGCGC TTTTAGAATCGAGTCCGTGCGAAAAGCATAGACACTCG TTTTTAGAATTGAGTCTGATTTTT TTTTTAGGTCCTTACTGCTTTTT TTTTTTGGCGGGCTTCTTATTTTT TTTTTCTGAAGCACTTATGTTTT TTTTCTCAACTTACCTGCTGAGGACGTCGGCCTTGACGGTCCGGTTTT TTTTTTGGGACGACGTAGTTAGAAAAGCATTAACTCTTGCTAAAC TTTTGTGTCGATGCTATGGCAATGCAGTCTGCTTATAGGTCCGGTCA TTTTCCGAGATGCTATCCTTTTT TTTTGGAGCGTTCAGTATATTTTT TTTTTCTCGTAGAAACCGTTTT TTTTCTGTGAGCATTTCATTTTT AGATATATTCGCGCGGAACATATGGAGAAGTTTGCCACCTGTCGTTTT CAACAGTGACCATCCCATGTGAATGGGTATGCGGCTTT CAATTCATACGCGGAGGTGTGAGGGTATACGAGTTTT TTTTGCGTCCCTATACGCTTTT TTTTGCTGACATTAGTTCGCTTTT TTTTCTGTGAGCGCTCGACTTTT TTTTGTGGAATTTCCGATTTTT</p>	<p>CATAGAAATTAATTCACAGGACCTGCGAATCCTCGTTTTttttTGGAGTCACAGATTGG</p> <hr/> <p style="text-align: center;">complementary handle sequence</p> <hr/> <p>CCAACTGTGACTCCA</p>

Table 8 Oligos for the nanocube, as adapted from as previously published³⁷. The complementary 16-nt handle sequence was appended to the 6HB bottom staple strands so that nanocubes could be bound to the megastructures to create patterns.

Supplementary references

53. Xin, Y., Shen, B., Kostiainen, M.A., Grundmeier, G., Castro, M., Linko, V. & Keller, A. Scaling Up DNA Origami Lattice Assembly. *Chemistry* **27**, 8564–8571 (2021).
54. Giovampaola, C.D. & Engheta, N. Digital metamaterials. *Nat. Mater.* **13**, 1115–1121 (2014).
55. Hartman, N.C. & Groves, J.T. Signaling clusters in the cell membrane. *Curr. Opin. Cell. Biol.* **23**, 370–376 (2011).
56. Ben Zion, M.Y., He, X., Maass, C.C., Sha, R., Seeman, N.C. & Chaikin, P.M. Self-assembled three-dimensional chiral colloidal architecture. *Science* **358**, 633–636 (2017).
57. Chatterjee, G., Dalchau, N., Muscat, R. *et al.* A spatially localized architecture for fast and modular DNA computing. *Nature Nanotech.* **12**, 920–927 (2017).
58. Ponnuswamy, N. *et al.* Oligolysine-based coating protects DNA nanostructures from low-salt denaturation and nuclease degradation. *Nat. Commun.* **8**, 15654 (2017).
59. Gerling, T. *et al.* Sequence-programmable covalent bonding of designed DNA assemblies, *Sci Adv.* **4**, eaau1157. (2018).